# Preliminary Study on Plate Girders with Corrugated Webs

Fatima Hlal

Mohammad Al-Emrani, Mozhdeh Amani

# Table of content

# Preliminary Study on Plate Girders with Corrugated Webs

## 1. Resistance to bending moment

The bending resistance of a simply supported girder supporting an evenly distributed load is simply the minimum axial resistances of the flanges times the distance between the flanges' centroids. This is particularly the case in girders with corrugated webs as the web stiffness along the beam is very low (a few tenths to a few hundredths of that of a flat steel web) due to "accordion effect".

### 1.1 Accordion effect

To study the accoridion effect and the moment capacity in corrugated web beams, Elamary et al., in 2017, conducted an experimental and analytical research. The authors compared the flexural capacity of standard steel I-beams (with flat web) and steel beams with corrugated webs (CW). Their tests revealed that the flexural capacity of steel beams with corrugated web is 10 to 20% lower than that of conventional steel I-beams with flat webs which is expected since the corrugated web does not contribute to the bending resistance. Moreover, the authors compared the moment capacity of composite concrete-steel beams with flat and with corrugated webs. The same manner of reduction was observed (Elamary et al., 2017).

The contribution from the web due to Accordion effect was neglected by Eurocode (EN_1993-1-5, 2006) and many other researchers. However, a recent study performed by (Inaam & Upadhyay, 2022) revealed that the contribution from the web could be considerable. Based on numerical studies performed by Inaam et al., three essential parameters that affect the accordion effect were identified. The slenderness ratio ($h_w/t_w$), enclosing effect (R), ref. Figure 1.8, and outstand ratio (O). If these parameters satisfy the conditions presented in Table 1.1, designers can utilize a minimum web participation factor of 10% (0.1 $t_w$) to determine moment resistance for steel trapezoidal corrugated I-girders with compact and laterally constrained flanges.

*Table 1.1 Conditions required for web utilization, (Inaam & Upadhyay, 2022)*

| $\dfrac{t_{w,eff}}{t_w}$ | $\dfrac{h_w}{t_w}$ | $R = \dfrac{(a_1 + a_4)a_3}{(a_1 + 2.a_4)b_f}$ | $O = \dfrac{b_f + a_3}{b_f - a_3}$ |
|---|---|---|---|
| 0.1 | $\leq 150$ | $< 0.18$ | $\leq 1.6$ |
| 0.2 | $\leq 125$ | $< 0.13$ | $\leq 1.2$ |
| 0.3 | $\leq 90$ | $< 0.09$ | $\leq 1.1$ |

### 1.2 Flange buckling resistance and Cross section classification

The bending resistance of I-girders might be affected by the compression flange local buckling if the flange plate is slender. Previous experimental and numerical studies have shown that when the compressed flange corresponds to cross-section class 4, the EN1993-1-5 bending moment resistance often results in resistances on the unsafe side (Jáger et al., 2017a). As a result, various design models were established in the past, however there are inconsistencies in the previous (current) design models when it comes to the consideration of flange width and web clamping effect (Jáger et al., 2017a).

Jager et al., in 2017, performed an experimental research program to investigate flange buckling behavior and bending moment capacity of corrugated web beams and a new model

to estimate flange buckling resistance of corrugated web girders was proposed (Jáger et al., 2017a).

This section presents and evaluate the model that has been suggested by Jager et al. and compare it to the design models given in the current version of (EN_1993-1-5, 2006) and a new model proposed in a draft version of (EN_1993-1-5, 2019).

It's worth mentioning that available models were developed with focus on carbon steel and no work could be found for stainless steel material.

### 1.2.1 Flange buckling resistance according to (EN_1993-1-5, 2006), current version
### 1.2.1.1 Flange buckling resistance for carbon steel
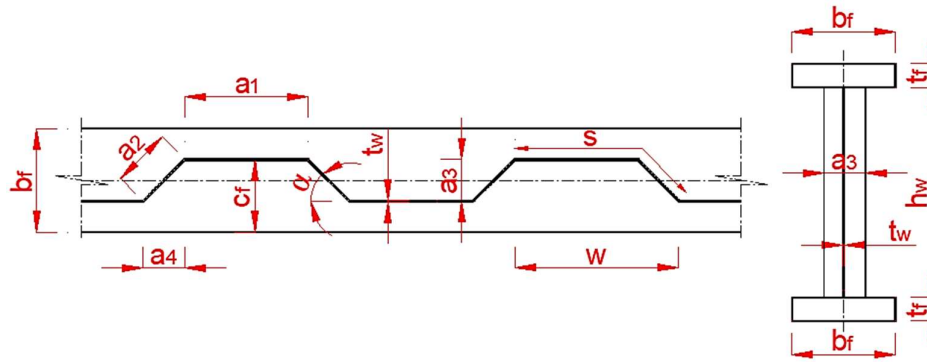


*Figure 1.1 Notations used for trapezoidal corrugated web*

When a thin plate's compression stress approaches its critical buckling stress, the plate buckles, reducing the effective resisting area. This reduction is proportional to the plate's slenderness.

The slenderness of a thin plate, in general, is defined as a square root of the ratio between yielding strength and the critical buckling stress.

$$\bar{\lambda}_p = \sqrt{\frac{f_y}{\sigma_{cr}}}$$

The critical buckling stress $\sigma_{cr}$ is a function of plate width, thickness, and the material properties (Poisson's ratio and modulus of elasticity). It can be obtained by the following formula:

$$\sigma_{cr} = k_\sigma * \sigma_E \quad \text{Where} \quad \sigma_E = \frac{\pi^2 E}{12(1-v^2)}\left(\frac{t}{b}\right)^2$$

$b$ and $t$ are the width and the thickness the plate.

The elastic buckling factor $k_\sigma$ depends on the plate support conditions (Internal or outstand element) and the stress variation along plate width, with lowest value when compression stress is uniform along the plate edge. The elastic buckling factor $k_\sigma$ for flanges in I-girder with flat web is set to 0.43 in (EN_1993-1-5, 2006).

According to (Al-Emrani, 2020), this buckling coefficient is 0.425 assuming three simply supported edges and reaches 1.277 having two simply supported edges and one fixed edge, see Figure 1.2.

k:  0.425        1.277
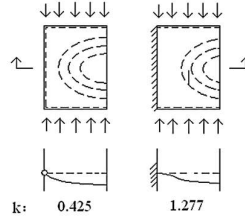
*Figure 1.2 Buckling coefficient for plates subjected to uniform compression having one edge free and three supported (Al-Emrani, 2020)*

The elastic buckling factor $k_\sigma$ for flanges in I-girders with corrugated webs is given in (EN_1993-1-5, 2006) an additional part $\left(\frac{c_f}{a}\right),^2$ due to the existence of the corrugation, with upper limit equal to 0.6.  It is thought that the buckling of the flange could occur in two different modes. The first buckling mode is buckling of the largest outstand of the flange. This mode is more relevant for webs with deep corrugations. The buckling factor $k_\sigma$ for this mode in given in the "case a" as following:

a-  $k_\sigma = 0{,}43 + \left(\frac{c_f}{a}\right)^2$   $where\ a = a_1 + 2a_4$

where  $c_f = \frac{b_f}{2} + \frac{a_3}{2}$ is the larger flange outstand from the toe of the weld to either free edge of the flange, see Figure 1.1.

Another buckling mode is rotation of the flange around the flange's centerline. This mode is more relevant for webs with shallow corrugations. The buckling factor $k_\sigma$ for this mode is given in the "case b" as following:

b-  $k_\sigma = 0{,}6\ and\ \bar{b} = \frac{b_f}{2}$

The most unfavorable situation between case a and b should govern.

Then the slenderness of the flange plate, is defined as following:

$$\bar{\lambda}_p = \sqrt{\frac{f_y}{\sigma_{cr}}} = \frac{\bar{b}/t}{28{,}4\varepsilon\sqrt{k_\sigma}}$$

$$where\ \varepsilon = \sqrt{\frac{235\text{MPa}}{f_y}}\ and\ \bar{b} = \frac{b_f}{2}$$

The buckling curve for flat and corrugated web is same in Eurocode, presented in Figure 1.3. However, the slenderness is different due to different buckling coefficient as illustrated above. The reduction factor is defined in sec 4.4 in  (EN_1993-1-5, 2006) as follows:

$$\rho = 1{,}0\ \ for\ \bar{\lambda}_p \leq 0{,}748$$

$$\rho = \frac{\bar{\lambda}_p - 0{,}188}{\bar{\lambda}_p^2} \leq 1{,}0\ \ for\ \bar{\lambda}_p > 0{,}748$$
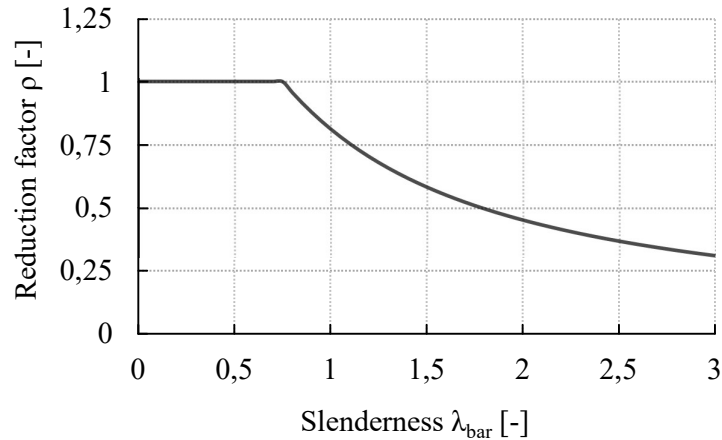
*Figure 1.3 Reduction factor, plate buckling EN1993-1-5 (2006)*

### 1.2.1.2 Flange buckling resistance for stainless steel

The buckling curve for stainless steel was defined firstly in (EN_1993-1-4, 2006) with different curves from that given for carbon steel. Later on, in an amendment of EN1993-1-4 (Amedment, 2015), this curve was adjusted to be the same as to carbon steel for outstand elements as following:

$$\rho = \frac{1}{\bar{\lambda}_p} - \frac{0,188}{\bar{\lambda}_p^2} \quad \text{but } \rho \leq 1,0$$

The elastic buckling factor $k_\sigma$ for corrugated beams was developed in Eurocode for carbon steel and has not been updated for stainless steel. Thus, until further studies, the predicted capacity due to flange buckling in stainless steel corrugated web girders can be checked with

the above-mentioned reduction factor with same elastic buckling coefficient for corrugated web beams with carbon steel, but with the specific material coefficients defined in Table 1.2.

*Table 1.2 Design values for material coefficients for carbon steel and stainless steel*

| Design values for material coefficients for carbon steel (EN_1993-1-1, 2005) | |
| --- | --- |
| Modulus of elasticity **E** | $E = 210$ GPa |
| Shear modulus **G** | $G = \dfrac{E}{2(1+v)} \approx 81000 \text{N/mm}^2$ |
| Poisson's ratio in elastic stage **v** | $v = 0,3$ |
| Coefficient of linear thermal coefficient **α** | $\alpha = 12 \times 10^{-6}$ perK (for $T \leq 100°C$) |
| Material parameter | $\varepsilon = \left[\dfrac{235}{f_y}\right]^{0.5}$ |
| **Design values for material coefficients for stainless steel (EN_1993-1-4, 2006)** | |
| Modulus of elasticity **E** | For ULS calculations:<br>$E = 200$ GPa for austenitic and austenitic-ferritic grades in Table 2.1 in (Amedment, 2015) excluding grades 1.4539, 1.4529, 1.4547<br>$E = 195$ GPa for austenitic grades 1.4539, 1.4529, 1.4547<br>$E = 220$ GPa for the ferricic grades in Table 2.1 in (Amedment, 2015)<br>In the second draft one value for E is given:<br>$E = 200$ GPa (EN_1993-1-4, 2020)<br>For SLS calculations:<br>The secant modulus of elasticity should be used according to section 4.2 in (EN_1993-1-4, 2006) |
| Shear modulus **G** | $G = \dfrac{E}{2(1+v)}$ |
| Poisson's ratio in elastic stage **v** | $v = 0,3$ |
| Coefficient of linear thermal coefficient **α** | The values suggested in the second draft (EN_1993-1-4, 2020) are:<br>$\alpha = 13 \times 10^{-6}$ perK (for $T \leq 100°C$) for Duplex stainlesss steel<br>$\alpha = 16 \times 10^{-6}$ perK (for $T \leq 100°C$) for austenitic stainless steel<br>$\alpha = 10 \times 10^{-6}$ perK (for $T \leq 100°C$) for ferritic stainless steel |
| Material parameter | In the current version (EN_1993-1-4, 2006):<br>$\varepsilon = \left[\dfrac{235}{f_y}\dfrac{E}{210000}\right]^{0.5}$<br>In the second draft (EN_1993-1-4, 2020):<br>$\varepsilon = \left[\dfrac{235}{f_y}\right]^{0.5}$ |

*Table 1.3 Design values for partial factors for carbon steel and stainless steel*

| Design values for partial factors for carbon steel (EN_1993-1-1, 2005) | |
|---|---|
| Resistance of cross-section whatever the class is | $\chi_{M0} = 1,00$ |
| Resistance of members to instability assessed by member checks | $\chi_{M1} = 1,00$ |
| Resistance of cross-section in tension to fracture | $\chi_{M2} = 1,25$ (1.2 in (Transportstyrelsens, 2018)) |
| Design values for partial factors for stainless steel (EN_1993-1-4, 2006) | |
| Resistance of cross-section whatever the class is | $\chi_{M0} = 1,1$ |
| Resistance of members to instability assessed by member checks | $\chi_{M1} = 1,1$ |
| Resistance of cross-section in tension to fracture | $\chi_{M2} = 1,25$ |

### 1.2.2  Flange buckling resistance according to (Jáger et al., 2017b)

In a study made by Jager et al., the authors collected available previous experiments that have been conducted to estimate the flange buckling resistance of beams with corrugated webs. In addition, a new experimental program was performed to study the effects that web and flange thicknesses have on the buckling resistance. The tests were also used to verify numerical models which were used to propose a new model for flange buckling resistance of corrugated web girders.

The results suggest that the Eurocode design curve for flange buckling resistance which is based on Winter-curve formula is not applicable for girders with corrugated webs. Figure 1.4 demonstrates that a significant fraction of capacity estimates based on Eurocode are placed below the curve. Based on these results, a new model was proposed for calculating the flange buckling resistance in beams with corrugated webs.
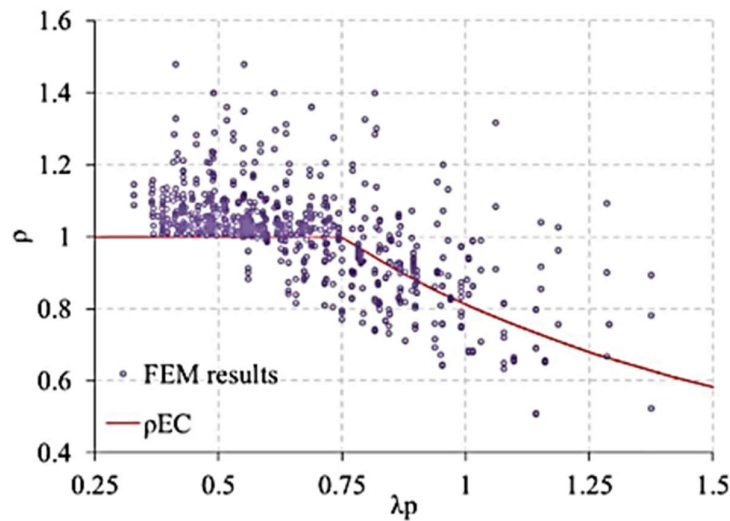


*Figure 1.4 GMNIA results compared to the design curve given in EN1993-1-5 (Jáger et al., 2017b)*

Imperfection sensitivity in flange buckling resistance, (Jáger et al., 2017b)

Fabrication tolerances for steel elements are set by EN1090-2. However, corrugated web beams are not covered in this standard. Annex C in Eurocode EN1993-1-5(2006) proposes a larger magnitude for equivalent geometric imperfection than the fabrication tolerances, thus covering the effect of residual stresses and geometric imperfections at the same time. The proposed value for flange subject to twist equals to $\frac{cf}{50}$, see Figure 1.5. However, this proposal is not specific to corrugated web girders (EN_1993-1-5, 2006).
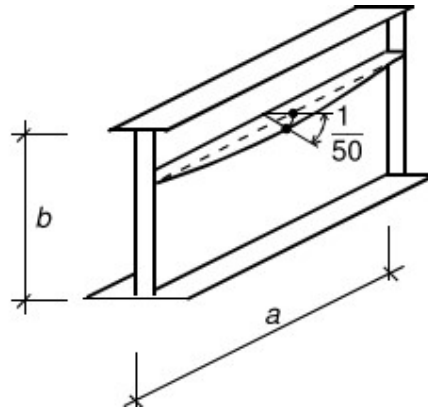


*Figure 1.5 Modelling equivalent geometric imperfection EN1993-1-5(2006)*

To investigate on the applicability of using $\frac{cf}{50}$ as the imperfection amplitude with the first eigen buckling mode as imperfection shape for corrugated web girders, an imperfection sensitivity study was performed by Jager et al. (Jáger et al., 2017b). In this study a numerical model was developed to estimate the moment capacity of corrugated web girders and the results were compared to test results from girders with different cross-section classes. Different imperfection amplitudes were studied all with the same shape of imperfection (1st mode of buckling). Figure 1.6 illustrates the results from the imperfection sensitivity analysis performed on some of the tested girders. It was noticed that the slenderer the flanges are, the more sensitive to initial imperfection they become, necessitating a bigger imperfection amplitude to achieve capacity less than those observed in the experiments. Moreover, the thicker the webs the less the flange sensitivity to initial imperfection (Jáger et al., 2017b).
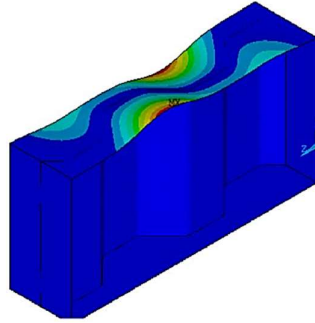
a) typical first eigenmode shape (4TP2-2)　　　　b) specimens 1-3
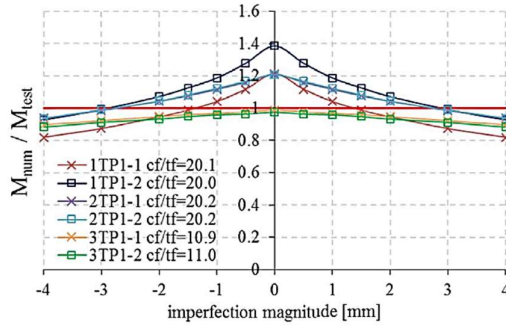
*Figure 1.6 Sensitivity analysis for initial imperfection on flange buckling resistance (Jáger et al., 2017b). The girders vary in flange slenderness cf/tf and in flange to web thicknesses ratio tf/tw (2.75, 2.70, 1.32, 1.32, 4.85, 5.11 for 1TP1-1, 1TP1-2, 2TP1-1, 2TP1-2, 3TP1-1, 3TP1-2 respectively).*

The capacities that have been resulted from the numerical model developed in this study using first eigen buckling mode with amplitude equal to $\frac{cf}{50}$ resulted in an average of 0.946 of the capacities reported from the experiments. Based on these results, it was concluded that an initial imperfection amplitude of $\frac{cf}{50}$ with first eigen buckling mode as imperfection shape gives good approximation for the flange buckling resistance of corrugated web girders in comparison with the test data (Jáger et al., 2017b).

Elastic buckling factor, $k_\sigma$ (Jáger et al., 2017b)

The model in Eurocode for flanges in beams with flat web considers two flange buckling modes, the normal stress buckling where the web is assumed to provide rigid support to the flange and the flange induced buckling where the web buckles. A buckling mode similar to the latter was also observed in the experimental program performed by Jager et al. However, according to a study performed by Elamary et al., the corrugated web beams exhibit just local flange buckling while the flat web beams could show local flange buckling followed by web local buckling (Elamary et al., 2017).

The authors considered various flange to web thickness ratios and it was observed that three buckling modes within the flange can occur, dependent on the rigidity of the support that the web provides to the flange. The change between fixed and pinned support happens at around $\frac{tf}{tw} = 2.5$. The three modes are illustrated in Figure 1.7 and can be differentiated as follows:

Separated local flange buckling when $\frac{tf}{tw} < 2.5$. Figure 1.7, b

Combined buckling mode when $5 > \frac{tf}{tw} > 2.5$. Figure 1.7, d

Flange induced buckling of the web when $\frac{tf}{tw} \geq 5$. Figure 1.7, a
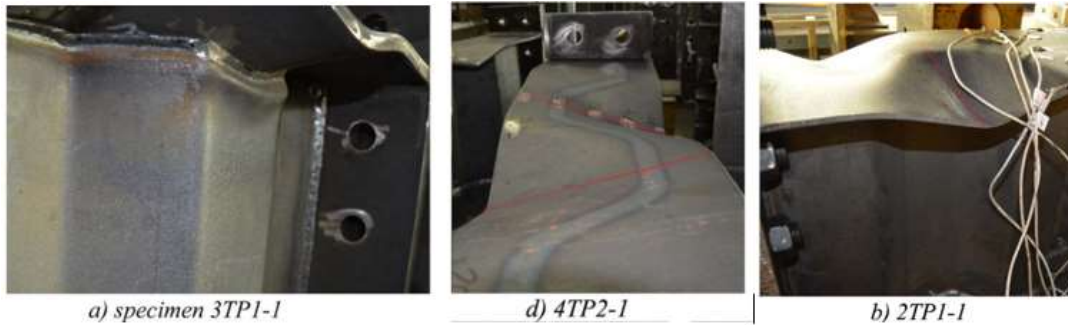
*Figure 1.7 Flange buckling modes according to Jager et al. experiments (Jáger et al., 2017b)*

The findings of Jager et al. study revealed that EN1993-1-5 for the buckling factor, kσ, needs be improved for the following reasons:

1. It ignores the effect of flange to web connection rigidity, which varies depending on the flange to web thickness ratio $\frac{t_f}{t_w}$. The numerical study showed that increasing $\frac{tf}{tw}$ leads to less rigid support from the web meaning a lower buckling factor. (Jáger et al., 2017b)

2. It doesn't take the true buckling length into account (in the case of $\frac{b_f}{a_3}$>2, the buckling (a) length could be larger than $(a_1 + 2 \cdot a_4)$. The numerical study showed that increasing $\frac{c_f}{a}$ increases the buckling factor, meaning that the buckling coefficient decrease with increasing the buckling length (Jáger et al., 2017b).

3. It doesn't consider the enclosing effect of the web, R, which specifies the size of the flange region cut by the web from the total flange width, see Figure 1.8. The numerical study showed that increasing $R$ decreases the buckling factor (Jáger et al., 2017b).
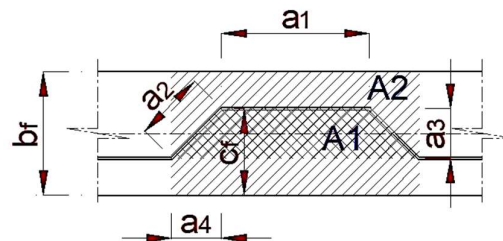


*Figure 1.8 Enclosing effect R=A1/A2*

A new formula for the buckling factor was suggested by (Jáger et al., 2017b) based on the experimental and numerical programs. The new formula considers all previous mentioned aspects with upper limit of 1.3 (one end is fixed). It is expressed by the following equation:

$$k_\sigma = min\left(1.3, 0.43 \cdot \left(2.5 \cdot \frac{t_w}{t_f}\right)^{(0.6+R)} + \left(\frac{c_f}{a_1 + 2 \cdot a_4}\right)^2\right)$$

<u>Reduction buckling factor, **ρ** according to (Jáger et al., 2017b)</u>

The design model developed by Jager et al. has been developed considering first buckling mode as initial imperfection shape with amplitude equal to $\frac{c_f}{50}$.

The buckling reduction factor can be calculated as:

$$\rho_a = min\left(1,\left(14 \cdot \varepsilon \cdot \frac{t_f}{c_f}\right)^\beta\right)$$

Factor $\beta$ considers the corrugation configurations and it is defined as follows:

$$\beta = 5 \cdot \eta \cdot R \cdot \left(\frac{1}{\tan(\alpha)}\right)^\eta \quad 0.5 \geq \beta \leq 1$$

The enclosing effect is defined as follows:

$$R = \left(\frac{A_1}{A_2} = \frac{(a_1 + a_4) \cdot a_3}{(a_1 + 2 \cdot a_4) \cdot b_f}\right) < 0.14$$

Factor $\eta$ that consider the flange to web thicknesses ratios is defined as follows:

$$\eta = 0.45 + 0.06 \cdot \frac{t_f}{t_w}$$

The larger outstand of the compression flange can be calculated as following:

$$c_f = \frac{b_f + a_3}{2}$$

### 1.2.3 Flange buckling resistance according to (EN_1993-1-5, 2019), new draft

Same procedure that was used in EN1993-1-5 (2006) for flange buckling resistance in corrugated web girder is also suggested in the new draft o Eurocode with change in the considered flange outstand from $b_f/2$ to $c_f$ as illustrated in Figure 1.9.
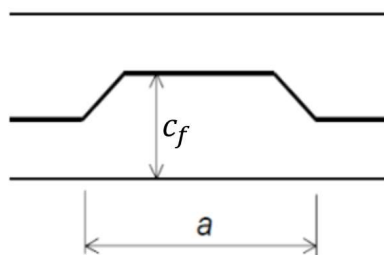


*Figure 1.9 Flange notation, (EN_1993-1-5, 2019)*

Elastic buckling factor, $k_\sigma$

The buckling factor should be determined as below:

$$k_\sigma = max\left(0.6, 0.43 + \left(\frac{c_f}{a}\right)^2\right) \quad where \ a = a_1 + 2a_4$$

And $c_f$ is the larger outstand from the toe of the weld to the free edge, illustrated in Figure 1.9.

Reduction buckling factor, $\rho$

The reduction factor according to sec 6.4 in (EN_1993-1-5, 2019)

$$\rho = 1{,}0 \quad for \ \bar{\lambda}_p \le 0{,}748$$

$$\rho = \frac{\bar{\lambda}_p - 0{,}188}{\bar{\lambda}_p^2} \le 1{,}0 \quad for \ \bar{\lambda}_p > 0{,}748$$

The non-dimensional slenderness is defined as:

$$\bar{\lambda}_p = \sqrt{\frac{f_y}{\sigma_{cr}}} = \frac{\bar{b}/t}{28{,}4\varepsilon\sqrt{k_\sigma}}$$

Here $\bar{b}$ is equal to the larger outstand $c_f$ as indicated in Figure 1.9

### 1.2.4   Discussion and recommendations
To achieve better understanding of the model proposed by Jager et al., a comparison of this model with the flat web model suggested in Eurocode has been conducted. Different values of factor β are considered and the results are presented in Figure 1.10. It can be observed that for deep corrugations, this model predicts lower flange buckling resistances for corrugated web girders than for flat webs. After a specific flange width (with very shallow corrugation beta = 0.5), however, the flange in beams with corrugated web will have higher capacity than in the flat web beam.

Moreover, as the corrugation gets deeper, the resistance will drop substantially and that is due to increasing the enclosing effect R (increases $\beta$), implying that shallow corrugations provide higher capacity.
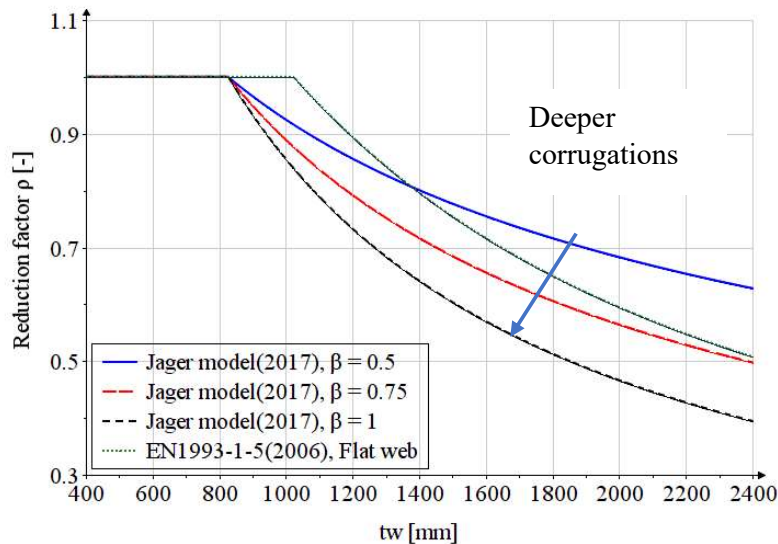


*Figure 1.10 Reduction factor variation with flange width for different β values, Jager model, dimensions presented in Table 1.4 with a3 = 200 mm*

Moreover, a plot for reduction factor variation with web thickness (changing $\frac{t_f}{t_w}$) for different corrugation depths is also performed and presented in Figure 1.11. It can be observed that

increasing the web thickness increases the reduction factor and that attributes to the increase in the support rigidity provided by the web.
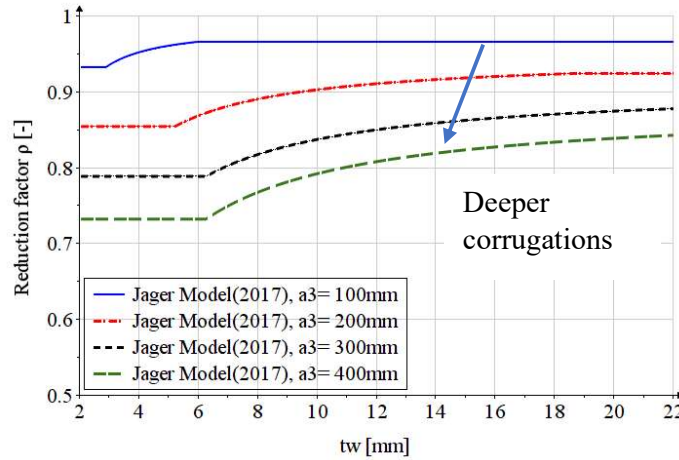


*Figure 1.11 Reduction factor variation with flange width for different web thicknesses, Jager model, dimensions presented in Table 1.4 with bf = 1000 mm and a3 = 200 mm*

Furthermore, a comparison between four buckling curves; (EN_1993-1-5, 2006), (Jáger et al., 2017b), (EN_1993-1-5, 2019) for corrugated web girders, and (EN_1993-1-5, 2006) for flat web girders has been performed.

For these models, the effect of increasing the flange width on the buckling reduction factor has been investigated for three corrugation depths. The other dimensions of the studied beam are illustrated in Table 1.4.

*Table 1.4 Dimensions of studied girders*

| $f_{yf}$ [MPa] | alpha [deg] | $a_1$ [mm] | $a_3$ [mm] | $t_w$ [mm] | $t_f$ [mm] | $b_f$ [mm] |
|---|---|---|---|---|---|---|
| **355** | 30 | 190 | 100, 200, 300 | 3 | 45 | 400 to 2400 |

Figure 1.12 present a comparison between the four models considering the buckling factor as a maximum of (0.6) and $\left(0.43 + \left(\frac{c_f}{a}\right)^2\right)$ for Eurocode models. Both versions of Eurocode offer very large values for flange buckling resistance, which is owing to the buckling factor being set to a maximum of (0.6) and $\left(0.43 + \left(\frac{c_f}{a}\right)^2\right)$. However, with the minimum buckling factor, the results will be more reasonable. For this reason, the buckling factor has been replaced with minimal value of (0.6) and $\left(0.43 + \left(\frac{c_f}{a}\right)^2\right)$, and later the comparison is repeated.
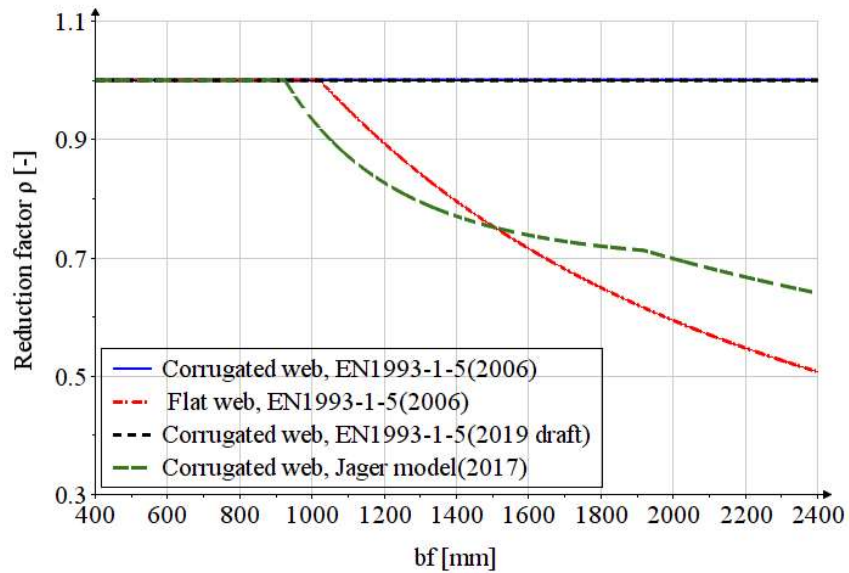
*Figure 1.12 EN2006, EN2019, Jager2017 and flat buckling reduction factor variation with bf, a3=100mm, maximal kσ*

Figure 1.13 to Figure 1.15 show the repeated comparison. As it can be observed, the current Eurocode draft gives more conservative results than the 2006 version. Two types of buckling were identified in 2006, one for rotational (torsional) buckling of the flange (restrained by the corrugated web) and the other for local flange buckling and flange outstand is set to $b_f/2$. In 2019 draft, however, the flange outstand is set to $c_f$.
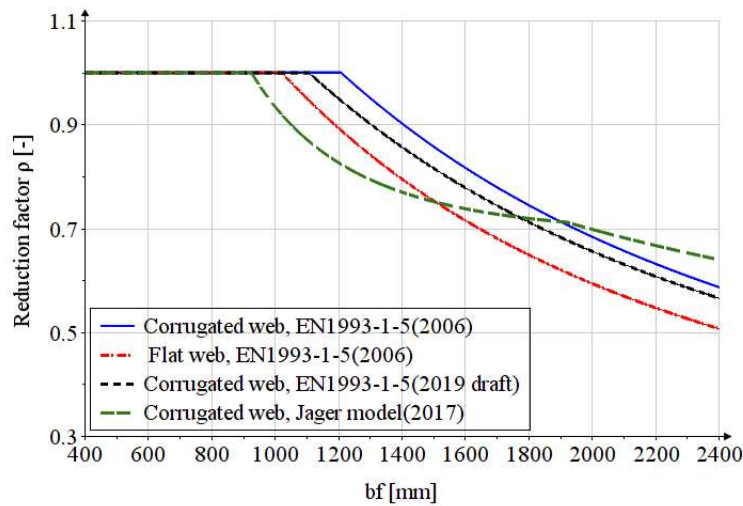


*Figure 1.13 EN2006, EN2019, Jager2017 and flat buckling reduction factor variation with bf, a3=100mm, minimal kσ*
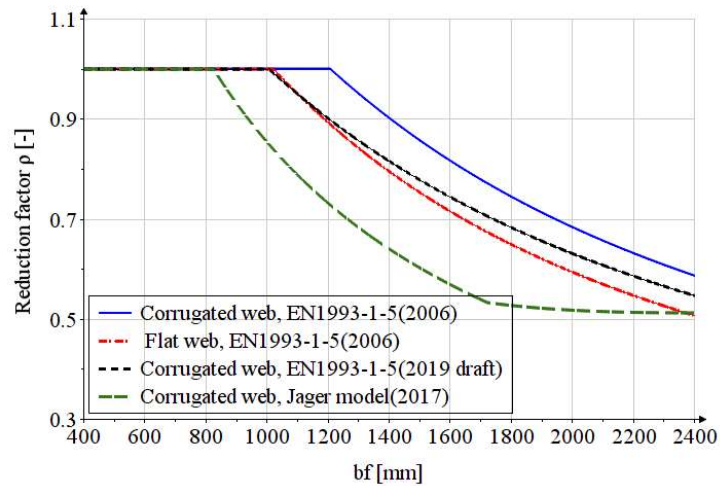
*Figure 1.14 EN2006, EN2019, Jager2017 and flat buckling reduction factor variation with bf, a3=200mm, minimal kσ*
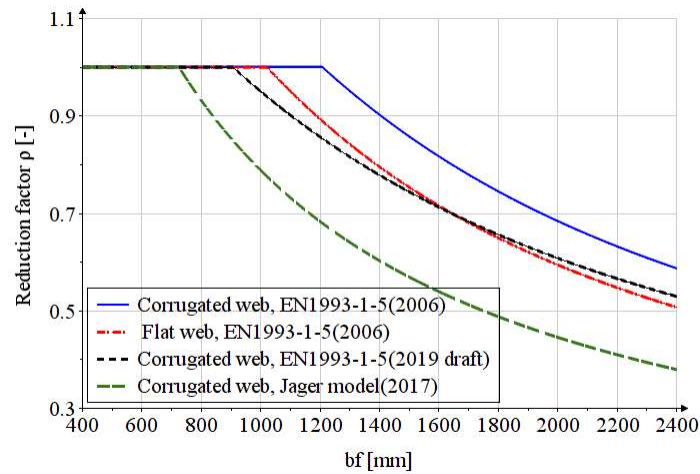


*Figure 1.15 EN2006, EN2019, Jager2017 and flat buckling reduction factor variation with bf, a3=300mm, minimal kσ*

Comparing the model proposed by Jager et al. to the Eurocode models, the model proposed by Jager et al. gives lower capacities compared to the Eurocode models for small flange widths, as seen in Figure 1.13. With increasing flange width, however, this tendency changes. In addition, as the corrugation gets deeper, Figure 1.14 and Figure 1.15 , Jager model estimate lower capacities than Eurocode versions.
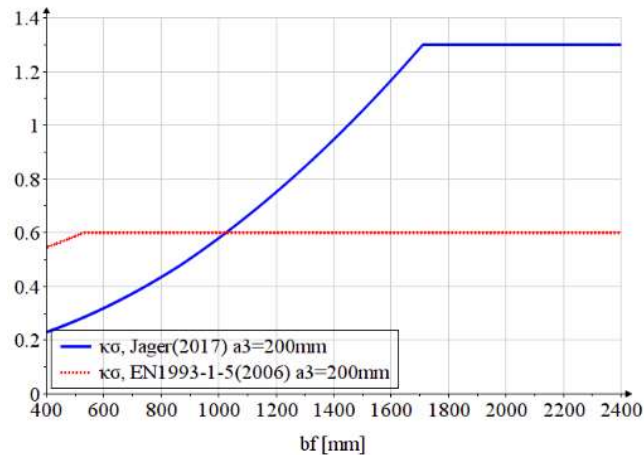
*Figure 1.16 Elastic buckling factor for Jager model and Eurocode model. The considered dimensions are presented in Table 1.4. The buckling factor according to Eurocode is considered minimum between case a and case b.*

Comparing the flange buckling resistance in a beam with corrugated web to that in a flat web beam, it's worth noting the current version of EN1993-1-5 predicts larger flange capacities for beams with corrugated webs than for that with flat web while the new draft considers the corrugation depth and as the corrugation gets deeper the corrugated web curve become close to the flat web. The Jager et al. model predicts that flanges in corrugated web girders will buckle more easily than that for flat web girders for small flange slenderness and shallow corrugation, see Figure 1.13 and Figure 1.16. And the same manner as in the Eurocode draft, for deeper corrugation the capacity is expected to be lower than that for flat web girders even for small flange slenderness.

Another study has been performed in this section. Herein, the moment resistances of several earlier performed tests with flange buckling failure were compared to the values predicted by the EN2006, EN2019, and Jager 2017 models. Both maximum and minimum buckling factors from the new draft are considered in the comparison. Table 1.5 and Figure 1.17 summaries the tests that were investigated. It can be observed that choosing the maximum value for the buckling factor according to the formulation in the EN2019 draft leads to unconservative results (test 5 and 6). However, when the buckling factor is set to the minimum value, however, we can observe that the EN2019 gives good results in comparison to the test results. In some cases, such as the GJ3-2 girder, the Jager model gives unconservative results, while in another girder, such as 5TP2-2, it yields relatively conservative results. It's worth noting that the reduction factor obtained here is applied to the whole flange width, as contrasted to Jager et al. calculations of flange buckling resistance according to Eurocode, which calculated the reduction factor for each outstand separately before adding them up (Jáger et al., 2017b).

It can be also noticed from the Table 1.5 that some girders like CB90-6, M09AR, and M32BR all models predict same moment capacity and that attributes to the fact that slenderness of these girders' flanges were small and no reduction due to flange buckling is noticed.

*Table 1.5 Previous tests capacities according to EN2006, EN2019, Jager2017 models and test results*

| Nr. | Specimen | Ref. | Test results [kNm] | EN2006 Model | EN2019 Model, $k_{\sigma.max}$ | EN2019 Model, $k_{\sigma.min}$ | Jager Model |
|---|---|---|---|---|---|---|---|
| 1 | CB90-6 | Koichi& Masahiro | 83.7 | 79.058 | 79.058 | 79.058 | 79.058 |
| 2 | 5TP2-2 | Kövesdi | 321.3 | 370.9 | 294.283 | 278.9 | 246.968 |
| 3 | M09AR | Elgaaly et al. | 180.9 | 177.595 | 177.595 | 177.595 | 177.595 |
| 4 | M32BR | Elgaaly et al. | 223.2 | 231.058 | 231.058 | 231.058 | 231.058 |
| 5 | GJ3-2 | Li et al. | 81 | 95.507 | 151.046 | 86.212 | 133.118 |
| 6 | 1TP1-2 | Kövesdi | 322.7 | 377.465 | 377.465 | 321.56 | 320.539 |

*Table 1.6 Dimensions of the studied girders*

| | CB90-6 | 5TP2-2 | M09AR | M32BR | GJ3-2 | 1TP1-2 |
|---|---|---|---|---|---|---|
| $f_{yf}$ [MPa] | 297 | 495 | 289 | 376 | 400 | 495 |
| $f_{yw}$ [MPa] | 301 | 392 | 682 | 682 | 524 | 392 |
| E [GPa] | 200 | 200 | 200 | 200 | 200 | 200 |
| Poisson ratio [-] | 0.3 | 0.3 | 0.3 | 0.3 | 0.3 | 0.3 |
| $h_w$ [mm] | 319.2 | 500 | 304.8 | 304.8 | 238.54 | 500 |
| $t_w$ [mm] | 3.26 | 5.95 | 0.607 | 0.76 | 2.06 | 2.93 |
| $b_f$ [mm] | 99.9 | 248 | 152.4 | 152.4 | 310 | 249 |
| $t_f$ [mm] | 8.14 | 7.69 | 12.7 | 12.7 | 5.73 | 7.92 |
| $a_1$ [mm] | 87 | 145 | 19.8 | 49.8 | 62 | 97 |
| alpha [deg] | 43.6 | 45 | 50 | 62.5 | 50.27 | 45 |
| $a_2$ [mm] | 87 | 145 | 18.53 | 57.25 | 50 | 97 |
| $a_4$ [mm] | 63 | 102.53 | 11.91 | 26.435 | 31.96 | 68.6 |
| $a_3$ [mm] | 60 | 102.53 | 14.195 | 50.781 | 38.45 | 68.6 |
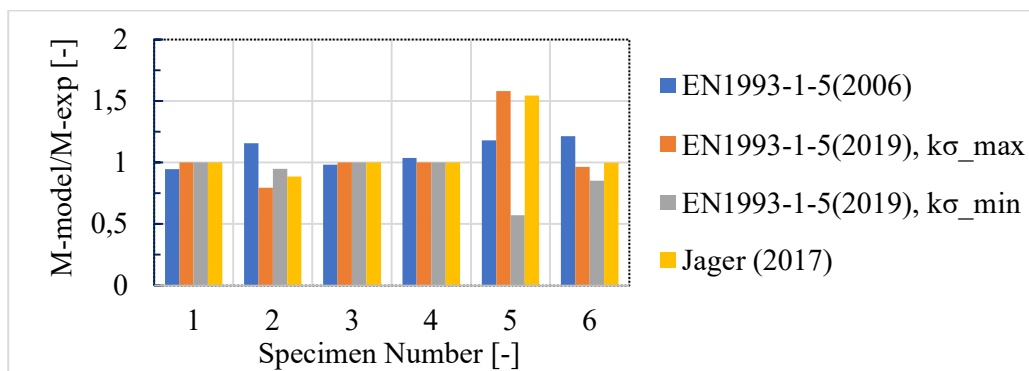


*Figure 1.17 Previous tests capacities according to (EN_1993-1-5, 2006), (EN_1993-1-5, 2019), (Jáger et al., 2017b) models and test results*

The last study in this section is a comparison between the buckling factor for carbon steel and stainless steel according to the new draft of EN1993-1-5. Herein, same dimensions as mentioned above is used. The studied stainless material is Duplex (Austenitic-ferritic steels) of grade 1.4162. The flange thickness is $75\ mm > b_f = 45mm > 13.5\ mm$ and the yield strength

is 450MPa (Amedment, 2015). The modulus of elasticity is given in section 2.1.3 in (EN_1993-1-4, 2006), $E = 200\ GPa$ for austenitic-ferritic grades except grades (1.4539, 1.4529, 1.4547). The buckling reduction factor is defined as following:

$$\rho = \frac{1}{\bar{\lambda}_p} - \frac{0,188}{\bar{\lambda}_p^2} \quad \text{but}\ \rho \le 1,0 \quad \text{(Amedment, 2015)}$$

The predicted capacity due to flange buckling is lower in stainless steel due to the difference in the material parameter ε. This factor is $\varepsilon = \sqrt{\dfrac{235\text{MPa}}{f_y}}$ in carbon steel and $\varepsilon = \left[\dfrac{235}{f_y}\dfrac{E}{210000}\right]^{0.5}$ in stainless steel (Amedment, 2015). Meaning that this factor is smaller for stainless steel leading to larger slenderness and higher reduction factor.
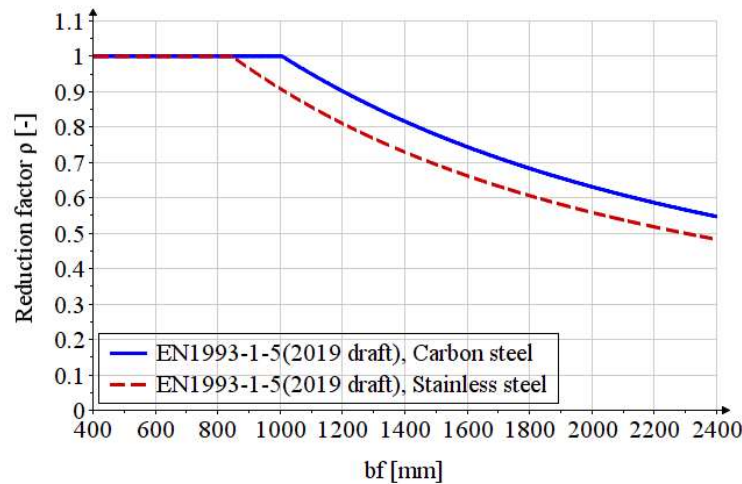


*Figure 1.18 Reduction flange buckling factor for carbon steel and stainless steel EN1993-1-5(2019 draft)*

The conclusions and recommendations that can be drawn from this study are:

1. The buckling factor in the new Eurocode draft should be changed from Max to Min.
2. The reduction factor is applied to the entire flange width in this study and needs to be clarified in Eurocode.
3. EN1993-1-5(2019) with minimal value for buckling factor can be utilized for carbon steel trapezoidal corrugated web girders. However, a more thorough investigation with various corrugation configurations is desired.
4. To modify the model of carbon steel or to adapt it for stainless steel, a parametric research for stainless steel material is essential.

## 1.3 Transverse bending moment, M-V interaction

Previous experiments have revealed that shear stress in the corrugated web implies a transverse bending moment, resulting in extra normal stresses in the flanges. In this kind of beams, the moment-shear interaction equation has different character. When the girder is subjected to shear and bending moment, the interaction can be taken by reduced bending resistance by factor $f_T$ which depends on the flange yield strength and the maximum stress coming from shear flow into the flange. (Kövesdi et al., 2016)

The maximum additional stresses $\sigma_x(M_z)$ can be calculated by applying transverse moment $M_z$ based on the shear load. Several researchers have investigated the method of estimating

the transverse bending moment and the resulting extra stresses in the flanges. This section compiles the Eurocode' model that accounts for these effects, as well as many of the approaches proposed in previous work.

### 1.3.1 Transverse bending moment according to (EN_1993-1-5, 2006), current version

#### 1.3.1.1 Transverse bending moment for carbon steel

The shear stress path in the junction between the web and the flange in corrugated web beams is not straight as that in flat web beams, it follows, however, the corrugation path as shown in Figure 1.19. The horizontal shear forces developing at the web-to-flange junction ($T_1$) results in moment $M_1$. In addition, the shear force ($T_2$) results in force ($F_y$) acts as transverse loads in the plane of flanges. These effects ($M_1, F_y$) resulting in additional normal stresses on the flanges.
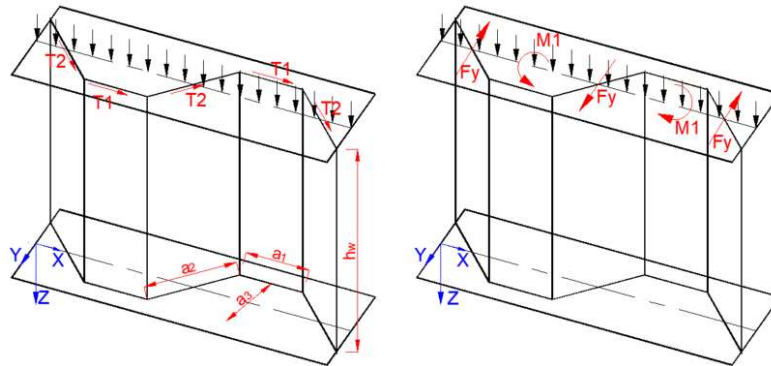


*Figure 1.19 Transverse actions due to shear flow introduction into the flange*

Eurocode considers the effect of this transverse bending moment by reducing the value of yield strength of the flange for both tension and compression flanges. The reduction is based on the amount of transverse bending stress induced in the flanges from the shear flow (EN_1993-1-5, 2006).

The reduced yield strength of the flange due to transverse moment is defined as follows:

$$f_{yf,r} = f_{yf*}f_T$$

The reduction factor due to transverse bending is defined as follows:

$$f_T = 1 - 0,4 \sqrt{\frac{\sigma_x(M_z)}{\frac{f_{yf}}{\gamma_{M0}}}}$$

$\sigma_x(M_z)$ the normal stress on the flange due to the transverse moment.

The transverse action due to shear flow in the flanges can be analyzed as shown in Figure 1.19. The horizontal forces can be determined as following:

$$T_1 = \frac{V}{h_w}a_1 \text{ and } T_2 = \frac{V}{h_w}a_2$$

V is the shear force.

Then the transverse moment $M_z$ can be obtained from conventional structural analysis of the flange as a beam subjected to $T_1$ and $T_2$ which can be substituted with the following loads:

$$F_y = T_2 \cdot \sin(\alpha) \text{ and } M_1 = T_1 \cdot a_3/2$$

According to (B. Johansson, 2007), the maximum transverse bending moment $M_{z,max}$ that can occur is when the inclined web part intersects the centerline of the flange, see Figure 1.20. In the absence of detailed analysis, this moment $M_{z,max}$ can be expressed as:

$$M_{z,max} = \frac{V}{h_w} \frac{a_3}{4} (2a_1 + a_4)$$
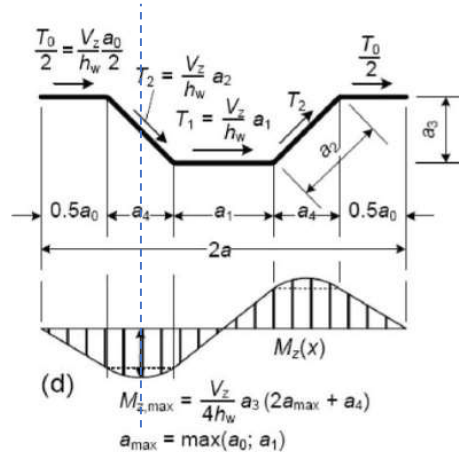


*Figure 1.20 Moment distribution in the part of the corrugation cut off the flange due to shear flow, (Baláž & Koleková, 2012). Note, $a_0 = a_1$*

To note here that a new draft of Eurocode (EN_1993-1-5, 2019) provides a new formula to estimate the transverse bending moment as following:

$$M_{z,max} = \frac{V}{h_w} \frac{a_3}{2} (2a_1 + a_4)$$

The maximum additional normal stress to the flange can then be obtained from:

$$\sigma_x(M_z) = \frac{M_z}{I_{fz}} \cdot \frac{b_f}{2}$$

Where $I_{fz}$ is the moment of inertia around the strong axis of the flange.

### 1.3.1.2  Transverse bending moment for stainless steel

The design model in Eurocode that consider transverse bending moment in corrugated web beams is developed for carbon steel and has not been modified for stainless steel. Therefore, the same model is recommended with the relevant partial and material factors that has been defined in Table 1.2 and Table 1.3 until further investigations is done.

### 1.3.2  Transverse bending moment according to  (Abbas et al., 2007)

Two different methods were presented by Abbas et al. (Abbas et al., 2007). The first method is called Fictious load method. This method was published earlier, and it gives closed form solution for transverse bending moment for sinusoidal profiles and profiles with linear folds.

This method was investigated by Abbas et al. for various web profiles and it was observed that transverse bending moment is related only to the area function of web profile. Thus, a simpler method which called the C-factor method was proposed by the authors.

C-factor method:

In this method, the transverse moment is to be calculated for sinusoidal corrugation with same wavelength and same corrugation depth. See Figure 1.21. Then transfer it to the new shape (trapezoidal, rectangular, or triangular) by the C-factor.
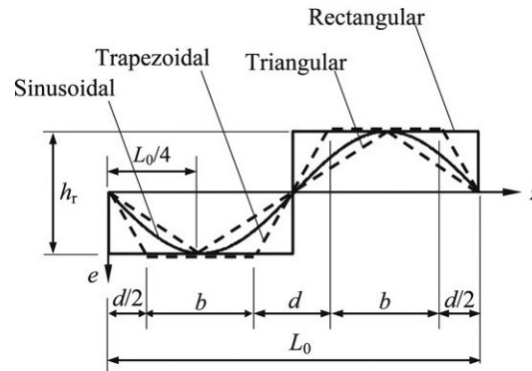


*Figure 1.21 Web profiles with equal wavelength and corrugation depth (Abbas et al., 2007)*

The notation that is used by the authors for sinusoidal corrugations are illustrated in Figure 1.22.
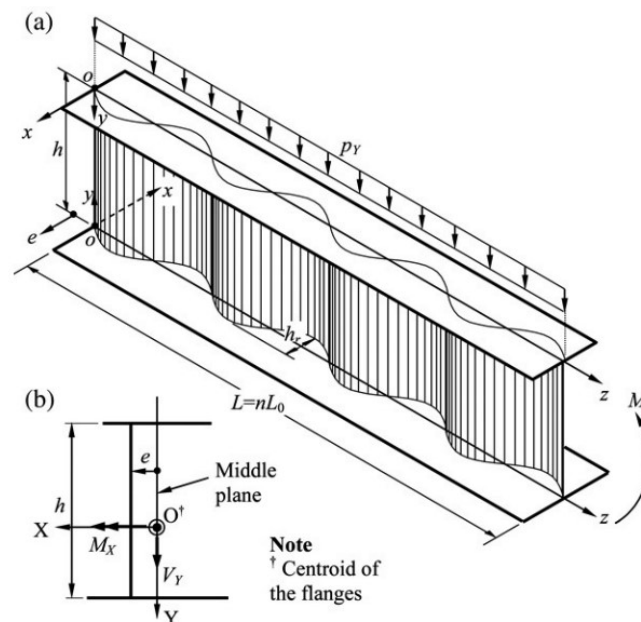


*Figure 1.22 Notations for Sinusoidal corrugated webs, (Abbas et al., 2007)*

The transverse moment for sinusoidal corrugated web girder under uniformly distributed load is defined as follows:

$$M_t = \frac{p_Y L^2 e_0}{h} \left\{ \frac{1}{\Pi^2} \left[ (1 - 2\zeta)\Pi c_\zeta + 2s_\zeta + (\Pi c_{11} - 2s_\Pi + \Pi)\zeta - \Pi \right] \right\}$$

where $\zeta = z/L$; $\Pi = 2\pi n$; $c_\zeta = \cos(2\pi n\zeta)$; $c_\Pi = \cos(2\pi n)$;
$s_\zeta = \sin(2\pi n\zeta)$; and $s_\Pi = \sin(2\pi n)$.

L is the span of the girder

$e_0 = h_r/2$ is the amplitude of corrugation

$p_Y$ is the uniformly distributed load applied on the girder.

$n$ is the number of corrugations

$z$ is the coordinate in the longitudinal axis

The total stress from in plane moment and transverse moment can be obtained as following:

$$\sigma = \frac{M_X Y}{I_X} + \frac{M_t x}{I_t}$$

The transverse moment can be transferred to another shape by the following equation:

$$\frac{M_t^I}{M_t^J} = \frac{C^I}{C^J}$$

Where C-factor can be taken from Table 1.7.

*Table 1.7 Area under one half wave and area ratio, C, relative to sinusoidal profile (Abbas et al., 2007)*

| Profile | Area under one half wave $\int_0^{L_0/2} e\,dz$ | Area ratio $C$ |
|---|---|---|
| Sinusoidal | $\frac{h_r L_0}{2\pi}$ | 1 |
| Trapezoidal | $\frac{h_r}{2}[b + d/2]$ | $\pi\left[\frac{b+d/2}{L_0}\right]$ |
| Triangular | $\frac{h_r L_0}{8}$ | $\pi/4$ |
| Rectangular | $\frac{h_r L_0}{4}$ | $\pi/2$ |

Fictitious load method:

 this approach calculates the transverse moment by applying fictitious transverse loads on the flange and analyzing the flange under these loads. Figure 1.23 shows an example for simply supported beam subjected to concentrated load on mid-span. The fictious applied loads are obtained from the geometry of the web profile and the main shear force.

The load is to be placed alternately on the top flange:

$$p_t = \frac{2}{h}\left[V_Y \frac{de}{dz} + e \frac{dV_Y}{dz}\right] \qquad \text{Eq.5 (Abbas et al., 2007)}$$

$\frac{de}{dz}$ is the change in eccentricity slope.

$\frac{dV_Y}{dz}$ is the change in shear slope.

In cases where the eccentricity or the shear force is not continuous, a fictious concentrated load is to be applied at the point of discontinuity. This load can be calculated as following:

$$P_t = \frac{2}{h} * e * \Delta V_Y \text{ when shear force is discontinuous.}$$

$$P_t = \frac{2}{h} * \Delta e * V_Y \text{ when eccentricity is discontinuous.}$$

$\Delta V_Y$ is the change in primary shear at the point of discontinuity

$\Delta e$ is the change in the web eccentricity at the point of discontinuity, i.e., the location of applied concentrated load on top flange.

$h$ is the height of the girder.
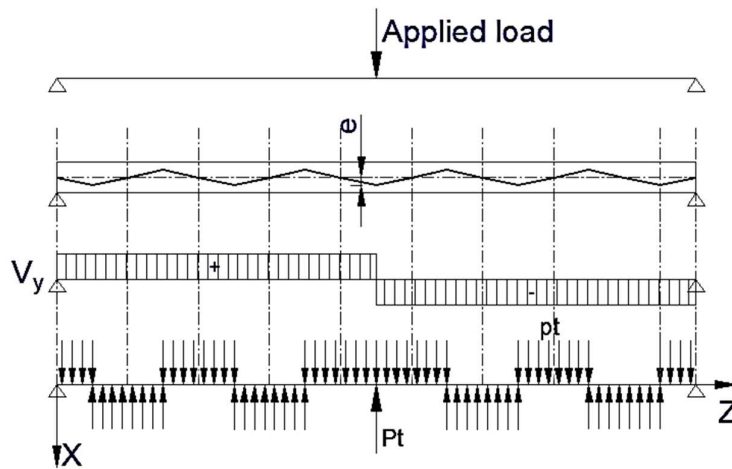


*Figure 1.23 Top flange fictitious transverse loads*

### 1.3.3 Transverse bending moment according to (Kövesdi et al., 2016)

In 2012, Baláž, I. & Koleková (Baláž & Koleková, 2012) have performed analysis of girders with trapezoidal corrugated webs and based on the results the authors proposed a simple formula to calculate the maximum transverse moment as expressed in the following equation:

$$M_{z,max} = \frac{V}{h_w} \frac{a_3}{4} (2a_1 + a_4)$$

Later, in 2016, the effects of geometric properties, corrugation geometry, lateral and end supports, and different loading conditions were extensively studied by Kövesdi et al. to find the most unfavorable case that gives maximum additional normal stress to the flange from the shear flow. The maximum transverse moment that obtained in this study was double of what has been founded in 2012 (Kövesdi et al., 2016). Therefore, the maximum transverse moment was proposed to be calculated using the following equation:

$$M_{z,max} = \frac{V}{h_w} \frac{a_3}{2} (2a_1 + a_4)$$

The maximum additional normal stress to the flange can then be obtained as:

$$\sigma_x(M_z) = \frac{M_{z,max}}{I_{fz}} \cdot \frac{b_f}{2}$$

where $I_{fz}$ is the second moment of area of the flange around the weak axis of the girder.

Moreover, the effect of lateral supports on the resulting additional stress on the flanges has been studied. It was concluded that the lateral supports might have a major effect on the extra normal stress distribution. In the case of the studied girder, transverse girders, or purlins, which provide lateral support to the girders, can lower the extra normal stresses in the region of the lateral supports by 35-40%, and continuous lateral support reduces the additional normal stresses by 75%.

Later, a parametric model based on material and geometric nonlinearity was created by the authors to investigate the true influence of shear force on the girder's bending resistance. The model was built to simulate both bending and shear failures. The model is validated by 6 large scale bending test specimens done by Elgaaly et al. and three large scale shear tests. The parametric research was then applied on 20 girders: 11 bridge girders, and 9 building geometries. The shear and moment resistances were determined first, followed by eight calculations for each girder with various shear-moment ratios.

As indicated by the research, the imperfection shape was set to the first buckling mode with equivalent amplitude according to (EN_1993-1-5, 2006). The different failure modes have been studied separately. The results for typical bridge girder and typical building girder are illustrated in Figure 1.24. It was observed that the moment resistance does not drop even when the shear force is close to the girder's shear resistance meaning that the additional normal stress in flanges due to shear flow has no effect on ultimate moment capacity of the girder. The same conclusion applies for the 20 studied girders, see Figure 1.25. It can be seen from Figure 1.25 that when (EN_1993-1-5, 2006) is taken as a reference for moment resistance, most cases ends in the conservative side ($M/M_{R,EC}$ =1 to 1.2). The highest reduction in bending resistance due to the combined M-V loading scenario is 4,7%. The observed resistance reduction is not greater than the bending resistance contribution from the web or the shear buckling resistance contribution from the flange. It was demonstrated that there is no relation between the size of the transverse bending moment and the ultimate bending resistance, (Kövesdi et al., 2016). Thus, for ultimate limit state design, the transverse bending moment can be neglected.
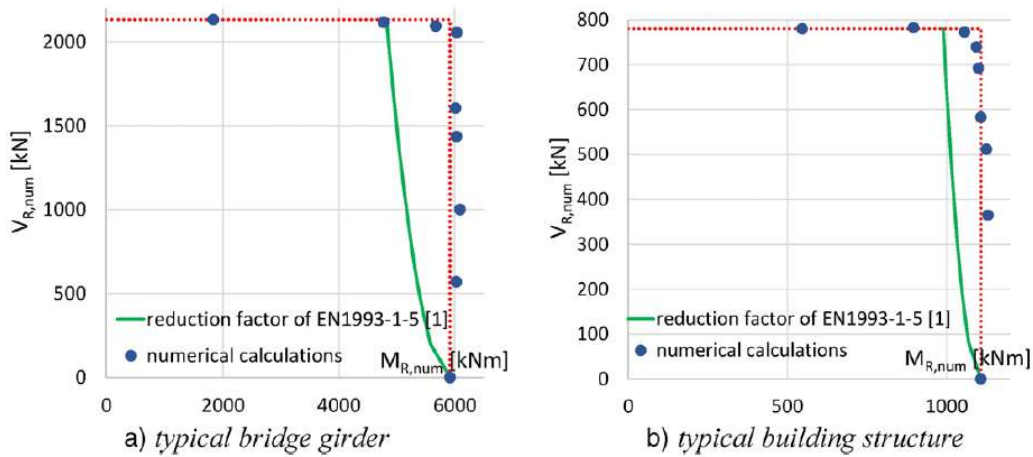
*Figure 1.24 Typical M-V interaction behavior (Kövesdi et al., 2016)*
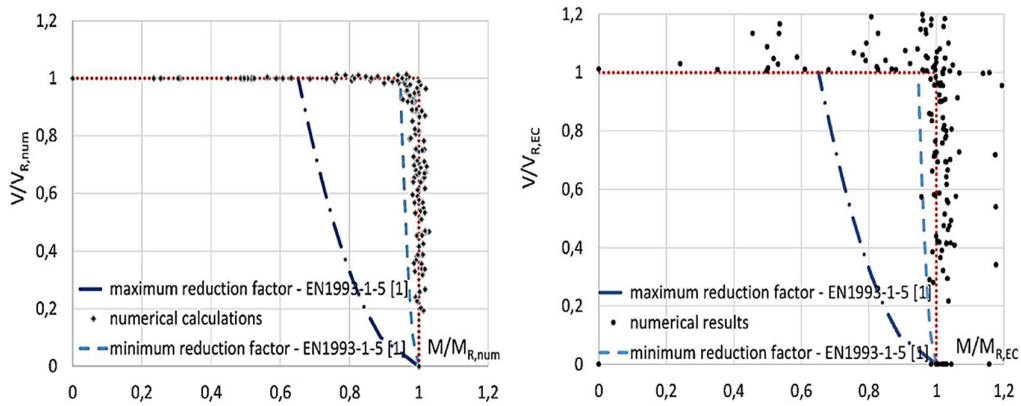


*Figure 1.25 Observed M-V interaction behavior using bending and shear resistances calculated according to (EN_1993-1-5, 2006) and bending and shear resistances calculated numerically*

### 1.3.4 Transverse bending moment according to (EN_1993-1-5, 2019), new draft

This draft of Eurocode suggests that the normal stresses that are induced by the shear force in the flange can be neglected for the design with reference to ultimate moment capacity $M_{Rd}$, regardless of the shear utilization ratio. However, these stresses should be considered in elastic analysis, e.g., in fatigue design (EN_1993-1-5, 2019).

An approximated equation for calculation of the transverse bending moment is suggested in case of the absence of detailed analysis as following:

$$M_{z,max} = \frac{V}{h_w}\frac{a_3}{2}(2a_1 + a_4)$$

V is the shear force in the analyzed cross section.

The shear flow and the approximated transverse moment are illustrated in Figure 1.26.
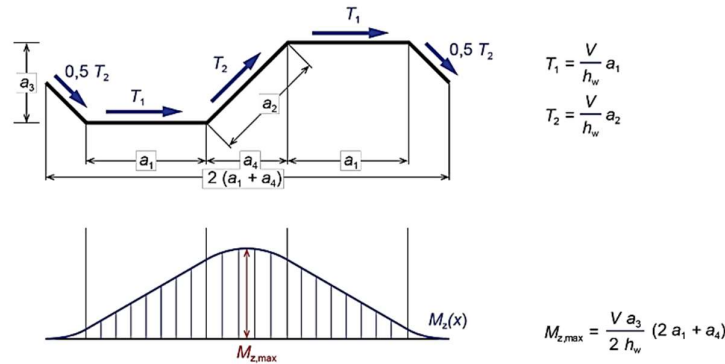


*Figure 1.26 Transverse actions due to shear flow introduction into the flange (EN_1993-1-5, 2019)*

### 1.3.5 Discussion and recommendations

It can be observed from the different studies that the transverse moment can have significant effect on the normal stress of the flanges for elastic response. The magnitude of additional normal stresses depends on the fold length, corrugation depth, the web height, and the girders support conditions. However, this effect is negligible in ultimate limit state.

In addition, the studies mentioned in this section are done on carbon steel. The magnitude of the transverse moment is not affected by the material but rather by the girder geometry, end supports, lateral supports and loading conditions. This, however, applies for carbon steel where it was proven that the effect of transverse bending is negligible in ultimate limit state and this attributes to the material plasticity and the stress redistribution. In case of high strength steel, on the other hand, the material behavior is different and the effect of transverse bending moment might be considerable. Thus, the same conclusion cannot be drawn for stainless steel and further investigation is desired.

### 1.4 Lateral torsional buckling

When a load is applied to a beam, it deflects vertically. The beam will also deflect out of the loading plane if it lacks sufficient lateral stiffness or lateral support along its length. The load that causes this buckling might be much lower than the beam's in-plane load bearing capacity. There will be no out-of-plane deformations in an assumed perfectly straight elastic beam until the applied moment exceeds the critical value, at which time the beam buckles by deflecting laterally and twisting. The applied moment creates a component torque about the deflected longitudinal axis, which causes the beam to deflect laterally (Denan et al., 2010).

The corrugated web girders are found to give higher resistance to lateral torsional buckling compared to flat web girders as the corrugation gives substantial transverse bending stiffness. This effect becomes stronger as the corrugation gets deeper (Denan et al., 2010).

The present section summarizes some of the previous findings on lateral torsional buckling resistance besides Eurocode design methods.

### 1.4.1 Lateral torsional buckling according to (EN_1993-1-5, 2006), current version

#### 1.4.1.1 Lateral torsional buckling for carbon steel

The out of plane buckling is considered in Eurocode by reducing the yielding moment capacity with reduction factor $\chi$ that is defined from Section 6.3 of EN1993-1-1.
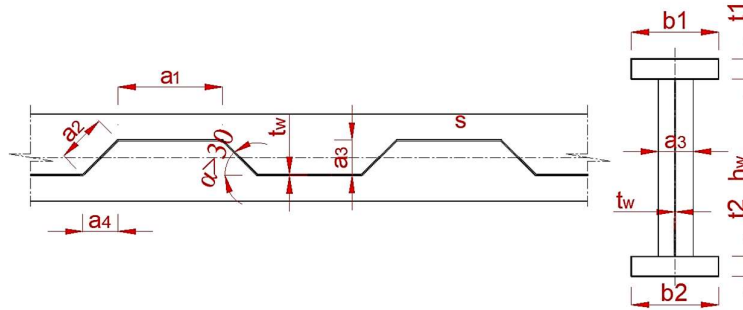


*Figure 1.27 Notations used for trapezoidal corrugated web*

The moment capacity for corrugated web girders with respect to lateral torsional buckling can be defined as following:

$$M_{y,Rd} = \underbrace{\frac{b_1 t_{f1} \chi f_{yf}}{\gamma_{M1}} \left( h_w + \frac{t_{f1} + t_{f2}}{2} \right)}_{\substack{\text{compression flange} \\ \text{for } \chi < 1.0}}$$

$b_1, t_{f1}, b_2, t_{f2}, h_w$ are illustrated in Figure 1.27.

For corrugated web beams, the reduction factor $\chi$ is advised in the same way as it is for flat web beams. For flat web beams, Eurocode gives an accurate approach for estimating lateral torsional buckling resistance as well as a simplified method that considers the flange as a compressed column.

The exact method, general case

This method is defined in Section 6.3.2.2 in (EN_1993-1-1, 2005).

The reduction factor $\chi$ due to lateral torsional buckling can be determined as follows:

$$\chi_{LT} = \frac{1}{\Phi_{LT} + \sqrt{\Phi_{LT}^2 - \bar{\lambda}_{LT}^2}} \text{ but } \chi_{LT} \leq 1,0$$

$$\text{where } \Phi_{LT} = 0,5\left[1 + \alpha_{LT}\left(\bar{\lambda}_{LT} - 0,2\right) + \bar{\lambda}_{LT}^2\right]$$

The relative slenderness is defined as following:

$$\bar{\lambda}_{LT} = \sqrt{\frac{W_y f_y}{M_{cr}}}$$

The imperfection factor $\alpha_{LT}$ can be determined from Table 6.3 in (EN_1993-1-1, 2005) and the appropriate buckling curve can be taken from Table 6.4 in (EN_1993-1-1, 2005).

$M_{cr}$ is the elastic critical moment for lateral-torsional buckling

$W_y$ is the section modulus

## The simplified method

This method is given in Section 6.3.2.4 in (EN_1993-1-1, 2005)

The reduction factor $\chi$ of the equivalent compression flange is determined as follows:

$$\chi = \frac{1}{\phi + \left[\phi^2 - \bar{\lambda}_f^{\,2}\right]^{0.5}} \leq 1$$

$$\text{where } \Phi = 0{,}5\left[1 + \alpha(\bar{\lambda}_f - 0{,}2) + \bar{\lambda}_f^{\,2}\right]$$

The relative slenderness for equivalent flange is defined as following:

$$\bar{\lambda}_f = \frac{k_c L_c}{i_{f,z}\lambda_1} \qquad \text{Eq. 6.59 (EN\_1993-1-1, 2005)}$$

$i_{f,z}$ is the radius of gyration of equivalent flange plus 1/3 of the compressed part of the web around the minor axis of the section.

$$i_{f,x} = \sqrt{\frac{I_{eff,f}}{A_{eff,f} + \frac{1}{3}A_{eff,w,c}}}$$

Where $\lambda_1 = \pi\sqrt{\dfrac{E}{f_y}} = 93{,}9\varepsilon \qquad and \qquad \varepsilon = \sqrt{\dfrac{235}{f_y}}$

$k_c$ is the slenderness correction factor for moment distribution between the restraints. It is given in Table 6.6 in (EN_1993-1-1, 2005)

If the slenderness of the compression flange satisfies $\bar{\lambda}_f \leq \bar{\lambda}_{c0}\dfrac{M_{c,Rd}}{M_{y.Ed}}$ the compression flange is not susceptible to lateral torsional buckling, $\chi = 1$.

Where $M_{y.Ed}$ is the design bending moment.

$M_{c,Rd}$ is moment resistance of the section $M_{c,Rd} = W_y\dfrac{f_y}{\gamma_M}$ with appropriate $W_y$ ; elastic or plastic or effective according to section class of the flange.

$\bar{\lambda}_{c0}$ is the slenderness limit $\bar{\lambda}_{c0} = \bar{\lambda}_{LT\cdot 0} + 0{,}1$

$\bar{\lambda}_{LT\cdot 0}= 0.4$ (maximum value) *Section 6.3.2.3, (EN_1993-1-1, 2005)*

The capacity should be magnified by factor $k_{fl}$ with recommended value of $k_{fl} = 1{,}10$

Curve d should be considered for welded section satisfies $\dfrac{h}{t_f} \leq 44\varepsilon$ and curve c for other sections

h is the overall height of the section

Same model is recommended for corrugated web girders. However, there is no formulation in Eurocode to estimate the elastic buckling moment so the simplified method would be more

relevant to be used noting that the web part considered in the equivalent compression flange should be disregarded in corrugated web girders due to accordion effect.

### 1.4.1.2 Lateral torsional buckling for stainless steel

For stainless steel <u>only the exact method</u> is provided in Eurocode to estimate lateral torsional buckling resistance of stainless-steel girders with flat web. It is defined in section 5.4.3 in (EN_1993-1-4, 2006) as following:

The reduction factor $\chi$ due to lateral torsional buckling can be determined as follows:

$$\chi_{LT} = \frac{1}{\Phi_{LT} + \sqrt{\Phi_{LT}^2 - \bar{\lambda}_{LT}^2}} \text{ but } \chi_{LT} \leq 1,0$$

$$\text{where } \Phi_{LT} = 0,5\left[1 + \alpha_{LT}(\bar{\lambda}_{LT} - 0,4) + \bar{\lambda}_{LT}^2\right]$$

The relative slenderness for equivalent flange is defined as following:

$$\bar{\lambda}_{LT} = \sqrt{\frac{W_y f_y}{M_{cr}}}$$

Whereas the imperfection factor is recommended as follows:

$\alpha_{LT} = 0.34$ for cold formed sections and hollow sections

$\alpha_{LT} = 0.76$ for welded open sections and other sections.

<u>The simplified model</u> in Eurocode to estimate lateral torsional buckling resistance is developed only for carbon steel and has not been updated for stainless steel. To use this method considering the flange as a column buckle around the minor axis of the girder, buckling curve d should be used stainless steel. Refer to Table 5.3 in (Amedment, 2021).

### 1.4.2 Lateral torsional buckling according to (Moon et al., 2009)

The lateral torsional buckling strength of an I-girder with corrugated webs is studied by Moon et al. (Moon et al., 2009) under uniform bending using finite element analysis. Firstly, the authors determined the location of shear center for corrugated web girders by moment equilibrium because it is essential to calculate the warping constant. The shear center (S) was found to be located at distance of 2d from the center of lower and upper flange, see Figure 1.28. Then it is assumed that the cross section to be composed of series of interconnected

plate elements. Each plate of length $L_{ij}$ and thickness $t_{ij}$ with two end points (i) and (j). An arbitrary path has been chosen to calculate the warping constant, see Figure 1.28.
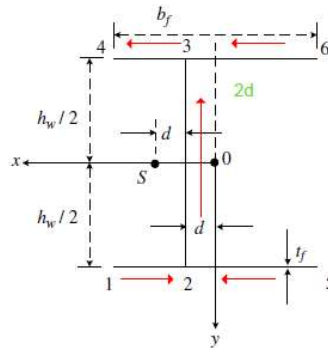


*Figure 1.28 Shear center location and the path used for warping constant calculation (Moon et al., 2009)*

The procedure to calculate the elastic buckling moment of corrugated web girders can be summarized as following:

1- Calculate the average corrugation depth:

$$d_{avg} = \frac{(2a+b)d_{max}}{2(a+b)}$$

The notations are illustrated in Figure 1.29
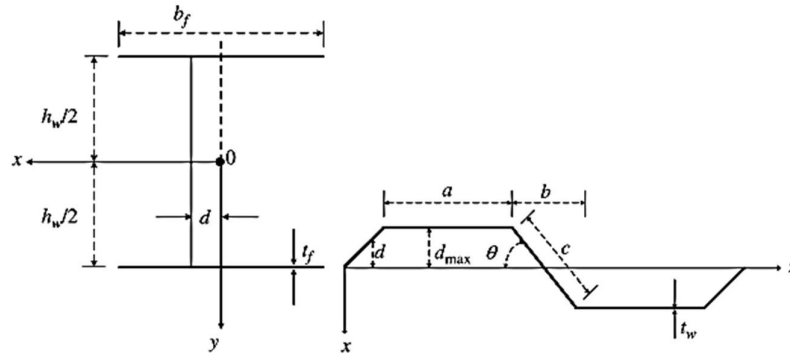


*Figure 1.29 Notations for corrugated web beams used in (Moon et al., 2009)*

2- Determine the normalized unit warping as following:

$$W_{n1} = \frac{2b_f^2 h_w t_f + b_f h_w^2 t_w}{8b_f t_f + 4h_w t_w}$$

$$W_{n2} = \frac{2b_f^2 h_w t_f + b_f h_w^2 t_w}{8b_f t_f + 4h_w t_w} - \left(\frac{b_f}{4} - \frac{d}{2}\right) h_w$$

$$W_{n3} = \frac{2b_f^2 h_w t_f + b_f h_w^2 t_w}{8b_f t_f + 4h_w t_w} - \left(\frac{b_f}{4} + \frac{d}{2}\right) h_w$$

$$W_{n4} = \frac{2b_f^2 h_w t_f + b_f h_w^2 t_w}{8b_f t_f + 4h_w t_w} - \frac{1}{2} b_f h_w$$

$$W_{n5} = W_{n4}$$

$$W_{n6} = W_{n1}$$

$$C_w = \frac{1}{3}\Sigma\left(W_{ni}^2 + W_{nj}W_{ni} + W_{nj}^2\right)t_{ij}L_{ij}$$

3- Determine the warping constant of corrugated web for all interconnected elements.
4- Determine the elastic lateral–torsional buckling moment of I-girder with corrugated webs as following:

$$M_{ocr} = \frac{\pi}{L}\sqrt{EI_{y,co}G_{co}J_{co}}\sqrt{1 + W^2}, \quad W = \frac{\pi}{L}\sqrt{\frac{EC_{w,co}}{G_{co}J_{co}}}$$

The shear modulus of corrugated web plated can be calculated as following:

$$G_{co} = \frac{a + b}{a + c}G$$

Where G is the shear modulus of flat plates.
The pure torsional constant can be defined as follows:

$$J_{co} = \frac{1}{3}\left(2b_f t_f^3 + h_w t_w^3\right)$$

The second moment of area around the weak axis is defined as follows:

$$I_{y,co} = \frac{t_f b_f^3}{6}$$

Later this <u>elastic</u> buckling moment is used by the authors to estimate the <u>inelastic</u> lateral-torsional buckling according to Eurocode as following:

$$\chi_{LT} = \frac{1}{\Phi_{LT} + \sqrt{\Phi_{LT}^2 - \lambda_{LT}^2}} \text{ but } \chi_{LT} \leqslant 1$$

$$\Phi_{LT} = 0.5[1 + \alpha_{LT}(\lambda_{LT} - 0.2) + \lambda_{LT}^2]$$

$$\lambda_{LT} = \sqrt{\frac{M_P}{M_{ocr}}}$$

According to Moon et al. study, the elastic buckling moment for corrugated web is higher than for flat web and the difference is more significant with increasing the corrugation depth (or corrugation angle), see Figure 1.30. In other words, for angles less than 45 degrees, where most practical cases can be found, there is almost no difference compared to flat web.

The pure torsional constant has been proven to be same for corrugated web and for flat web. However, for flat webs, the warping constant is lower, and the shear modulus is larger than for corrugated webs according the Moon et al. study, see Figure 1.31
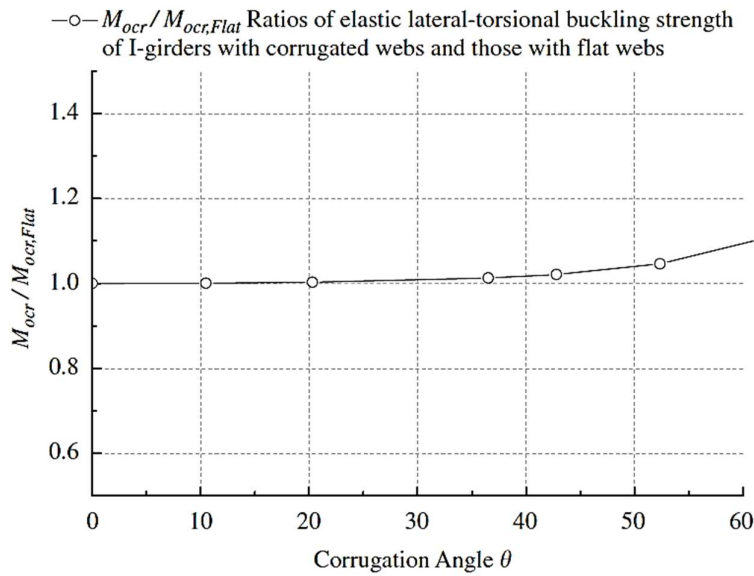


Figure 1.30 Variation in Mocr/Mocr, Flat with corrugation angle(Moon et al., 2009).
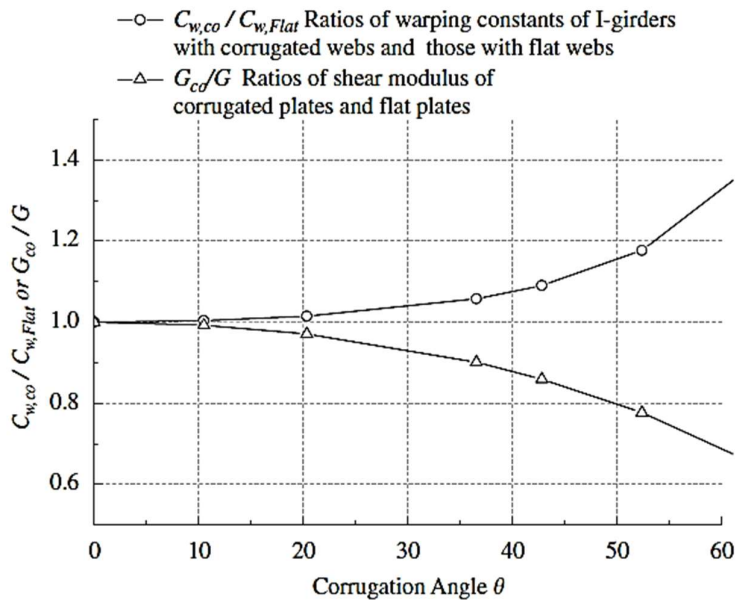


Figure 1.31 Variation of warping constant Cw,co/Cw,Flat and shear modulus Gco/G with corrugation angle (Moon et al., 2009)

### 1.4.3   Lateral torsional buckling according to (Nguyen et al., 2011)

A FEM program was created by Nguyen et al. in 2011 to investigate the moment modification factors of I-girder with trapezoidal web corrugations when subjected to a concentrated load. Different load positions; On top flange, on shear center and on bottom flange, and different end boundary conditions; Simply supported, warping fixed, lateral bending fixed and completely fixed, have been studied. See Figure 1.32.
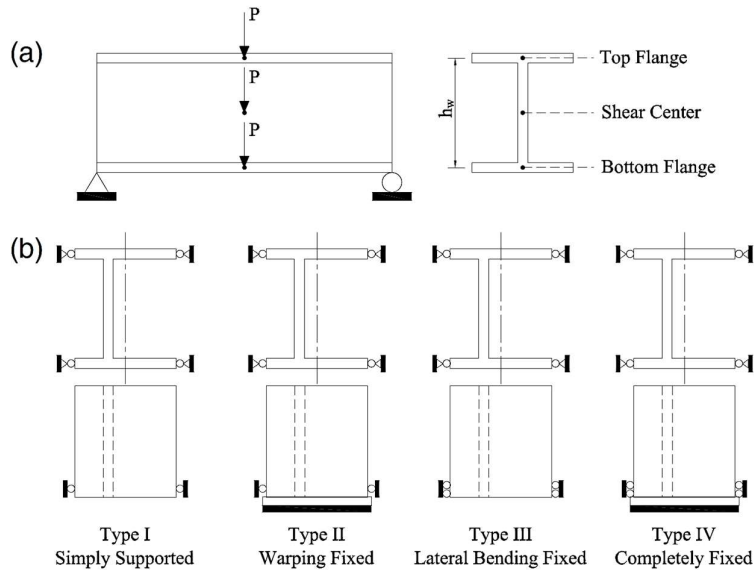
*Figure 1.32 (a) Position of concentrated load, (b) End restraint conditions (Nguyen et al., 2011).*

It has been proposed that the elastic lateral torsional buckling moment under uniform load may be defined for a simply supported I-girder with trapezoidal web corrugations that is restricted from lateral deflection and twisting at the supports but free to warp as following:

$$M_{ocr} = \frac{\pi}{L_b} \sqrt{EI_{y,c} G_c J_c} \sqrt{1 + W_c^2}$$

The beam parameter for corrugated beam girders can be calculated as following

$$W_c = \frac{\pi}{L_b} \sqrt{\frac{EC_{w.c}}{G_c J_c}}$$

The pure torsional constant for I-girder with corrugated web is the same for flat web and can be calculated as follows

$$J_c = \frac{2b_f t_f^3 + h_w t_w^3}{3}$$

The warping constant for corrugated web girders is defined as following

$$C_{w,c} = \frac{h_w^2 t_f b_f \left(6t_f b_f^3 + t_w h_w b_f^2 + 12d^2 t_w h_w\right)}{24\left(6t_f b_f + t_w h_w\right)}$$

The shear modulus for corrugated web girders is defined as following

$$G_c = \frac{a + b}{a + c} G$$

G is the shear modulus of flat plates

a is the longitudinal flat fold length

b is the projection of inclined fold length

c is the inclined fold length

d is the corrugation depth

This critical buckling moment then should be modified by factor $C_b$ which depends on the boundary conditions and the concentrated load position. The factor $C_b$ can be calculated as following:

$C_{b,c} = \frac{A_c}{B_c}$ for load on top flange

$C_{b,c} = A_c$ for load at shear center

$C_{b,c} = A_c * B_c$ for load at the bottom flange

The values for $A_c$ & $B_c$ can be taken from table.4 in the paper (Nguyen et al., 2011).

### 1.4.4   Lateral torsional buckling according to  (EN_1993-1-5, 2019), new draft

This draft, as for the current version, provides two methods to estimate the lateral torsional buckling resistance, the exact solution method and the simplified method. The two methods were adjusted in this draft and explained in this section.

The exact solution method

The out of plane buckling is considered by reducing the yielding moment capacity by reduction factor $\chi$ that can be defined from section 8.3 of (EN_1993-1-1, 2019).

The moment capacity with respect to lateral torsional buckling can be defined as following:

$$M_{y,Rd} = \underbrace{\frac{b_1 t_{f1} \chi f_{yf}}{\gamma_{M1}} \left( h_w + \frac{t_{f1} + t_{f2}}{2} \right)}_{\substack{\text{compression flange} \\ \text{for } x < 1.0}}$$

The relative slenderness for lateral torsional buckling  $\bar{\lambda}_{LT}$ should be taken as:

$$\bar{\lambda}_{LT} = \sqrt{\frac{M_{Rk}}{M_{cr}}}$$

$M_{cr}$ is the elastic critical moment for lateral torsional buckling

$M_{Rk}$ is the characteristic value of the resistance to bending detailed in Section 8.2.2.6 in (EN_1993-1-5, 2019)

$$M_{y,Rk} = W_y f_y$$
$$M_{z,Rk} = W_z f_y$$

$W_y, W_z$ follow the section class of the flange. See Table 1.8

*Table 1.8 Section properties according to the class of the cross-section, table 8.1 EN1993-1-1, 2019*

| Class | 1 | 2 | 3 | 4 |
|---|---|---|---|---|
| Section area $A_i$ | $A$ | $A$ | $A$ | $A_{eff}$ |

| | | | | |
|---|---|---|---|---|
| Section modulus $W_y$ | $W_{pl,y}$ | $W_{pl,y}$ | $W_{el,y}^{a,b}$ | $W_{eff,y}$ [b] |
| Section modulus $W_z$ | $W_{pl,z}$ | $W_{pl,z}$ | $W_{el,z}^{a,b}$ | $W_{eff,z}$ [b] |

The reduction factor for doubly symmetric I and H sections and fork boundary condition on both ends is defined as following
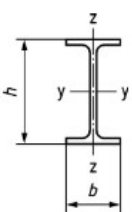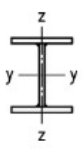
$$\chi_{LT} = \frac{f_M}{\Phi_{LT} + \sqrt{\Phi_{LT}^2 - f_M \bar{\lambda}_{LT}^2}} \qquad \text{but} \qquad \chi_{LT} \leq 1,0$$

Where:

$$\phi_{LT} = 0,5 \left[ 1 + f_M \left( \left( \frac{\bar{\lambda}_{LT}}{\bar{\lambda}_z} \right)^2 \alpha_{LT}(\bar{\lambda}_z - 0,2) + \bar{\lambda}_{LT}^2 \right) \right]$$

$\alpha_{LT}$ is the imperfection factor corresponding to the appropriate buckling curve (which differs from the previous version of Eurocode) can be taken from Table 8.5 in the new draft (EN_1993-1-1, 2019). See Table 1.9.

*Table 1.9 Imperfection factor $\alpha_{LT}$ for lateral torsional buckling of doubly symmetric I- and H-sections, (EN_1993-1-1, 2019)*

| Cross-section | | | Limits | | $\alpha_{LT}$ |
|---|---|---|---|---|---|
| Rolled I-sections |  | $h/b > 1,2$ | $t_f \leq 40$ mm | $0,12 \sqrt{\dfrac{W_{el,y}}{W_{el,z}}}$ but: $\alpha_{LT} \leq 0,34$ |
| | | | $t_f > 40$ mm | $0,16 \sqrt{\dfrac{W_{el,y}}{W_{el,z}}}$ but: $\alpha_{LT} \leq 0,49$ |
| | | $h/b \leq 1,2$ | — | $0,16 \sqrt{\dfrac{W_{el,y}}{W_{el,z}}}$ but: $\alpha_{LT} \leq 0,49$ |
| Welded I-sections |  | | $t_f \leq 40$ mm | $0,21 \sqrt{\dfrac{W_{el,y}}{W_{el,z}}}$ but: $\alpha_{LT} \leq 0,64$ |
| | | | $t_f > 40$ mm | $0,25 \sqrt{\dfrac{W_{el,y}}{W_{el,z}}}$ but: $\alpha_{LT} \leq 0,76$ |

$f_M$ is factor that accounts for the effect of the bending moment distribution between discrete lateral constraints. In cases when the diagrams in Table 8.6 (EN_1993-1-5, 2019) cannot be estimated, it can be conservatively assumed as 1. See Table 1.10.

*Table 1.10 Moment distribution factor, EN1993-1-1, 2019*

| Load case | Factor $f_M$ | Factor $k_c$ |
|---|---|---|
| $M =$ uniform | 1,00 | 1,00 |
| $M$ ⬚ $\psi M$   $-1 \le \psi \le +1$ | $1,25 - 0,1\,\psi - 0,15\psi^2$ | $\dfrac{1}{1,33 - 0,33\psi}$ |
| � | 1,05 | 0,94 |
| $M_h$ ⬚ $M_0$ $M_h$ ⬚ $M_0$ | For $0 \le \dfrac{M_0}{M_h} < 2,0$: $1,0 + 1,35\dfrac{M_0}{M_h} - 0,33\left(\dfrac{M_0}{M_h}\right)^3$  For $\dfrac{M_0}{M_h} \ge 2$: 1,05 | $\dfrac{M_0}{M_h} < 1,0$: 1,00  $\dfrac{M_0}{M_h} \ge 1,0$: 0,90 |
| $M_h$ ⬚ $M_0$ | For $0 \le \dfrac{M_0}{M_h} < 1,47$: $1,25 + 0,5\left(\dfrac{M_0}{M_h}\right)^2 - 0,275\left(\dfrac{M_0}{M_h}\right)^4$  For $\dfrac{M_0}{M_h} \ge 1,47$: 1,05 | $\dfrac{M_0}{M_h} < 0,5$: 0,75  $\dfrac{M_0}{M_h} \ge 0,5$: 0,91 |
| ⬇triangle | 1,10 | 0,86 |
| $M_h$ ⬚ $M_0$ $M_h$ ⬚ $M_0$ | For $0 \le \dfrac{M_0}{M_h} < 2,0$: $1,0 + 1,25\dfrac{M_0}{M_h} - 0,30\left(\dfrac{M_0}{M_h}\right)^3$  For $\dfrac{M_0}{M_h} \ge 2,0$: 1,10 | $\dfrac{M_0}{M_h} < 1,0$: 1,00  $\dfrac{M_0}{M_h} \ge 1,0$: 0,77 |

$\bar{\lambda}_z$ is the relative slenderness for weak axis flexural buckling, as defined in 8.3.1.2, with the buckling length $L_{cr,z}$ between the lateral restraints.

$$\bar{\lambda} = \frac{L_{cr}}{i}\frac{1}{\lambda_1} \quad for\ Class\ 1,2\ and\ 3$$

$$\bar{\lambda} = \frac{L_{cr}\sqrt{\dfrac{A_{eff}}{A}}}{i}\frac{1}{\lambda_1} \quad for\ class\ 4$$

$$\lambda_1 = \pi\sqrt{\frac{E}{f_y}} = 93,9\varepsilon$$

i is the radius of gyration around the relevant axis considering the gross cross section.

$L_{cr}$ is the buckling length in the considered plane.

The elastic critical buckling moment

Eurocode does not provide a formula to calculate the critical buckling moment for corrugated web girders. However, the modified version of Linder provide a good estimation of the critical buckling moment (EDVARDSSON, 2014). This formulation, suggested by Larsson & Persson (LARSSON & PERSSON, 2013), considers the effect of corrugation by additional part $\frac{c_w}{G}$ to the torsional constant of flat web beams instead of additional part $c_w\frac{L^2}{E\pi^2}$ suggested by Linder to be added to the warping constant of flat web beams.

For a laterally unrestrained beam, the critical buckling moment is defined as following:

$$M_{Cr} = \frac{\pi^2 E I_z}{L^2} \sqrt{\frac{I_w}{I_z} + \frac{L^2}{\pi^2 E I_z}(G I_t + c_w)}$$

The moment of inertia about the weak axis $I_z$, the warping constant $I_w$ and the torsion constant $I_t$ can be calculated using the same expressions as for girders with flat webs.

The contribution of the web to the moment of inertia around the weak axis can be neglected and can be defined as following:

$$I_z = 2 \cdot \frac{t_f b_f^3}{12}$$

The torsion constant can be calculated according to the following equation:

$$I_t = \frac{1}{3}(b_{f1} t_{f1}^3 + b_{f2} t_{f2}^3 + h_w t_w^3)$$

The warping constant for doubly symmetric I-profiles is defined as following:

$$I_w = \frac{I_z(h - t_f)^2}{4}$$

The larger torsion constant $c_w$ obtained for girders with corrugated webs is attributed to the larger critical lateral-torsional buckling moment achieved. The torsion constant can be obtained as following:

$$c_w = \frac{(2d)^2 h_w^2}{8 u_x (a + b)}$$

$$\text{Where } u_x = \frac{h_w}{2 G a t_w} + \frac{h_w^2 (a+b)^3}{25 a^2 E b_f t_f^3}$$

The notations are illustrated in Figure 1.29.

The simplified method for beams with restraints in building

This method is summarized in Section 8.3.2.4 (EN_1993-1-1, 2019). The design buckling resistance $M_{\mathrm{b,Rd}}$ can be calculated based on the flexural buckling resistance of the equivalent compression flange and should satisfy $\frac{M_{\mathrm{Ed}}}{M_{\mathrm{b,Rd}}} \leq 1{,}0$.

The equivalent compression flange's relative slenderness should be determined as follows:

$$\bar{\lambda}_{\mathrm{c,z}} = \sqrt{\frac{A_c f_y}{N_{\mathrm{cr,c,z}}}} \qquad \textit{Eq.8.85 (EN\_1993-1-5, 2019)}$$

$$A_c = \begin{cases} A_f + \frac{1}{2} \cdot A_w & \textit{for load applied at the compression flange} \\ A_f + \frac{1}{6} \cdot A_w & \textit{for load applied at the shear center} \\ A_f & \textit{for load applied at the tension flange} \end{cases}$$

$A_f$ is the area of compression flange $A_f = b_f t_f$

$A_w$ is the total area of the web $A_w = h_w t_w$

$N_{cr,c,z}$ is elastic critical axial force of the equivalent compression flange for weak axis buckling of the section

$$N_{cr,c,z} = \frac{\pi^2 \cdot E \cdot I_{c,z}}{L_{cr}^2}$$

$I_{c,z}$ is the moment of inertia around the strong axis of the equivalent compression flange.

$L_{cr}$ is the length between the lateral restraints.

The modified relative slenderness of the equivalent compression flange is defined as follows:

$$\bar{\lambda}_{c,z,mod} = k_c \cdot \beta_c \cdot \bar{\lambda}_{c,z}$$

Where:

$$\beta_c = \sqrt{\frac{0,06\dfrac{h}{t_{f,max}}}{\lambda_{c,z} + \dfrac{t_{f,max}}{t_{f,min}}}} \text{ but } \beta_c \leq 2$$

$k_c$ is correction factor for moment distribution. See Table 1.10.

$t_{f,max}$ is maximum thickness of top and bottom flange of the section.

$t_{f,min}$ is minimum thickness of top and bottom flange of the section.

The reduction factor due to lateral torsional buckling is defined as follows:

$$\chi_{LT} = \frac{1}{\phi_{LT} + \left(\phi_{LT}^2 - \bar{\lambda}_{c,z,mod}^2\right)^{0.5}}$$

$$\phi_{LT} = 0.5 \cdot \left[1 + \alpha_{LT} \cdot (\bar{\lambda}_{c,z,mod} - 0.2) + \bar{\lambda}_{c,z,mod}^2\right]$$

For $\alpha_{LT}$ buckling curve "c" should be taken for hot rolled sections and curve "d" for welded sections.

### 1.4.5 Some remarks and conclusions

The capacity against lateral torsional buckling is related to the elastic critical buckling moment. The elastic buckling moment has been studied by several authors and it was found that this moment varies depending on the bending moment diagram, boundary conditions, load application point and, of course, the geometric dimensions of the girder.

Regarding the geometric dimensions, it can be concluded from the previous mentioned studies that the elastic buckling moment for girders with corrugated webs does not show a significant increase (less than 5%) compared to that for flat web when the corrugation angles are less than 45 degrees.

Regarding the effect of lateral supports and load application point, it is concluded these factors has considerable effect on lateral torsional buckling resistance. To better understand this effect, one girder with different load position applications and different boundary

conditions is analyzed using the model proposed by (Nguyen et al., 2011). The studied girder's dimensions, the boundary condition effect and the load application effect are illustrated in Table 1.11, Figure 1.33, and Figure 1.34 respectively.

It can be seen that the capacity to lateral torsional buckling is largest when the load is applied on the tension flange followed by when load is applied at the shear center and the capacity is lowest when the load is applied at the compression flange. This considered in the newest version of Eurocode in the simple method of equivalent compression flange by the considered area $A_c$ in calculation of flange slenderness. The considered area is largest when the load applied on compression flange which increase in its turn increase equivalent flange relative slenderness.

Moreover, the lateral supports have considerable effect on the lateral torsional buckling resistance according to (Nguyen et al., 2011) and it can be seen that fixing the ends of the beam against warping would give considerable increase in terms of lateral torsional buckling moment.

*Table 1.11 Dimension of the girder considered*

| a1 [mm] | a3 [mm] | $\alpha$ [degree] | $t_w$ [mm] | $h_w$ [mm] | E [GPa] | $b_f$ [mm] | $t_f$ [mm] | $L_{cr}$ [m] |
|---|---|---|---|---|---|---|---|---|
| 80 | 43 | 32 | 4.2 | 1421 | 200 | 394 | 29 | 8 |
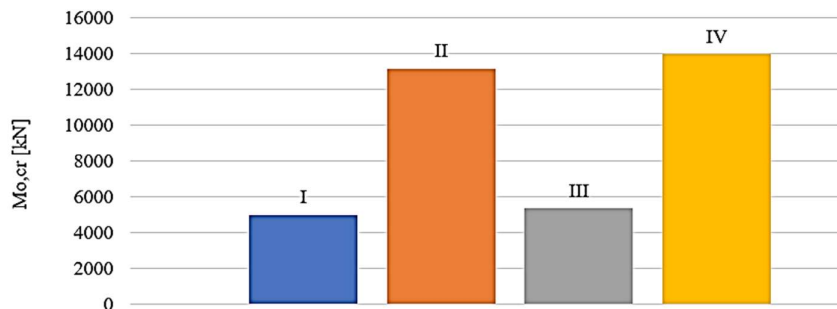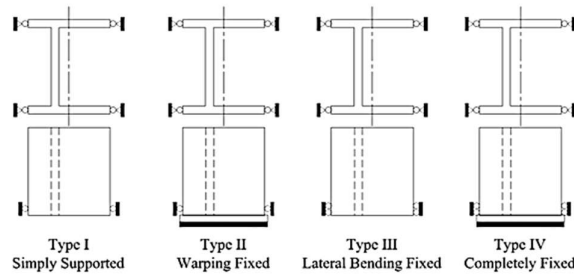




*Figure 1.33 Elastic critical buckling moment for different boundary conditions, the calculation according to (Nguyen, Han et al. 2011)*
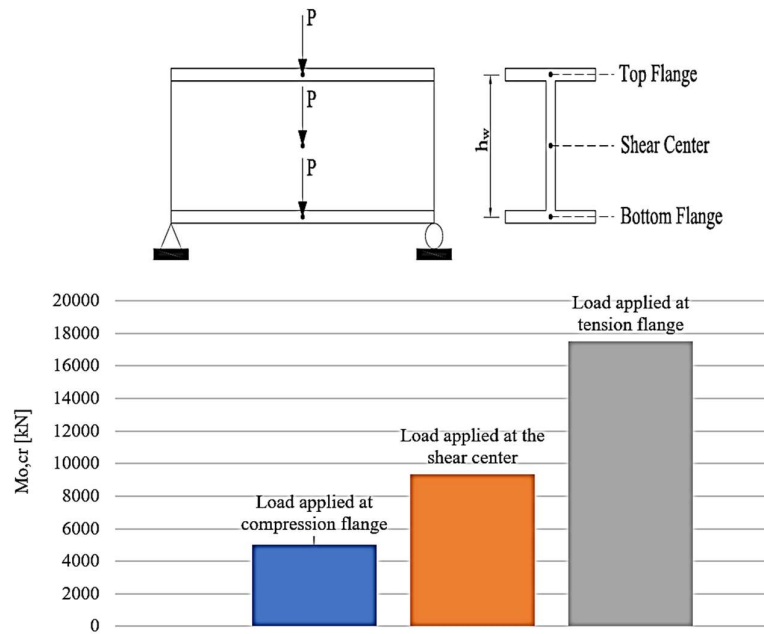
*Figure 1.34 Elastic critical buckling moment for different load application position, the calculation according to (Nguyen, Han et al. 2011)*

Regarding the inelastic resistance against lateral torsional buckling, Moon et al. conducted as study on two beams with two different corrugations. The dimensions of the studied beams are presented in Table 1.12.

*Table 1.12 Dimensions o analyzed girders by (Moon et al., 2009)*

| Model name | $a$ (mm) | $b$ (mm) | $d_{max}$ (mm) | $\theta$ (°) | $t_w$ (mm) | $h_w$ (mm) | $b_f$ (mm) | $t_f$ (mm) |
|---|---|---|---|---|---|---|---|---|
| C.P.1 | 180 | 140 | 50 | 35.5 | 8 | 1500 | 300 | 25 |
| C.P.2 | 330 | 270 | 100 | 36.5 | 12 | 2000 | 500 | 40 |

The beams were studied for perfect shapes, shape of first buckling mode with imperfection amplitude equal to L/1000 and shape of first buckling mode with imperfection amplitude equal to L/500. Then the lateral torsional slenderness was varied for each case and the results were plotted together with Eurocode buckling curve d, see Figure 1.35.

It was concluded that the method suggested by Eurocode is applicable and gives conservative results (Moon et al., 2009). However, this comparison has been done with curve d only. Moreover, the considered imperfection amplitudes (L/1000 and L/500) are less than Eurocode recommendation.
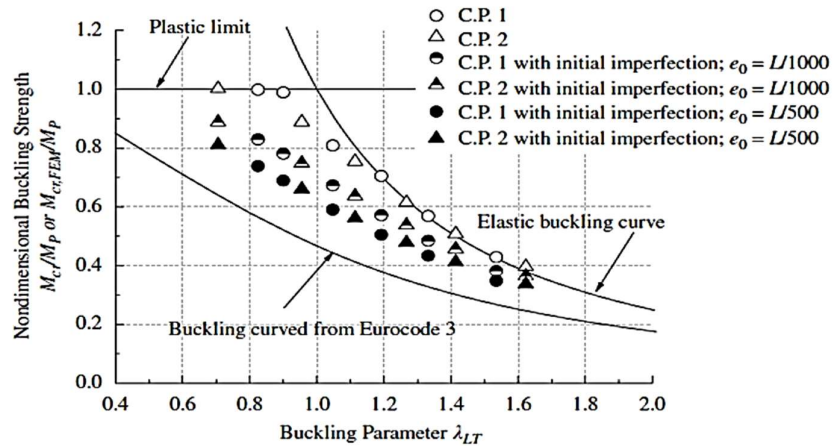
*Figure 1.35 Results of inelastic buckling from FEM, (Moon et al., 2009), $M_{cr}$ is calculated according to the equation suggested by Moon. $M_{cr,FEM}$ is the buckling moment obtained from the analysis (Moon et al., 2009).*

Eurocode recommendation for initial imperfection is given in Section 5.3.4 in (EN_1993-1-1, 2005). The initial imperfection that accounts for lateral torsional buckling for members in bending can be taken equal to:

$$k * e_{0,d}$$

Where $e_{0,d}$ is the initial bow imperfection of the weak axis of the considered profile. This factor is given in Table 5.1 in (EN_1993-1-1, 2005), see Table 1.13. The recommended value for k is 0.5. For buckling curve d in Eurocode, the initial imperfection should be taken as $0.5 * \frac{L}{100} = \frac{L}{200}$ for plastic analysis which is much larger that the amplitude considered by Moon.

*Table 1.13 Design values for initial local bow imperfection $e_0$, L is the member length.*

| Buckling curve acc. to Table 6.1 | elastic analysis | plastic analysis |
|---|---|---|
| | $e_0 / L$ | $e_0 / L$ |
| a$_0$ | 1 / 350 | 1 / 300 |
| a | 1 / 300 | 1 / 250 |
| b | 1 / 250 | 1 / 200 |
| c | 1 / 200 | 1 / 150 |
| d | 1 / 150 | 1 / 100 |

<u>Worth noting here</u> that a new draft of EN1993-1-5 (EN_1993-1-1, 2019) gives different recommendations for initial imperfection consideration. According to Section 7.3.3.2 in this draft, the initial imperfection that accounts for lateral torsional buckling or members in bending can be taken equal to:

$$e_{0,LT} = \beta_{LT}\frac{L}{\varepsilon}$$

Where $\beta_{LT}$ is the reference relative bow imperfection for lateral torsional buckling defined in Table7.2 in this draft, see Table 1.14.

$\varepsilon$ is the material parameter and $L$ is the member length.

*Table 1.14 Reference relative bow imperfection $\beta_{LT}$ for lateral torsional buckling*

| Cross-section | Condition | Elastic cross-section verification | Plastic cross-section verification |
|---|---|---|---|
| rolled | $h/b \leq 2{,}0$ | 1/250 | 1/200 |
| | $h/b > 2{,}0$ | 1/200 | 1/150 |
| welded | $h/b \leq 2{,}0$ | 1/200 | 1/150 |
| | $h/b > 2{,}0$ | 1/150 | 1/100 |

Another study regarding inelastic resistance against lateral torsional buckling were performed by (EDVARDSSON, 2014) in their master thesis at Chalmers. The authors performed a linear buckling analysis to see how restraints on the tension flange of a girder with corrugated web affect the lateral-torsional buckling resistance. It was concluded that the critical buckling moment may be estimated precisely using Modified Lindner's approach. This approach is a reformulation of the original approach but which adds the effect of corrugation to the torsion constant instead of warping constant giving same results as for the original approach (EDVARDSSON, 2014).

Furthermore, a nonlinear finite element analysis has been performed by (EDVARDSSON, 2014) and the results has been compared to Eurocode. It was concluded that the Eurocode 3 design model for lateral torsional buckling is conservatively applicable to restrained girders with corrugated web as for flat web.

### 1.4.6   Recommendations

It can be observed from the previous sections that the elastic lateral torsional buckling moment has been studied by several scholars. However, there is not enough studies on corrugated web girders' inelastic capability in terms of lateral torsional buckling. The same method as for flat webs is recommended by Eurocode. This appears to be a conservative estimation, given that corrugated web girders have been shown to have a higher buckling moment.

Furthermore, all previous research has focused on carbon steel and to propose buckling curves for corrugated web girders for carbon steel, a parametric study of inelastic capacity is needed. Moreover, a study of this problem for stainless steel are later needed.

Versions EN1993-1-5, 2005 and EN1993-1-5, 2019 draft provide a simplified method to calculate the moment resistance of the equivalent flange considering it as a column with buckling length equal to the distance between the lateral supports. This method has been modified in the draft of the upcoming version of Eurocode (2019) in many aspects summarized as below:

1- Consideration of the location of load application relative to the shear center.
2- The section stiffness around the weak axis of the girder is considered by modifying the relative slenderness.
3- The imperfection factor $\alpha_{LT}$, considers in the new draft the ratio of section modulus around the weak and the strong axes of the girder.
4- No modification factor ($k_{fl}$=1.1) is considered in 2019.

The simplified method of the new draft yields more conservative results compared to the method in the current version. This can be explained by the following attributes of the new proposed model:

1. Increase the slenderness by factor (βc).
2. No magnifying factor ($k_{fl}$).
1. The considered area from the web can also affect for case of flat web, increase Ac would increase slenderness. However, for corrugated webs, the web is disregarded.

## 2    Resistance to shear force

The research on shear buckling resistance of corrugated web beams began in 1969. Numerous studies have been conducted. Shear buckling was found to be the most common cause of failure for girders with corrugated webs under shear loading. Three shear buckling modes has been observed from the previous tests: local, global, and interactive buckling.

The current edition of Eurocode provides a design model to estimate the shear capacity of corrugated web beams. Local and global buckling modes are included separately in this model while the interactive buckling mode is not considered. The other researchers, on the other hand, were concentrating on describing the interaction between the local and global buckling modes in order to predict the shear resistance of corrugated web beams.

In this section the three shear buckling shapes are presented, followed by a compilation of the current edition of the EN1993-1- 5 design model for shear buckling as well as various models extracted from the literature. Moreover, the most influential parameters on shear buckling resistance, such as the initial imperfection and other geometric parameters, are addressed. Furthermore, a comparison between Eurocode design model and several other models has been performed based on previous experiments on corrugated web beams of carbon steel. Finally, the same comparison is repeated for the tested girders of stainless-steel in the SUNLIGHT project.

### 2.1    Shear buckling mode shapes

Shear failure of corrugated web girders may occur in three different shapes; local buckling mode where the buckling occurs in one-fold, global buckling mode where the buckling extends over many folds extended over the web height, and the interactive buckling mode where the buckling extends over few folds. The three different modes are illustrated in Figure 2.1.
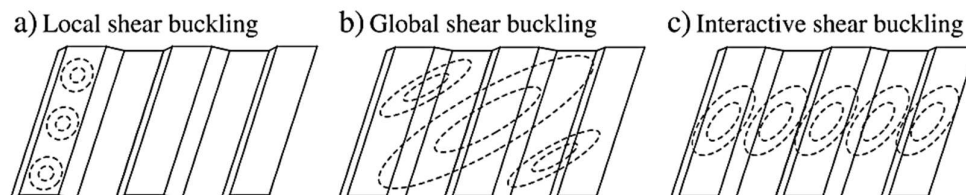


*Figure 2.1 Three different shear buckling modes of trapezoidal corrugated steel webs  (Jian-Guo Nie & Mu-Xuan Tao, 2013)*

## 2.2 Resistance to shear force according to (EN_1993-1-5, 2006), current version

### 2.2.1 Resistance to shear force for carbon steel
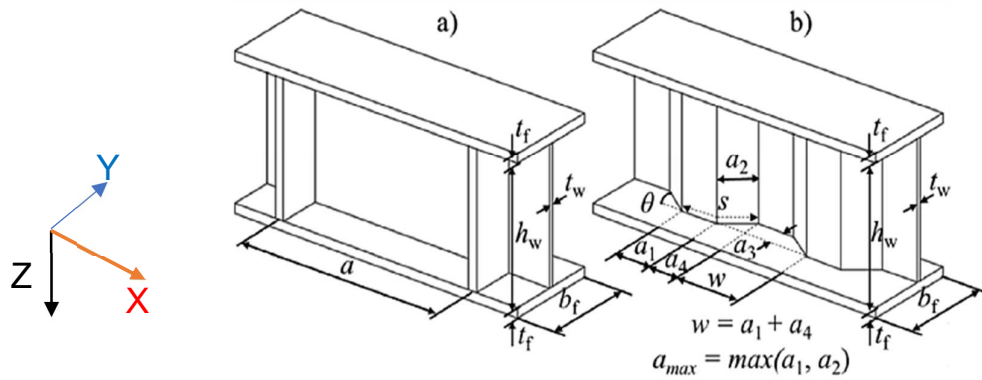


*Figure 2.2 Geometric notations of a. Flat web b. Corrugated web, (Kollár & Kövesdi, 2019)*

The shear buckling resistance of corrugated web girders is defined in Annex D in (EN_1993-1-5, 2006) as follows:

$$V_{bw,Rd} = \frac{\chi_c f_{yw} h_w t_w}{\sqrt{3}\gamma_{M1}}$$

The interactive buckling mode is neglected in Eurocode and the reduction factor is taken as minimum between local and global reduction factors as following:

$$\chi_c = min(\chi_{c,l}, \chi_{c,g})$$

The local slenderness is defined as follows:

$$\bar{\lambda}_{c,l} = \sqrt{\frac{f_{yw}}{\sqrt{3}\tau_{cr,l}}}$$

The local reduction factor is defined as follows:

$$\chi_{c,\ell} = \frac{1{,}15}{0{,}9 + \bar{\lambda}_{c,\ell}} \le 1{,}0$$

Where global slenderness is calculated as follows:

$$\bar{\lambda}_{c,g} = \sqrt{\frac{f_{yw}}{\tau_{cr,g}\sqrt{3}}}$$

The global reduction factor is defined as follows:

$$\chi_{c,g} = \frac{1.5}{0.5 + \bar{\lambda}_{c,g}^2} \le 1.0$$

The critical local shear stress where isotropic buckling plate theory is used is defined as follows:

$$\tau_{cr,\ell} = 4{,}83E\left[\frac{t_w}{a_{max}}\right]^2$$

The critical global shear stress where orthotropic buckling plate theory is used, the plates that are assumed to be hinges at the edges, is defined as follows:

$$\tau_{cr,g} = \frac{32{,}4}{t_w h_w^2} \sqrt[4]{D_x D_z^3}$$

The longitudinal bending stiffness per unit length is defined as follows:

$$D_x = \frac{Et_w^3}{12(1-v^2)}\frac{w}{s}$$

Where w is the length of one-half wave.

s is the unfolded length of one-half wave.

The transverse bending stiffness per unit length is defined as follows

$$D_z = \frac{EI_z}{w} = \frac{E \cdot t_w a_3^2}{12} \cdot \frac{3 \cdot a_1 + a_2}{a_1 + a_4}$$

$I_z$ is the second moment of area of one corrugation of length w around Z-axis as illustrated in Figure 2.2.

The buckling curve for shear buckling of corrugated web girders according to Eurocode is illustrated in Figure 2.3.
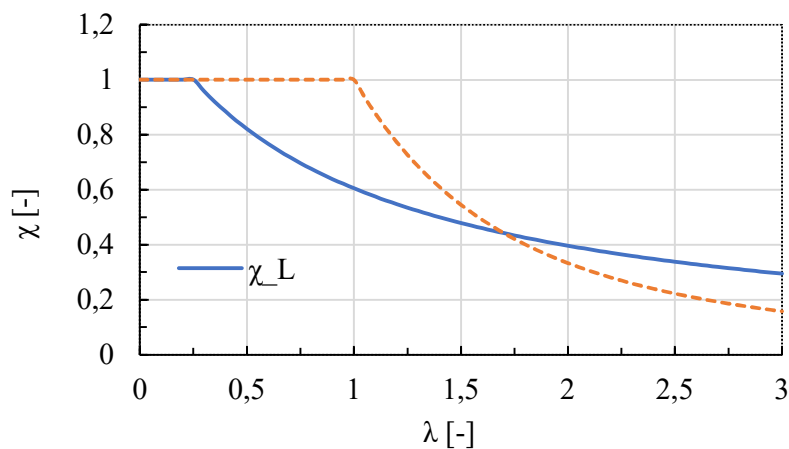


*Figure 2.3 Shear Buckling Curves according to EN1993-1-5*

### 2.2.2  Resistance to shear force for stainless steel

The design model for the shear strength of corrugated web girders in Eurocode is developed for carbon steel and has not been updated to stainless steel. Therefore, the shear capacity of a corrugated web girder in stainless steel can be checked based on the above-mentioned model

but with specific material coefficients and partial factors for stainless steel as in Table 1.2 and Table 1.3 until further research is done.

## 2.3 Resistance to shear force according to (Driver et al., 2006)

According to (Driver et al., 2006), the stress strain behavior, the residual stresses induced by fabrication and geometric imperfections are expected to be different for thin sheets material and plate material used in real bridges than that for small scale beams. For that reason, Driver et al., in 2006, have performed two large scale tests (G7A and G8A), with similar scale to the ones used in real bridges.

The authors suggested that when the elastic shear buckling stress become larger than 80% of shear yield stress, the critical buckling stress can be considered as inelastic buckling and can be taken from the following equation (Eq.4 in Figure 2.5):

$$(\tau_{cr})_{inel} = \sqrt{0.8\tau_y(\tau_{cr})_{el}} \leqslant \tau_y$$

Where $(\tau_{cr})_{el} = (\tau_{cr,L})_{el}$ in case of local buckling stress and $(\tau_{cr})_{el} = (\tau_{cr,G})_{el}$ in case of global buckling stress.

For local buckling, the plate stability theory has been used to predict the local shear buckling stress of corrugated web girders. The elastic local buckling stress can be obtained from the following equation (Eq.1 in Figure 2.5):

$$(\tau_{cr,L})_{el} = k_L \frac{\pi^2 E}{12(1 - v^2)(w/t_w)^2}$$

$k_L$ is local shear buckling coefficient that depends on the boundary conditions and fold aspect ratio $\frac{w}{h_w}$

$w$ is maximum fold length $w = \max(b, c)$, see Figure 2.4.
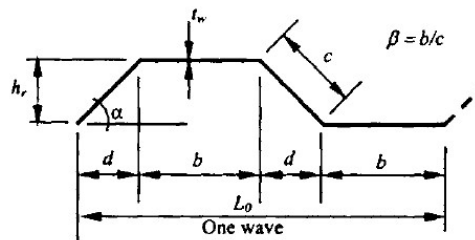


*Figure 2.4 Corrugation geometric notations, (Driver et al., 2006)*

For simply support edges, the local buckling coefficient, $k_L = 5.34$ and for fixed edges, $k_L = 8.98$

For global buckling, the corrugated web can be analyzed as orthotropic flat web with elastic buckling coefficient. The elastic global buckling stress is defined as follows:

$$\left(\tau_{cr,G}\right)_{el} = k_G \frac{E t_w^{\frac{1}{2}} b^{\frac{3}{2}}}{12 h_w^2} F(\alpha, \beta)$$

$F(\alpha, \beta)$ is a factor that considers the corrugation geometry, and it is defined as following:

$$F(\alpha, \beta) = \sqrt{\frac{(1+\beta)\sin^3\alpha}{\beta + \cos\alpha} \cdot \left\{\frac{3\beta + 1}{\beta^2(\beta + 1)}\right\}^{\frac{3}{4}}}$$

$\alpha$ is the corrugation angle

$\beta$ is the ratio between the longitudinal fold to the inclined fold

For simply support edges, the global buckling coefficient is $k_G = 31.6$ and for fixed edges, $k_G = 59$

Many previous test results together with the performed tests, where local buckling or yielding governed, have been plotted with the proposed equation for inelastic buckling stress and it was observed that the shear strength is overestimated by this equation for the webs with low slenderness values. See Figure 2.5. Thus, a new formula, Eq.10 in Figure 2.5, has been further suggested by the authors to estimate the shear strength of the girder taking the combination of local and global buckling as following:

$$\tau_n = \sqrt{\frac{\left(\tau_{cr,L} \cdot \tau_{cr,G}\right)^2}{\tau_{cr,L}^2 + \tau_{cr,G}^2}}$$

Where $\tau_{cr,L}$ and $\tau_{cr,G}$ are being calculated through equation

$$(\tau_{cr})_{inel} = \sqrt{0.8 \tau_y (\tau_{cr})_{el}} \leqslant \tau_y$$
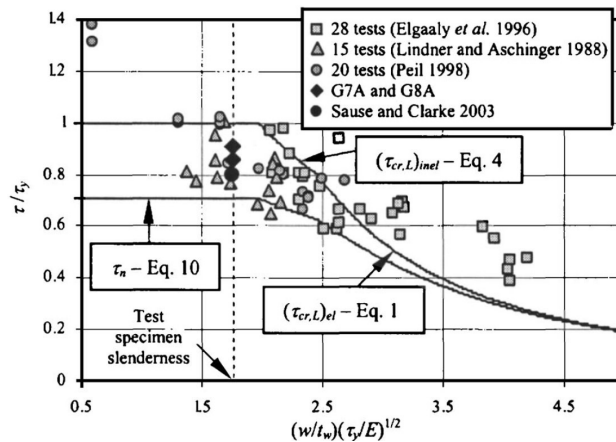


*Figure 2.5 Results of tests where local buckling or yielding governs, (Driver et al., 2006)*

It was also observed by Driver et al. that a significant loss in shear strength is accompanied with global buckling. Therefore, the authors recommended to prevent the global buckling by satisfying the following equation:

$$\frac{h_w}{t_w} \leqslant 1.91\psi \sqrt{\frac{E}{F_y}\left(\frac{b}{t_w}\right)^{1.5} F(\alpha, \beta)}$$

$\psi$ is set to 0.9 to provide safety for the design for global buckling strength

Then, the nominal shear strength can be determined based on only the local buckling according to the following equations:

$if \; \lambda_L \leqslant 2.586$

$$V_n = 0.707 \left(\frac{F_y}{\sqrt{3}}\right) h_w t_w$$

If $\; 2.586 < \lambda_L \leqslant 3.233$

$$V_n = \sqrt{\frac{1}{1 + 0.15\lambda_L^2}} \left(\frac{F_y}{\sqrt{3}}\right) h_w t_w$$

If $\lambda_L > 3.233$

$$V_n = \sqrt{\frac{1}{1 + 0.014\lambda_L^4}} \left(\frac{F_y}{\sqrt{3}}\right) h_w t_w$$

Where the normalized local buckling slenderness

$$\lambda_L = \frac{w}{t_w} \sqrt{\frac{F_y}{E}}$$

These equations are applicable when $\frac{b}{t_w}$ satisfy this condition:

$$\frac{b}{t_w} \leqslant 2.586 \sqrt{\frac{E}{F_y}}$$

b is the width of the longitudinal fold

<u>Imperfection sensitivity according to (Driver et al., 2006):</u>

An imperfection sensitivity analysis has also been conducted in this study. Firstly, the first buckling mode has been considered as imperfection shape and the amplitude has been taken as percentage of the web thickness (from 0% to 100% of $t_w$). It was concluded that the shear strength decreases with increasing the imperfection amplitude. See Figure 2.6.
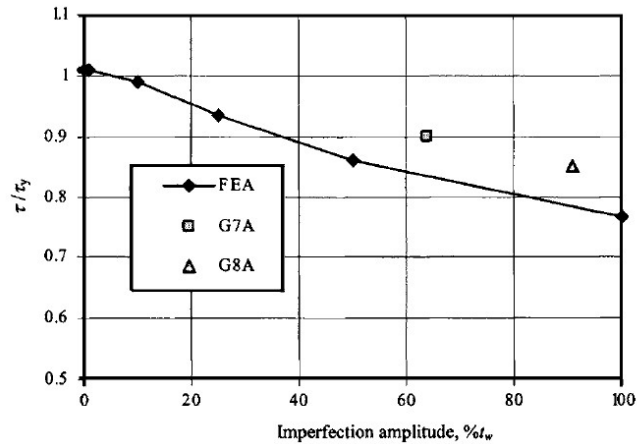
*Figure 2.6 Shear strength variation with imperfection amplitude (Driver et al., 2006)*

Secondly, the imperfection amplitude is kept to 100% of $t_w$ while the imperfection shape was taken from the various shear buckling modes revealed in the linear elastic buckling study. The shear stress capacity was found to rise with the mode number, with the first mode providing the most critical condition.

## 2.4 Resistance to shear force according to (Jiho Moon & Byung H. Choi, 2009)

A new design formula for shear buckling of corrugated web girders has been proposed by Moon. To validate the postulated formulae, several experimental studies were carried out (M12:M14) and a comparison of shear strength for the testes girders as well as some previous tests on shear buckling has been performed. It was concluded that the design shear buckling strength may be determined directly, without having to calculate local and global buckling separately, based on a first-order interactive buckling equation (Jiho Moon & Byung H. Choi, 2009)

The design model proposed by Moon et al. is illustrated in Figure 2.7 and can be summarized in the following steps:

1- Determine the shear slenderness

$$\lambda_s = 1.05 \cdot \sqrt{\frac{\tau_y}{k_I \cdot E}} \cdot \left(\frac{h_w}{t_w}\right)$$

$k_I$ is the interactive shear buckling coefficient that can be calculated as:

$$k_I = \frac{30.54}{5.34 \cdot \left(\frac{a_3}{t_w}\right)^{-1.5} + 5.72 \cdot \left(\frac{max(a_1, a_2)}{h_w}\right)^2}$$

2- Calculate the shear strength from the following equations, illustrated also in Figure 2.7. The proposed model considers material inelasticity, residual stress, and initial imperfections.

$$\text{if} \quad \lambda_s \leq 0.6 \qquad\qquad \frac{\tau_{cr}}{\tau_y} = 1$$

$$\text{if} \quad \sqrt{2} \geq \lambda_s \geq 0.6 \qquad \frac{\tau_{cr}}{\tau_y} = 1 - 0.614 \cdot (\lambda_s - 0.6)$$

$$\text{if} \quad \sqrt{2} < \lambda_s \qquad\qquad \frac{\tau_{cr}}{\tau_y} = \frac{1}{\lambda_s^2}$$

Where $\tau_{cr}$ is the shear buckling stress and $\tau_y$ is the shear yield stress.
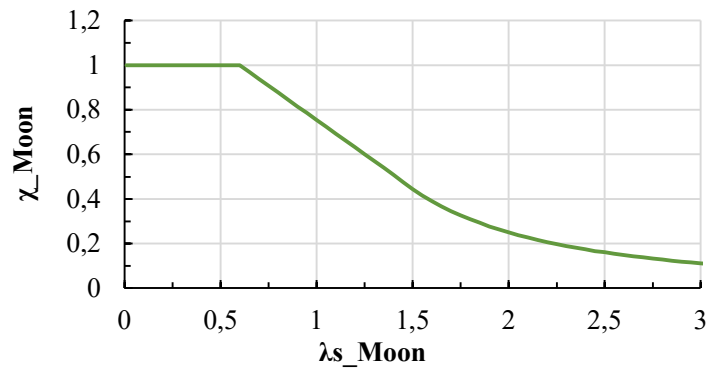


*Figure 2.7 Shear buckling curve according to Moon*

It is also recommended by Moon that to maximize the shear buckling strength of corrugated web girders, the shear slenderness should be kept less than 0.6 and that can be achieved by satisfying the following equation:

$$1.10 \left[ \frac{5.34(d/t_w)^{-1.5}(h_w/t_w)^2 + 5.72(w/t_w)^2}{30.54} \right] \frac{\tau_y}{E} \leq 0.36$$

## 2.5   Resistance to shear force according to (Richard Sause & Braxtan, 2011)

Sause and Braxtan, in 2011, have collected more than 100 test results from previous studies, categorized and analyzed based on test specimen parameters. Based on these test results they suggested a new equation to determine the ultimate shear strength for bridge girders with corrugated webs. The suggested formula doesn't include the test data where the shear strength is controlled by global elastic buckling. Moreover, this formula does not evaluate whether the corrugated webs tend to reach yielding as the girder become stocky. It was derived theoretically and not verified by previous test data where $\lambda_G$ and $\lambda_L$ are less than 0.6 (stocky girders) (Richard Sause & Braxtan, 2011).

The design model proposed by Sause and Braxtan is illustrated in Figure 2.8 and the procedure to estimate the shear buckling strength can be summarized as following:

The interactive buckling stress is defined as follows:

$$\tau_{n,S,3} = \tau_y \left( \frac{1}{(\lambda_{I,3})^6 + 2} \right)^{1/3}$$

The interactive slenderness $\lambda_{I,3}$ parameter to be estimated using an interactive order of n = 3 as follows:

$$\lambda_{I,n} = \lambda_L \lambda_G \left( \left( \frac{1}{\lambda_L} \right)^{2n} + \left( \frac{1}{\lambda_G} \right)^{2n} \right)^{1/2n}$$

The local buckling slenderness is defined as follows:

$$\lambda_L = \sqrt{\frac{12(1 - v^2)\tau_y}{k_L \pi^2 E}} \frac{w}{t_w}$$

The global buckling slenderness is defined as follows:

$$\lambda_G = \sqrt{\frac{12h_w^2 \tau_y}{k_G F(\alpha, \beta) E t_w^{0.5} b^{1.5}}}$$

The geometric factor is defined as follows:

$$F_{\alpha,\beta} = \sqrt{\frac{(1 + \beta) \cdot \sin(\alpha_c)^3}{\beta + \cos(\alpha_c)} \cdot \left( \frac{3 \cdot \beta + 1}{\beta^2 \cdot (\beta + 1)} \right)^{3/4}}$$

$\beta$ is the ratio between the longitudinal fold to the inclined fold

$\alpha_c$ is the corrugation angle
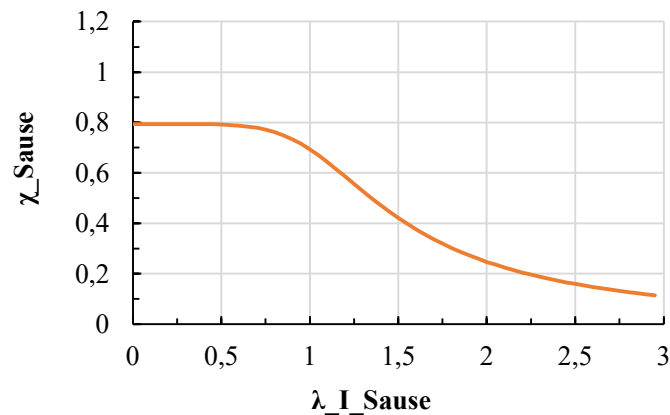


*Figure 2.8 Shear buckling curve according to Sause & Braxtan*

## 2.6   Resistance to shear force according to (Hassanein & Kharoob, 2013)

In 2013, Hassanein and Kharoob conducted a numerical parametric study to assess the real behavior at the intersection of the corrugated web and the flanges. The juncture was considered simple when $\frac{t_f}{t_w} < 3$ and fixed when $\frac{t_f}{t_w} > 3$.

The authors performed their parametric study on the following range (same notations as in Figure 2.4):

1. Corrugation depth-to-web thickness ratio (hr/tw); (9.72-29.17).

2. Web flat panel width-to-depth ratio (b/hw); (0.135–0.325).

3. Aspect ratio of the web panel (a/hw); (1.0–2.4).

4. Web plate slenderness (hw/tw); (56–400).

5. Flange thickness-to-web thickness ratio (tf/tw).

The results were compared to many previous design models on shear buckling of corrugated web beams. It was revealed that the 1st-order interactive buckling strength design model, as proposed by Sause and Braxtan (Richard Sause & Braxtan, 2011), is adequate for corrugated webs with simple junction, but it is unconservative for corrugated webs with fixed juncture. Thus, for the case of a fixed junction, a new interactive shear buckling strength formula was proposed by (Hassanein & Kharoob, 2013) as following:

The local buckling stress is defined as follows:

$$\tau_{cr.L} = k_L \cdot \frac{\pi^2 \cdot E}{12 \cdot (1 - \nu^2)} \cdot \left(\frac{t_w}{a_{max}}\right)^2$$

The local buckling coefficient is defined as follows:

$$k_L = 5.34 + 4 \cdot \left(\frac{a_{max}}{h_w}\right)^2$$

The global buckling stress is defined as follows:

$$\tau_{cr.G} = k_G \cdot \frac{D_x^{0.25} \cdot D_y^{0.75}}{t_w \cdot h_w^2}$$

The global buckling coefficient is defined as following:

$$k_G = 31.6$$

The interactive buckling stress is defined as:

$$\tau_{cr.I} = \frac{\tau_{cr.L} \cdot \tau_{cr.G}}{(\tau_{cr.G}{}^n + \tau_{cr.L}{}^n)^{\frac{1}{n}}}$$

Where the interaction of order:

$$n = 0.6 \quad \text{where} \quad \frac{t_f}{t_w} > 3$$

The interactive slenderness $\lambda_{I,0.6}$ parameter to be estimated using an interactive order of n = 0.6 as follows:

$$\lambda_{I,n} = \lambda_L \lambda_G \left(\left(\frac{1}{\lambda_L}\right)^{2n} + \left(\frac{1}{\lambda_G}\right)^{2n}\right)^{1/2n}$$

Then the shear buckling resistance is defined as follows:

$$\tau_n = \tau_y \times \left(\frac{1}{\left(\lambda_{I,0.6}\right)^6 + 2}\right)^{1/3}$$

Recently, in 2022, (Deng et al., 2022) performed an experimental program on a small-size girders with corrugated webs. Moreover, the authors performed a similar parametric study to that done by (Hassanein & Kharoob, 2013). However, the studied ranges for the most influencing parameters were wider and only fixed juncture is considered. Besides, the flanges are kept compact to avoid flange deformation (by satisfying $0.5 b_f / t_f \leq 0.38 \sqrt{\frac{E}{F_y}}$ ). The considered parameters ranges are:

1. Corrugation depth-to-web thickness ratio (hr/tw); (7.5-60).

2. Web flat panel width-to-depth ratio (b/hw); (0.1-0.33).

3. Aspect ratio of the web panel (a/hw); (1.08-2.57).

4. Web plate slenderness (hw/tw); (66.7-500).

For girders with equal flat and inclined folds, Hassanien and Kharoob's previous model yields the best estimate for shear buckling strength, according to this research. The Moon design approach, on the other hand, provides a more accurate estimation of capacity for situations with different fold lengths  (Deng et al., 2022).

## 2.7    Resistance to shear force according to (Leblouba, Barakat, et al., 2017)

In 2017 Leblouba et al. have published two papers on shear behavior of corrugated web girders. In the first paper, "*Shear buckling and stress distribution in trapezoidal web corrugated steel beams*" (Leblouba, Junaid, et al., 2017), they have performed five tests, collected around 22 tests from literature, and compared different models for the design purpose of shear buckling of corrugated web girders against the tests data. The authors concluded that the design model in EN-1993-1-5 is accurate and conservative enough for an economic design. See Figure 2.9.

Furthermore, there has been some disagreement in the literature as to whether corrugated beams can approach shear yield strength. It was demonstrated in this work that stocky girders with corrugated webs may reach shear yield strength.
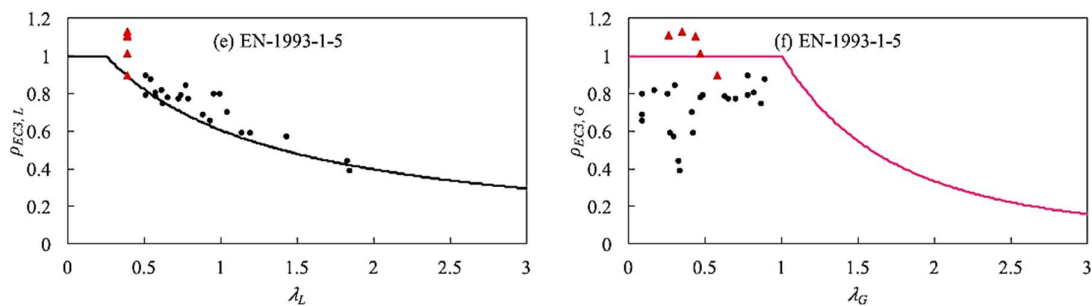


*Figure 2.9 Shear strength versus slenderness ratio compared with test data (27 tests),  (Leblouba, Junaid, et al., 2017)*

In the second paper "*Normalized shear strength of trapezoidal corrugated steel webs*",(Leblouba, Barakat, et al., 2017) they considered a larger range on experiments (around 125 experiments) and they suggested a new design model for interactive buckling based on Richard's equation which yielded in better results in comparison to the test data (only 5.6% of the 125 tests, the ratio $\rho_{M-1}/\rho_e$ were larger than one).

The shear buckling reduction factor according to Leblouba et al. can be defined as follows:

$$\rho_{M-1} = \frac{1}{\left(1 + \left(\frac{\lambda_{I.4}}{1.58}\right)^{1.6}\right)^{1.15}}$$

The interactive slenderness $\lambda_{I,4}$ parameter to be estimated using an interactive order of n = 4 as follows:

$$\lambda_{I,4} = \sqrt{\frac{\tau_y}{\tau_{I,4}}}$$

$$\tau_y = F_y/\sqrt{3}$$

$$\left(\frac{1}{\tau_{I,n}}\right)^n = \left(\frac{1}{\tau_L}\right)^n + \left(\frac{1}{\tau_G}\right)^n + \left(\frac{1}{\tau_y}\right)^n$$

The local buckling stress is defined as following:

$$\tau_L = k_L \frac{\pi^2 E}{12(1 - v^2)\left(\frac{w}{t_w}\right)}$$

$k_L$ is set to 5.38 for simply supported edges and to 8.98 for clamped edges.

The global buckling stress is defined as following:

$$\tau_G = k_G \frac{D_x^{\frac{3}{4}} D_y^{\frac{1}{4}}}{t_w h_w^2}$$

$k_G$ is set to 31.6 for simply supported edges and to 59 for clamped edges.

The longitudinal bending stiffness $D_x$ can be obtained from:

$$D_x = \frac{E}{b + d}\left(\frac{bt_w(d * \tan{(\theta)}^2)}{4} + \frac{t_w(d * \tan{(\theta)}^3)}{12\sin{(\theta)}}\right)$$

The transverse bending stiffness $D_y$ can be obtained from:

$$D_y = \frac{b + d}{b + d * \sec{(\theta)}} \frac{Et_w^3}{12}$$

The dimensional geometric properties $b, d, \theta$ are given in Figure 2.10.
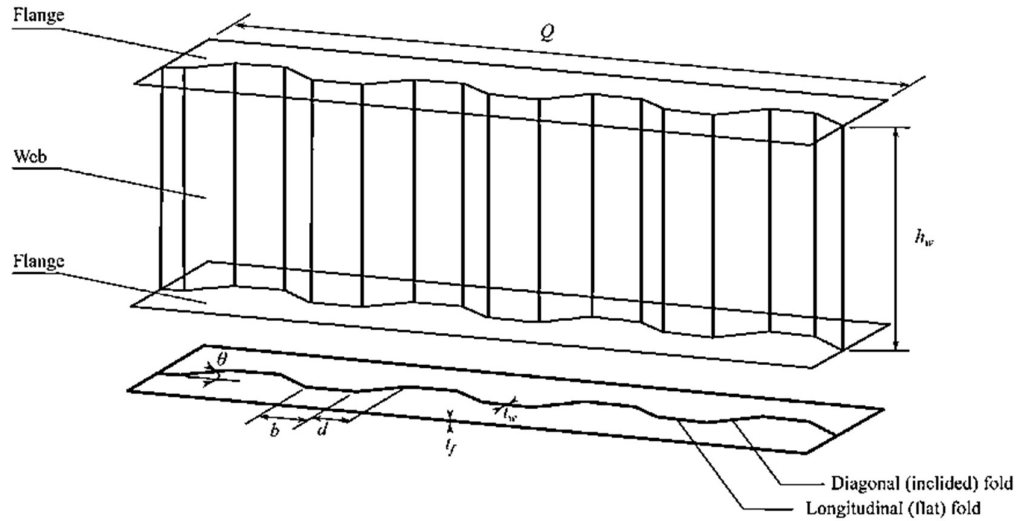
*Figure 2.10 Definitions and geometric properties of a trapezoidal corrugated web (Leblouba et al., 2019)*
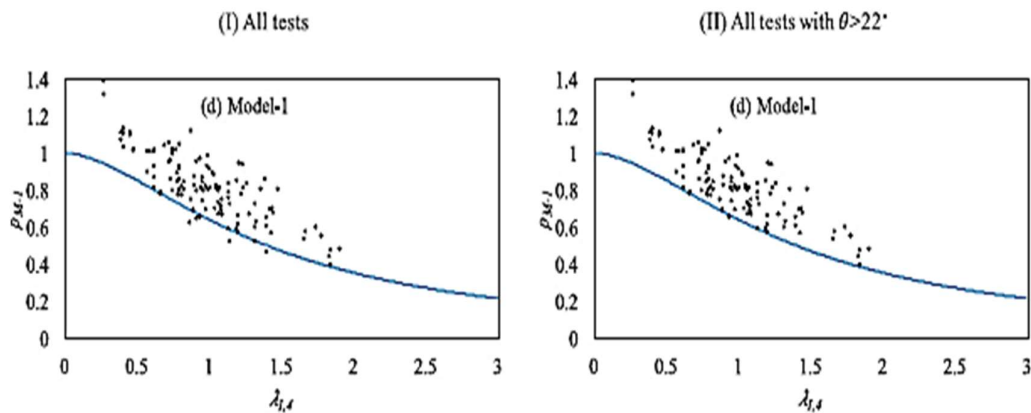


*Figure 2.11 Normalized shear strength versus $\lambda_{1,4}$ (Leblouba, Barakat, et al., 2017)*

The results for the proposed model together with the tests data are shown in Figure 2.11. The model gives good estimation for shear buckling strength when corrugation angle is larger than 22 degrees.

## 2.8 Resistance to shear force according to (EN_1993-1-5, 2019), new draft

In this draft, no adjustments to the existing version's shear resistance model of corrugated web girders are suggested.

## 2.9 Stress distribution of corrugated web under pure shear according to (Zhang et al., 2020)

In 2020, Zang et al. have studied the stress distribution on corrugated web under shear theoretically and verified it by experiment. The rotated stress field theory has been adopted, for the first time, to analyze the stresses in corrugated web girders (Zhang et al., 2020). The stress state has been summarized in the following three stages:

1.  <u>Pre-buckling stage</u>: the web is under pure shear, with shear stresses distributed equally throughout the web height as and a direction angle of primary strain of around 45 degrees. Because there is no vertical or horizontal membrane stress in the web $\tau = \sigma_1 = |\sigma_2|$.
2.  <u>Buckling stage</u>: at the time of buckling, the shear stresses and principal stresses attain their maximum values $\tau_u = \sigma_{1,max} = |\sigma_2|_{max}$
3.  <u>Post-buckling stage:</u> At the post-buckling stage, stresses redistribute, and the extent of redistribution is related to the development of out-of-plane deformation. The shear stress that causes critical buckling is lowered to (47-68%) of its nominal value (the resistance from the web is no longer present). The principal tensile stresses fall first, then rise again when deep creases appear in the body and a frame system (made up of flanges, transverse stiffeners, and an inclined tension zone in the web anchored to the flanges) resists and transfers the shear stress, see Figure 2.12. Finally, the girder is subject to its <u>ultimate failure</u> when plastic hinges develop in the flanges.
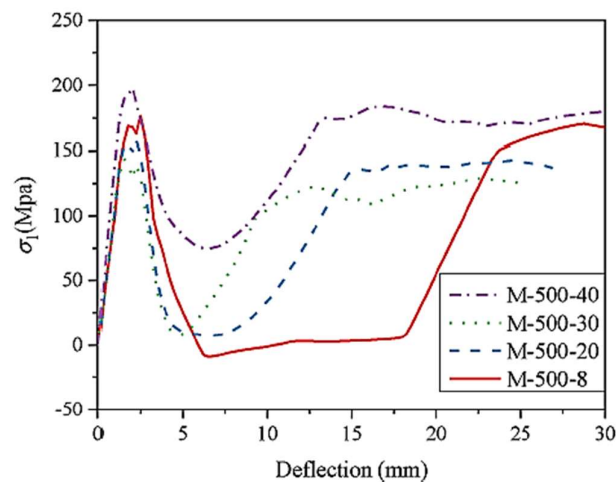


*Figure 2.12 First principal stress, 500 denotes the web width in mm and 40 denotes the flange width in mm, (Zhang et al., 2020).*

Figure 2.13 shows the stress state at the different stages. The "accordion effect" reduces the longitudinal stiffness of a corrugated steel web to a few tenths to a few hundredths of that of a flat steel web. As a result, no longitudinal membrane stress is expected in the corrugated steel web, and the end stiffeners' anchoring force is set to zero $\sigma_h = 0$.
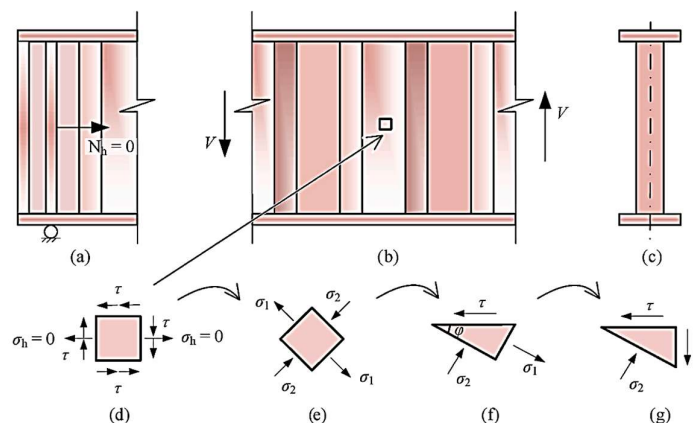
The verification with the test results is illustrated in **Error! Reference source not found.**.
The membrane stresses $\sigma_h = 0$ and $\sigma_v = 0$ throughout the test. The out-of-plane
displacement increases significantly when buckling takes place. Moreover, the orientation of
principle strain change from 45 to around 35.
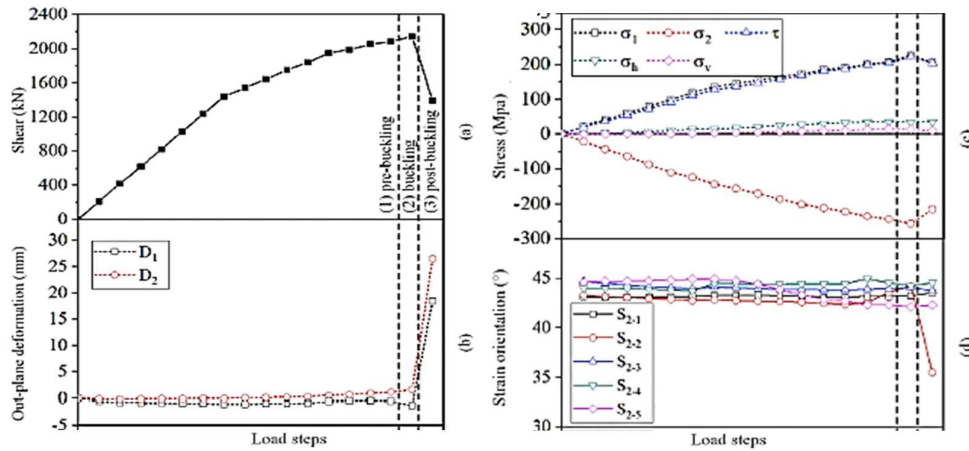


*Figure 2.14 Deformation and stress states in the corrugated web: (a) shear force in the beam
section; (b) out-of-plane deformation; (c) stress in the web (d) inclination angle of the principal
stress. Test performed by (Zhang et al., 2020).*

Furthermore, Zang et al. used an NLFEA to investigate the behavior of corrugated web
girders in the post-buckling stage. In the post-buckling stage, the CWGs are stated to exhibit
residual shear resistance. A frame system created composed of flanges, stiffeners, and an
inclined tension zone anchored to the flanges resists the shear force at this stage. This residual
capacity might range between 47% and 145% of the shear buckling load. This proportion is
determined by two factors:

1. The bending stiffness of the flanges, the residual shear capacity increases with
   increasing the bending stiffness of the flange (which rises as the flange thickness
   increases). Figure 2.15 illustrates the effect of flange thickness on the residual shear
   resistance.
2. The web width/height, the residual shear capacity increases with decreasing the web
   width/height ratio (the reason might be that when stiffeners are close (low ratio), the
   anchorage from the stiffeners would increase meaning increase in the frame system
   resistance). Figure 2.15 illustrates the effect of web width/height on the residual shear
   resistance.

(b) M-500-20



(d) M-500-40
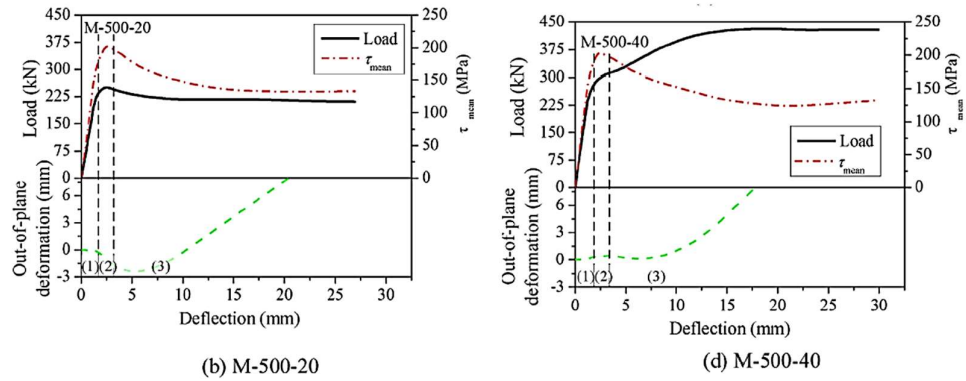
*Figure 2.15 load mean shear stress/out-of-plane deformation - deflection relation curves and shear buckling modes. Note: (1) in the pre-buckling stage (2) in the buckling stage stage (3) in the post-buckling stage (Zhang et al., 2020). Different flange thicknesses 20mm & 40mm*



(d) M-500-40



(h) M-750-40
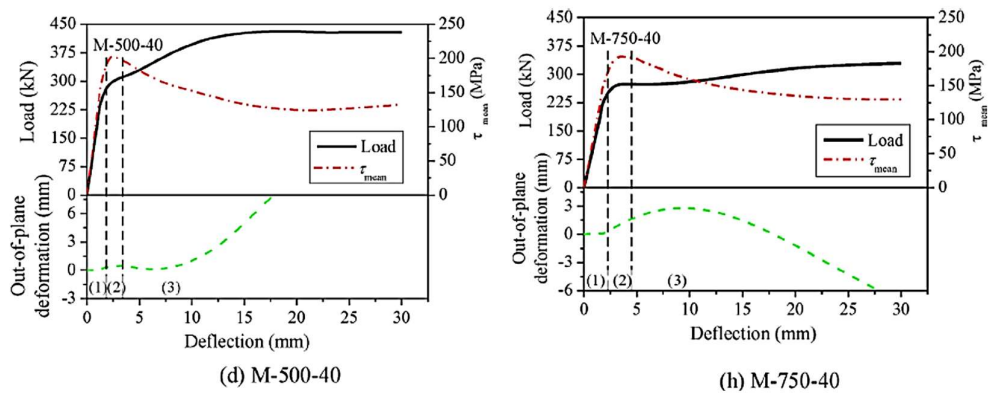
*Figure 2.16 load mean shear stress/out-of-plane deformation - deflection relation curves and shear buckling modes. Note: (1) in the pre-buckling stage (2) in the buckling stage (3) in the post-buckling stage (Zhang et al., 2020). Different web widths 500mm & 750mm.*

They concluded that three different collapse mechanisms might be distinguished in corrugated web girders. See Figure 2.17 .They are categorized based on the previous mentioned two factors (web width/height ratio and the bending stiffness of the flanges) as following:

1. Quasi mid-section mechanism: it happens when the flanges are flexible, and the web width/ height ratio is large.
2. Girder mechanism: it happens when the flanges are rigid, and the web width/ height ratio is quite low.
3. Mid-section mechanism: it is a transition between the previous two extreme cases.
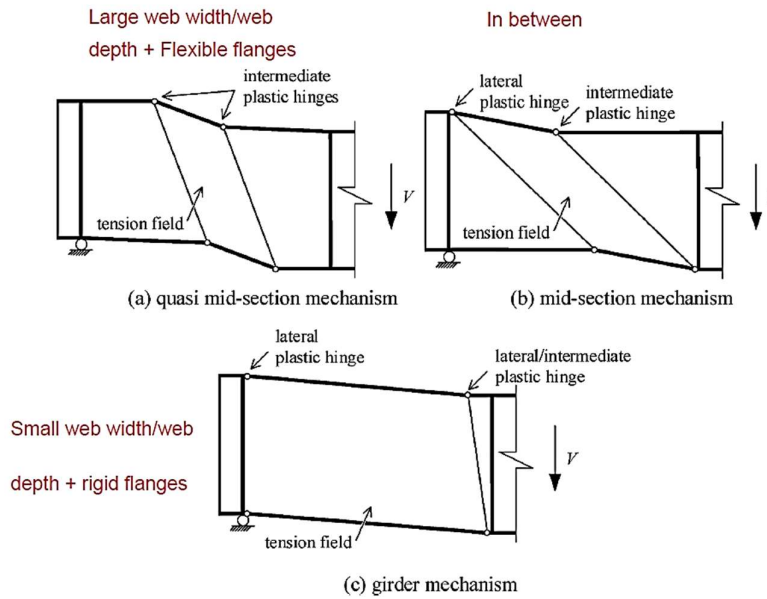
*Figure 2.17 Collapse mechanisms of corrugated steel web beams, (Zhang et al., 2020)*

## 2.10 Most influencing parameters on shear resistance of corrugated web girders

In this section the most influencing parameters on shear resistance of corrugated web beams are collected from the available literature and summarized in Table 2.1.
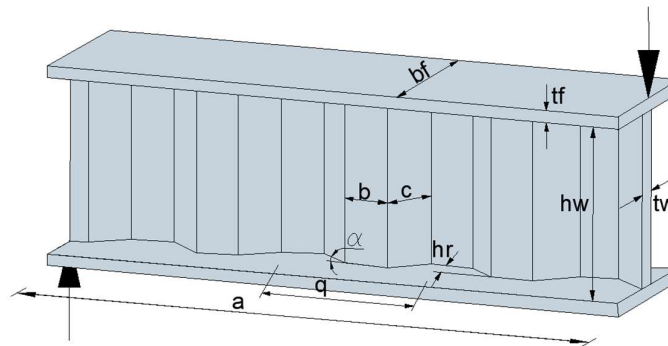


*Figure 2.18 Corrugated web beams notations*

*Table 2.1  Most influencing parameters on shear resistance of corrugated web girders, Notations in Figure 2.18*

| Ref. | Method | Parameter (s) | Results |
|---|---|---|---|
| Driver et al.(**Driver et al., 2006**) | Experiment + FEM | Imperfection amplitude | Increasing the imperfection amplitude decrease the shear buckling strength significantly |
| Nie et al. (**Jian-Guo Nie & Mu-Xuan Tao, 2013**) | Experiment | 1) Shear span, a 2) corrugation Configuration, q | $(\tau_{cr}/\tau_y)$ relationship is unrelated to the corrugation configuration (q) and shear span ratio (a/$h_w$) |
| | FEM | 1) Initial imperfection 2) (a/ q) | In case of yielding strength smaller than buckling strength: the ultimate loading capacity decreases significantly with increase imperfection at the descending stage, shear buckling occurs after yielding. In case of yielding strength larger than buckling strength: the ultimate loading capacity decreases with increasing |

| | | | imperfection whereas the descending capacity is independent on the imperfection. The shear capacity is insensitive to initial imperfection when $\lambda > 2, 3$. However, the shear capacity decreases fast when $\lambda$ between 0,75 and 2,3. In this range there is the largest effect of initial imperfection on shear strength. |
|---|---|---|---|
| | | 1) b/$h_w$ <br> 2) $h_r/t_w$ | Increasing b/$h_w$ change the mode from global to local. Increasing $h_r/t_w$ change the mode from global to local. Increasing both parameters together fasten the change of mode from global to local. |
| | | Corrugation configuration, q | The shear capacity is unrelated to the corrugation configuration (q) |
| | | Shear Span | The shear capacity is unrelated to shear span ratio |
| Kollár and Kövesdi 2018 (Kollár & Kövesdi, 2018) | Experiment and FEM | 1) Corrugation angle effect on 2) Initial imperfection | The virtual testing and the experiment give good agreement with the three angles with maximum difference with angle 60 deg which was within the tolerance, so initial imperfection is not related to the angle and an imperfection amplitude of $h_w/200$ is applicable but needs more research. |
| | | alpha | Shear strength increases with increasing of Alpha |
| Hassanein et al. 2017 (Hassanein et al., 2017) | FEM | 1) $t_w$ <br> 2) $h_w$ <br> 3) $h_r$ | 1) Increasing web thickness and height leads to significant increase in yielding region in the Web, thus raises the strength of the girders. <br> 2) Small web thicknesses are more economical. <br> 3) Smaller web heights have higher post buckling strength. <br> 4) Smaller $h_w$ is more efficient. <br> 5) Increasing corrugation depth ($h_r$) decrease the possibility of PHs (plastic hinges) development which only become visible in global shear failure due to increased rigidity of flanges besides the higher shear strength that does not result in differential deflection between upper and bottom flange to form PHs. Increasing $h_r$ increases shear strength considerably. |
| Jongwon Yi, Heungbae Gilb (et.al., 2008) | FEM | 1) b/$h_w$ <br> 2) $h_r/t_w$ | 1) When b/hw ratio increases, $\tau_{cr,g}/\tau_{cr,l}$ increase which means local buckling (Not mentioned). <br> 2) When $h_r/t$ ratio increases, $\tau_{cr,g}/\tau_{cr,l}$ increase which means local buckling (Not mentioned). <br> 3) The elastic buckling analysis results showed that the interactive shear buckling mode and strength was not influenced by material inelasticity or yielding, but rather by the geometry of the corrugated plate. |
| Moussa Leblouba, Samer Barakat, 2019 (Leblouba et al., 2019) | Experiment | 1) Shear span, a <br> 2) $h_w$ <br> 3) Corrugation angle | 1) Increasing corrugation angle leads to increasing shear strength and better usage of material strength and shear capacity. <br> 2) Shear span doesn't have an effect the shear strength. |
| Hassanein and Kharoob 2013 (Hassanein & Kharoob, 2013) | FEM | 1) $h_r/t_w$ <br> 2) b/$h_w$ <br> 3) a/$h_w$ <br> 4) $h_w/t_w$ | 1) For every web depth, raising the $h_r/t_w$ ratio reduces the critical shear stress ($h_w$). When the $h_r/t_w$ ratio approaches 30, the critical shear stress for any web depth ($h_w$) studied is nearly the same. <br> 2) Increasing the b/$h_w$ ratio (by decreasing $h_w$) raises the critical shear stress linearly. <br> 3) For any corrugated configuration, increasing the a/$h_w$ ratio (with the same a) The critical shear stress is increased. This demonstrates that the square corrugated webs are the most critical. However, this situation is incompatible with the real corrugated web bridge dimensions. Girders utilized in practice where the vertical stiffeners are spaced apart is far larger than the depth of the web ($h_w$). |

| | | | 4) For any web thickness, increasing the $h_w/t_w$ ratio lowers the critical shear stress. The crucial value for $h_w/t_w$ is 150 over which the decrease in stress becomes almost constant. |
|---|---|---|---|
| Moussa Leblouba, Samer Barakat and Zaid Al-Saadon **(Leblouba et al., 2018)** | Experiment and FEM | 1) $h_w$ <br> 2) b <br> 3) $t_w$ | Longitudinal fold b and $t_w$ are the most influential, followed by $h_w$, then the rest of the parameters; the modulus of elasticity E is noninfluential within the range [190–210] GPa. |
| Basinski, Witold **(Basinski, 2019)** | Experiment | Support stiffener rigidity | When reinforced support stiffeners are used, the linear range of variations in the shear angle is increased. The shear buckling resistance value then rises to 42%. |

## 2.11 Initial imperfection effect on shear buckling resistance

The initial imperfection is found to be one of the most effective factors on the girder's shear resistance. Apart from the manufacturing process, this imperfection is caused by the welding process and the accompanying residual stresses.

Both the amplitude and the shape of the initial geometric web imperfections play a major role in the shear strength and behavior of corrugated web steel girders.

In a study performed by Sause et al. to evaluate the effect of imperfection amplitude on the shear buckling capacity of corrugated web beams, it was revealed that the shear buckling capacity can reach yielding shear strength with an imperfection amplitude of up to 10% of $t_w$. However, increasing the amplitude of the imperfection drastically reduces the shear buckling strength. (Sause et al., 2003), see Figure 2.6.

Considering the size of the panels in the webs of real bridge girders, Hassanein et al. indicated that an imperfection magnitude equal to the corrugated web thickness ($t_w$) is practical (Hassanein & Kharoob, 2013).

Kollár and Kövesdi, in 2018, have performed three experiments to verify the virtual manufacturing and residual stresses with test results. Then they utilized the virtual manufacturing residual stresses as input for virtual testing to determine shear buckling resistance. It is concluded the imperfection amplitude suggested by EN 1993-1-5:2006 ($h_w$/200) to calculate shear buckling strength is applicable, however more research is needed (Kollár & Kövesdi, 2018).

On the other hand, in 2019, Kollár and Kövesdi applied virtual manufacturing techniques to simulate the residual stresses and deformation due to the manufacturing process, considering different web thicknesses (3mm, 2mm, and 1.2mm), presented that the residual stress in the corrugated webs can be neglected and the realistic imperfection amplitude is much smaller than $h_w$/200 suggested by EN 1993-1-5:2006. Thus, they suggested a more advanced modeling that considers the real initial imperfection (Kollár & Kövesdi, 2019).

Regarding the imperfection shape, the first buckling mode has been always thought of as an imperfection shape in earlier studies. An imperfection sensitivity study that has been conducted by Driver et al. has revealed that the first buckling mode shape is the most critical imperfection shape for shear buckling resistance (Driver et al., 2006).

## 2.12 Discussion and recommendation

In this section four design buckling curves for shear buckling resistance of corrugated web girders are compared. Several prior shear buckling resistance tests were compared between (Jiho Moon & Byung H. Choi, 2009), (EN_1993-1-5, 2019), Leblouba et al. (Leblouba, Barakat, et al., 2017) and (Richard Sause & Braxtan, 2011) design curves. The tests that were investigated for carbon steel are summarized in Table 2.2. As can be observed, in case of carbon steel tests, all models deliver conservative results compared to the test results. see Figure 2.19.

Table 2.2 Previous tested girders in carbon steel. References, A12-305-30 and A12-305-45 (Leblouba, Barakat, et al., 2017), Zang test (Zhang et al., 2020) and G7A (Driver et al., 2006)

| Tested girder | a1 [mm] | a3 [mm] | α [deg] | $t_w$ [mm] | $h_w$ [mm] | $F_{yw}$ [MPa] | $b_f$ [mm] | $t_f$ [mm] | $\tau_e$ [MPa] | $\tau_e/\tau_y$ |
|---|---|---|---|---|---|---|---|---|---|---|
| G7A | 300 | 150 | 36.9 | 6.3 | 1500 | 465 | 450 | 50 | 244 | 0.91 |
| A12-305-30 | 40 | 20 | 30 | 1.2 | 305 | 230 | 150 | 12 | 136.07 | 1.025 |
| A12-305-45 | 40 | 28.284 | 45 | 1.2 | 305 | 230 | 150 | 12 | 147.26 | 1.108 |
| Zang test | 340 | 160 | 45 | 6.4 | 1500 | 405 | 250 | 50 | 225 | 0.962 |
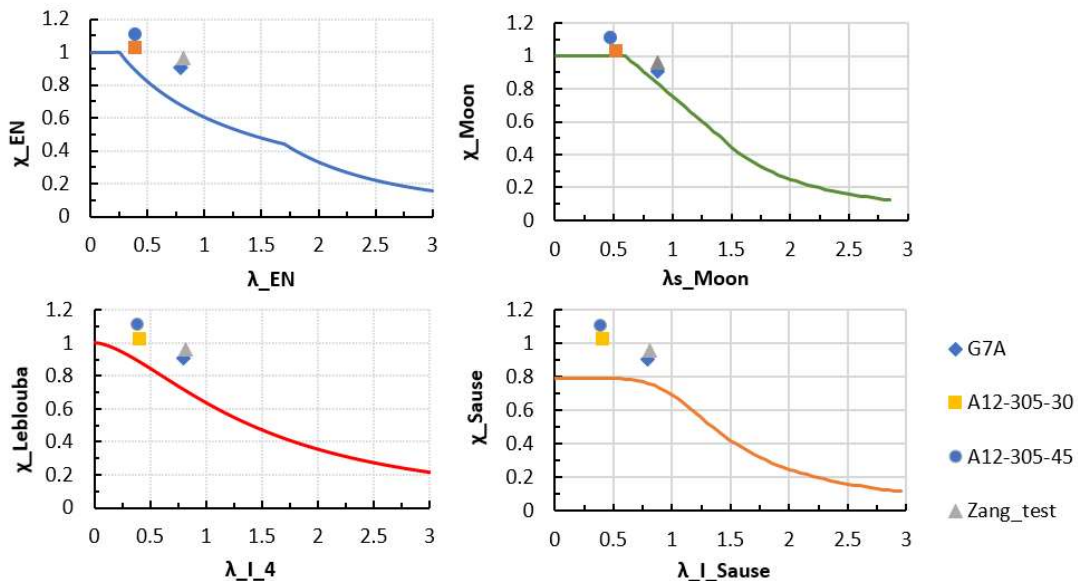


*Figure 2.19 Previous tests in carbon steel on Eurocode, Moon, Leblouba and Sause design curves.*

Looking at the shear design model in Eurocode, the shear capacity is defined based on the minimum between the local and global buckling modes. However, the design models in the literature consider interaction between the local and global buckling modes. Refer to Figure 2.19, although some of the proposed design models (Moon model) provide results closer to the test results, there is no indication here or in the studied literature that the Eurocode model is unsafe.

Regarding stainless steel, In SUNLIGHT testing program four girders with different geometric parameters of the corrugation were fabricated and tested in three-point bending. Lateral restraints were provided to prevent lateral-torsional buckling. The dimensions of the

flange plates (250 mm×25) were chosen to eliminate the risk of flange buckling and to ensure shear failure occurs in the web before other failure modes. All the girders were made of LDX 2101 stainless steel delivered by Outokumpu. The girders all had an approximate length of 4.0 m and height of 1.45 m. Detailed dimensions are presented in Table 2.3.

In SUNLIGHT-PROJECT, experiments were designed and performed to more accurately investigate the shear behavior of girders made of stainless steel and corrugated web plates. Four full-scale girders were tested. 3D DIC was used to monitor the initial geometry and deformations of the web panel during loading. The applied load, maximum vertical deflection, and the strains were all measured. Based on the conducted tests, a finite element model was developed and validated.

The results of tested girders in SUNLIGHT have been compared with the four mentioned models. As can be seen from Figure 2.20, the four studied models give quite conservative strengths in comparison with the test results.

*Table 2.3 Tested girders in stainless steel. Ref. SUNLIGHT Project*

| Speci men | a1 [mm] | a3 [mm] | α [deg] | $t_w$ [mm] | $h_w$ [mm] | $F_{yw}$ [MPa] | $b_f$ [mm] | $t_f$ [mm] | Failure load [kN] | $\tau_{ult}$ [MPa] | $\tau_e/\tau_y$ |
|---|---|---|---|---|---|---|---|---|---|---|---|
| 1001 | 170 | 60 | 35 | 4 | 1450 | 460 | 250 | 25 | 3188 | 274.83 | 1.04 |
| 1002 | 170 | 60 | 45 | 4 | 1450 | 460 | 250 | 25 | 3500 | 301.73 | 1.14 |
| 1003 | 170 | 100 | 35 | 4 | 1450 | 460 | 250 | 25 | 3303 | 284.74 | 1.07 |
| 1004 | 170 | 100 | 45 | 4 | 1350 | 460 | 250 | 25 | 3202 | 296.48 | 1.12 |
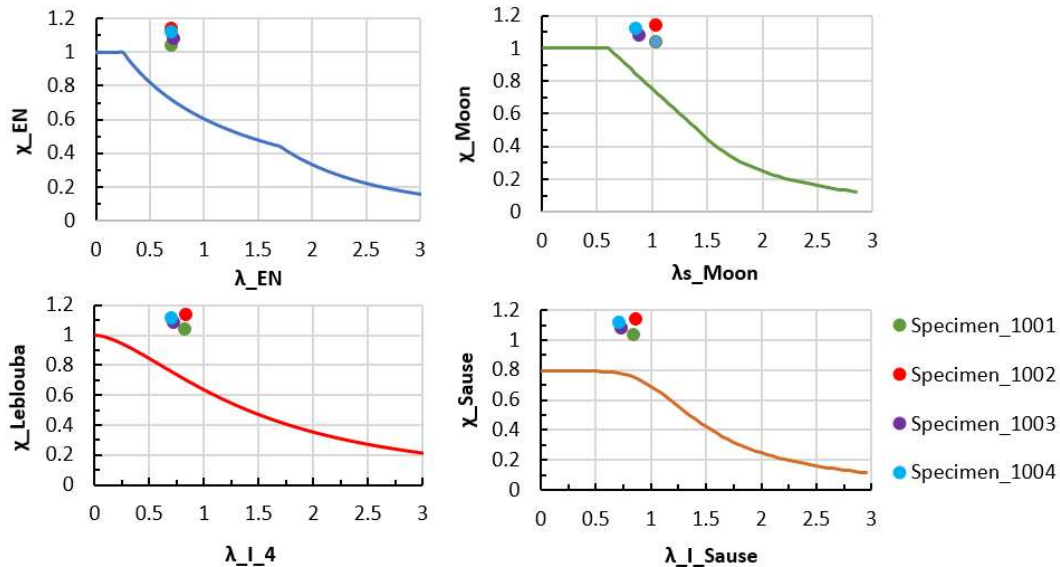


*Figure 2.20 Current tests on stainless steel on Eurocode, Moon, Leblouba and Sause design curves.*

To conclude, the shear capacity of corrugated web girders is studied expensively by different authors. The ultimate shear capacity of corrugated web girders is stated to be governed by buckling load of the web according to many authors like (Jiho Moon & Byung H. Choi, 2009) and (Richard Sause & Braxtan, 2011). Zang et al., on the other hand, suggested that the flanges can also contribute to the shear resistance and give considerable increase to the shear resistance by the frame system that develop after buckling (Zhang et al., 2020). This is dependent on the bending stiffness of the flanges and the aspect ratio of the web (NOTE, in

real bridge girders the distance between the stiffeners is large and the flanges are too flexible to provide this kind of frame action. Thus, the shear resistance is expected to be limited by the buckling of the web). Limiting the shear resistance to the web buckling will give conservative values (additional capacity can be obtained by stain-hardening). Eurocode consider the shear resistance to be the minimum local and global buckling load. Leblouba et al. have confirmed that the use of Eurocode design curve will give conservative values for local and global buckling (Leblouba, Junaid, et al., 2017). However, they proposed a new equation for shear strength (Interaction of order n = 4) based on 125 previous performed tests (Leblouba, Barakat, et al., 2017).

For stainless steel material, two master theses have been performed in CHALMERS by (Karlsson, 2018) and (Hlal, 2021). A limited parametric study was conducted. It was concluded that using the current design model in EN1993-1-5 yields results on the safe side. Furthermore, a new design model was proposed by (Karlsson, 2018) for stainless steel. However, due to the sensitivity of shear behavior to initial imperfections, corrugation parameters, and other parameters, ref. Table 2.1, evaluating the current design models in Eurocode is not possible without extensive parametric studies. After comparing parametric studies and design models, the final comment on the current shear design models for corrugated web stainless steel girders in Eurocode will be possible.

# 3 Resistance to transverse forces (Patch loading)

Few studies have provided models to estimate the patch loading resistance of corrugated web girders, and this the topic is not yet covered in the current Eurocode. However, a suggested design model is included in a draft for the coming version of Eurocode.

Previous research in the field has been exclusively devoted to beams made of carbon steel. The patch load capacity of corrugated web beams made of stainless steel has – to the knowledge of the author – not been studied.

This section summarizes some of the previous research on the patch load resistance of beams with corrugated webs. The design model provided in a draft of Eurocode (EN_1993-1-5, 2019) is also presented and examined in view of previous work.

## 3.1 Resistance to transverse force according to (EN_1993-1-5, 2006), current version

The current version of Eurocode, EN1993-1-5 (2006), does not include a design model for carbon steel or stainless-steel beams with corrugated webs' resistance to patch loading.

## 3.2 Resistance to transverse force according to (Luo & Edlund, 1996)

In 1996, Lou and Edlund (Luo & Edlund, 1996) conducted a parametric study using nonlinear finite element analysis to determine the ultimate load capacity of trapezoidal corrugated web girders under patch loading. Based on this work, an empirical model for estimating the patch loading resistance was proposed. The parameters were considered in the parametric study and their effect on patch loading capacity of corrugated web beams are the following:

- Material model: the ultimate strength of the studied girders- different web thicknesses and different corrugation angles are considered to study the effect of material model on patch loading capacity- is found to be roughly 8-12% percent greater with a

Ramberg-Osgood strain-hardening model for webs than with an elastic-perfectly plastic model.

- Initial imperfections (local and global): a small global initial imperfection has little effect on load-carrying capacity, but a local initial imperfection in the web near the load has a significant impact on the load-deflection curve. A small imperfection with an amplitude of about half the web thickness ($\frac{t_w}{2}$) was found to reduce the ultimate load by around 7%.
- Corner effects (strain hardening due to cold forming): Cold-forming of corrugation in webs causes a local increase in yield stress, i.e., strain-hardening of the material in a small region around the corner of the web profile, which is commonly referred to as corner-effects. The effect of local increase in yield strength due to stain hardening on the ultimate strength was found to be negligible.
- Loading position, the loading position is studied by applying a knife load on different positions, at the center of oblique part, at the center of flat part and at the corner. It was concluded that when a knife-load is applied to the center of the oblique part of the corrugation, the investigated girder has the greatest ultimate load, whereas when load is applied to the center of the flat part of the webs, the girder has the lowest ultimate load.
- Load distribution length: the ultimate load for a girder subjected to a knife-load is found to be approximately 40% and 20% lower when the knife-load is substituted with a uniformly distributed patch load with lengths of 115.2 mm and 50 mm, respectively.
- variation of geometric parameters, corrugation angle: for angles lower than75 degrees, the ultimate strength of a girder grows as the corrugation angle increases, however, the ultimate load for corrugation angle of 90 degrees is nearly equal to that for 75 degrees.
- variation of geometric parameters, web thickness: the ultimate load increases almost proportionally to the web thickness.
- variation of geometric parameters, flange thickness: the ultimate load increases almost proportionally to the flange thickness.
- Girder length & height: the panel dimensions H and L do not have much effect on the ultimate strength for girders with flange thickness $t_f = 10\ mm$, except when H is extremely small (around 200 mm).

The design model proposed by Lou and Edlund is illustrated as following:

The patch loading resistance is defined as following:

$$F_R = \gamma \cdot t_f \cdot t_w \cdot f_{yw}$$

$$\gamma = 10.4 \cdot \gamma_\alpha \cdot \gamma_c$$

$$\gamma_\alpha = \frac{a_1 + a_2}{a_1 + a_2 \cdot \cos{(\alpha)}} \text{ for } \frac{t_f}{t_w} \geq 3.82$$

$$\gamma_\alpha = 1 \text{ for } \frac{t_f}{t_w} < 3.82$$

$$\gamma_c = 1 + \eta \cdot s_s$$

Where the correction coefficient η is set to 1/240.

$s_s$ is loading length

## 3.3 Resistance to transverse force according to (Elgaaly, 1997)

In 1997, (Elgaaly, 1997), Elgaaly et al. performed a parametric study utilizing FEM to propose a simple design model for patch loading capacity based on tests to failure under partial compressive edge loading -fork and distributed-. Furthermore, new suggested equations for (patch loading & shear) and (patch loading & moment) interactions were provided. The parameters that have been considered are:

- The thickness and yield stress of the web
- Flange material
- The corrugation profile.
- The width of the patch load
- Three different positions for the load
    a. Over a parallel fold.
    b. Over an inclined fold.
    c. Over the fold line between two folds.

The findings revealed that there are two main failure modes:

- Web yielding followed by crippling and vertical bending of the flange into the crippled web.
- Web crippling and Flange collapse mechanism.

The design model proposed by Elgaaly is illustrated below:

1- Patch loading resistance due to web crippling is defined as following:

$$F_R = P_{fl} + P_w$$

The contribution from the flange can be obtained as:

$$P_{fl} = \frac{4 \cdot M_{pl,f}}{a - \frac{S_S}{4}}$$

Where the distance between two plastic hinges (a) in the flange at the positive and negative bending moment is defined as following:

$$a = \left(\frac{f_{yf} \cdot b_f \cdot t_f^2}{2 \cdot f_{yw} \cdot t_w}\right)^{0.5} + \frac{s_s}{4}$$

The flange plastic moment capacity $M_{pl,f}$ is defined as follows:

$$M_{pl,f} = \frac{f_{yf} \cdot b_f \cdot t_f^2}{4}$$

The contribution from the web can be obtained as:

$$P_w = \left(E \cdot f_{yw}\right)^{0.5} t_w^2$$

2- Patch loading resistance due to web yielding

$$F_R = (b + b_a) \cdot t_w \cdot f_{yw}$$

$$b = \frac{a_4 + a_1}{2}$$

$$b_a = \alpha_b \cdot t_f \cdot \left(\frac{f_{yf}}{f_{yw}}\right)^{0.5}$$

$$\alpha_b = 14 + 3.5\beta - 37\beta^2 \geq 5.5$$

$$\beta = a_3/b_f$$

3- The ultimate load capacity is taken as the minimum of the two cases (web crippling and web yielding)

## 3.4 Resistance to transverse force according to (Kövesdi, 2010)

In 2010 Kövesdi et al. conducted an experimental program where 12 large scale girders that are simply supported were tested. The tests' goal was to determine the patch loading resistance of corrugated web girders with a corrugation profile typical for a bridge girder. The ultimate loads were determined, and structural behavior and failure modes were investigated and explained. A previously developed design method by Braun and Kuhlmann was verified and improved based on the test findings.

The tested girders had the same corrugation configuration, see Figure 3.1, same web thickness and same web height. Three different loading lengths were investigated; 90, 200 and 380 mm so the load was applied on one or more than one-fold. The length of the specimens and the thickness of the flange were also varied.
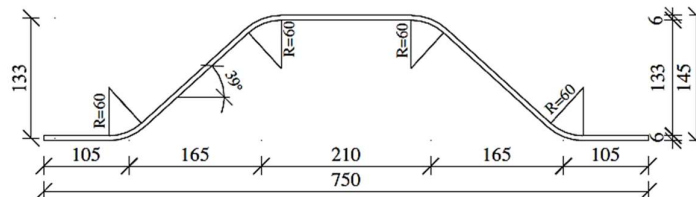


*Figure 3.1 Corrugation configuration for the girders tested by Kövesdi et al. (Kövesdi & Dunai, 2011)*

Two different failure modes were observed during the tests:

Web crippling: web buckling is limited to one-fold when the loading length is small, and the buckled shape's wavelength along the web depth is relatively short. If buckling occurs in adjacent folds, all buckling waves will have the **same** direction as shown in "case a" in Figure 3.2.

Local web buckling: for loading length larger than one-fold, more than one-fold will be involved in the load bearing. Web buckling occurs in all loaded folds at the same time. As seen in "case b" in Figure 3.2 , the buckling zone spreads over more folds and is longer than the preceding one. Bucking waves in neighboring folds **alternate** direction every time in this failure condition.

*a, web crippling*             *b, local web buckling*

*Figure 3.2 Observed failure modes, Kövesdi tests*

Furthermore, a parametric study using nonlinear FEM to estimate the resistance of corrugated web beams to transverse load w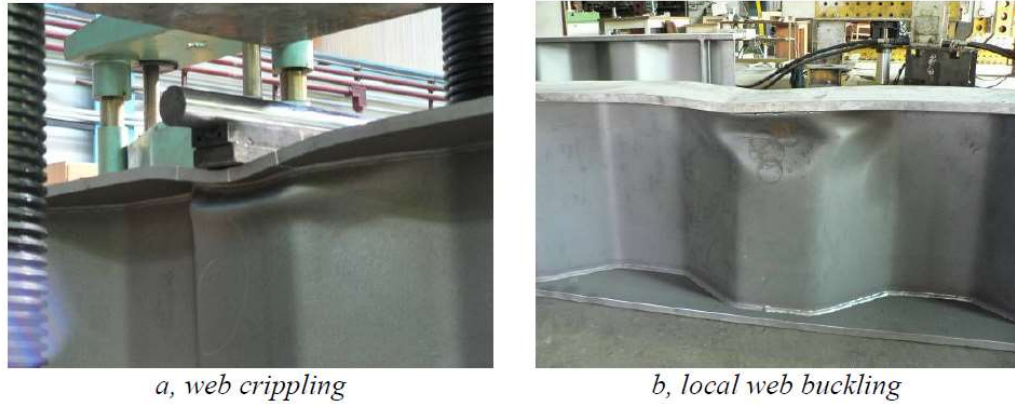as performed by the author. Different parameters were considered, loading length, fold ratio $\frac{a_i}{t_w}$, web ratio $\frac{h_w}{t_w}$, corrugation angle and flange width and thickness. A third buckling mode, global buckling mode, was observed in the finite element simulation, when the fold ratio was small the web ratio became decisive. Global buckling mode is main for girders with large web ratio. This mode together with the previous mentioned modes are illustrated in Figure 3.3.
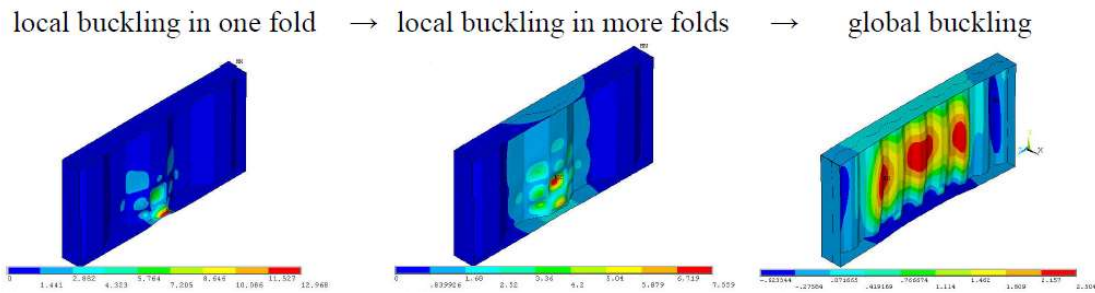


*Figure 3.3* Different failure modes (Kövesdi, 2010)

The considered parameters and their effects on patch loading resistance for corrugated web beams that have been concluded from this study are:

- Loading length: It was revealed that increasing the loading length corresponds to a linear increase in patch loading resistance regardless the web ratio and other parameters.
- Fold ratio: if the failure mode is local buckling, increasing the fold ratio $\frac{a_i}{t_w}$ reduces the load bearing capacity. If the failure mode is global buckling, this has no effect.
- Web ratio: increasing the web slenderness $\frac{h_w}{t_w}$ reduces load carrying capacity in the global buckling domain; however, if the failure mode is local buckling, this has no effect.
- Corrugation angle: to evaluate the effect of corrugation angle, the loading length has been considered as a multiple of corrugation wavelength to study the effect of changing corrugation angle without changing the loading length. It was concluded that as the corrugation angle increases, the patch loading resistance increases with the same ratio (39% to 45% for angles 20 degrees to 65 degrees) regardless the web or fold ratio.

- Flange thickness: increasing the thickness of the flange results in a linear increase in patch loading resistance.
- Flange width: the patch loading resistance is increased with increasing the flange width.

Furthermore, a modified design model was developed by (Kövesdi, 2010). This proposed design method has the same formulation as Braun and Kuhlmann's model, with the exception that interactions between shear & transverse force and bending & patch loading were not considered. The model by (Kövesdi, 2010) for patch loading resistance developed firstly for centric patch load and was based on the following range of parameters:

*Table 3.1 Parameter range of experimental and numerical investigations,(Kövesdi, 2010)*

| Web ratio $h_w/t_w$ | $200 - 300 - 400 - 500$ |
|---|---|
| Fold ratio $a_i/t_w$ | $2.5 - 25 - 50 - 75 - 100 - 116.7($ in all cases $a_1 = a_2)$ |
| Loading length $s_s/h_w$ | $0.4 - 0.6 - 0.8$ |
| Corrugation angle $\alpha$ | $15° - 30° - 45° - 65°$ |
| Flange thickness $t_f$ | $20 - 40 - 60 - 80 - 100$mm |
| Flange width $b_f$ | $150 - 300 - 400 - 500$mm |

The design model proposed by Kövesdi can be summarized as follows:

The patch loading resistance <u>when the whole flange width is loaded</u> is defined as:

$$F_R = 2 \cdot \sqrt{n \cdot M_{plf} \cdot t_w \cdot \chi \cdot f_{yw}} + \chi \cdot t_w \cdot f_{yw} \cdot s_s \cdot k_\alpha$$

The reduction factor due to buckling is defined as follows:

$$\chi = \begin{cases} 1.0, & \bar{\lambda}_p \leq 1.273 \\ \dfrac{1.9}{\bar{\lambda}_p} - \dfrac{0.8}{\bar{\lambda}_p^2}, & \bar{\lambda}_p > 1.273 \end{cases}$$

Factor n considers how many plastic hinges can develop in the flange. This factor is determined by the ratio $\frac{t_f}{t_w}$. When $\frac{t_f}{t_w} < 4$ , the entire yield line in the web as well as all four plastic hinges in the flange can evolve during the failure mechanism. When the flange is more dominant like when $\frac{t_f}{t_w} > 4$, the web failure mechanism is activated earlier, and all four plastic hinges are unable to develop, resulting in a lower patch loading resistance. This decrease in resistance can be factored into the amount of flange plastic hinges that are considered as follows:

$$n = \begin{cases} 4, & \dfrac{t_f}{t_w} < 4 \\ 3, & 4 \leq \dfrac{t_f}{t_w} \leq 7 \\ 2, & \dfrac{t_f}{t_w} > 7 \end{cases}$$

The relative slenderness can be calculated as following:

$$\bar{\lambda}_p = \sqrt{\frac{f_{yw}}{\sigma_{cr}}}$$

Elastic buckling stress is determined as follows:

$$\sigma_{cr} = \frac{k_\sigma \cdot \pi^2}{12 \cdot (1 - v^2)} \cdot E \cdot \left(\frac{t_w}{a_i}\right)^2$$

$k_\sigma$ is a constant set to $k_\sigma = 1.11$

The factor $k_\alpha$ that consider the effect of corrugation angle

$$k_\alpha = \frac{a_1 + a_2}{a_1 + a_4}$$

$a_i$ is the loaded fold length or the maximum fold length when there are more than one loaded fold.

$M_{plf}$: plastic moment capacity of the flange
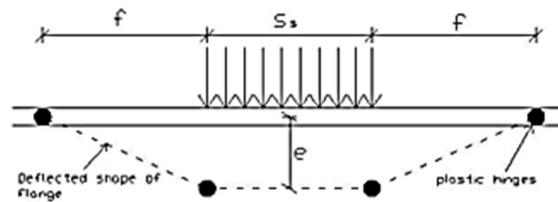


*Figure 3.4 Flange mechanism under patch loading failure*

The author then modified the model to consider the effect of <u>loading width</u> on the patch loading resistance as following:

$$F_R^{red} = F_R \cdot \{1 - m \cdot [a_4 \cdot (1 - b) - ss_a]\}$$

$m$: decreasing tendency, this value changes for long and short loading length, ref. Figure 3.5.

$b$: shifting ratio of the breaking point, this value changes for long and short loading length

$ss_a$: loading width

*Figure 3.5 Design method development, (Kövesdi, 2010)*

Furthermore, the model is modified to consider the eccentricity of the transverse force by applying a reduction on the previous resistance as following:

$$F_R^{red2} = F_R^{red} \cdot \left(1 - m_3 \cdot \frac{e}{b_f}\right)$$

$m_3$: slope of the resistance decreasing tendency. Refer to Equations (51-55) in (Kövesdi, 2010).

$e$: eccentricity of the applied load.

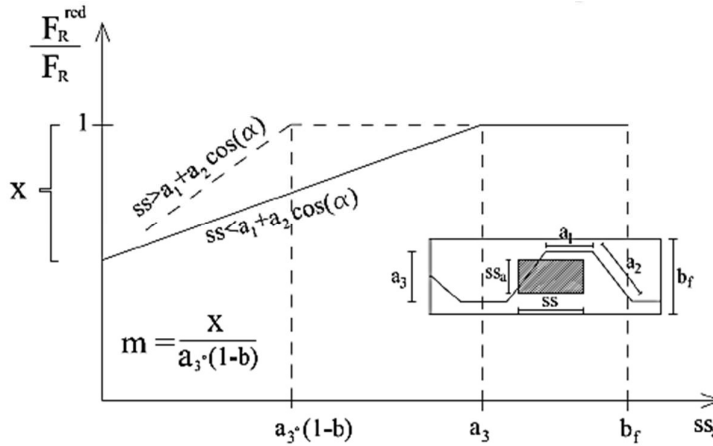$F_R^{red}$: patch loading resistance reduced to loading width.

To note here that this model was developed without considering the interaction of bending and transverse force. The bending moment could have significant reduction of flange contribution in patch loading resistance.

Imperfection sensitivity for patch loading resistance according to (Kövesdi & Dunai, 2011)

In 2011, Kövesdi and Dunai performed an imperfection sensitivity analysis to establish an FEM-based design model. Nonlinear FEM analyses along with 12 tests were conducted to create a set of imperfection shapes and scaling factors that can be used to estimate the patch loading resistance of corrugated web girders. Different parameters were considered like the position of the applied load (parallel, inclined fold or corner area), the loading length (90–380 mm), the span (1140–1875 mm), the flange thickness (20–30 mm), and the effect of the loading eccentricity. Four imperfection shapes are analyzed, the first critical buckling mode, the ultimate shape (The highest point of the load–deflection curve obtained without initial imperfections is used to determine the ultimate shape), the sine wave imperfection shape, and a modified sine wave imperfection shape are investigated. The analysis showed that the relevant scaling factor is the fold length divided by 200 if the first buckling mode or the modified sine wave shape is chosen as an equivalent geometric initial imperfection. Referring to Figure 3.6, for imperfection amplitude of around (b/200 = 210mm/200 = 1.05mm), the predicted capacity will be less than the test results.
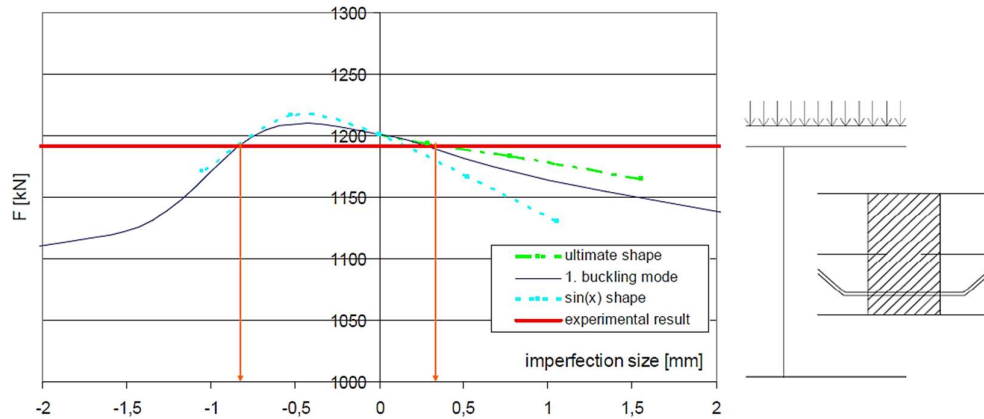
*Figure 3.6 Imperfection sensitivity - asymmetrical case (parallel fold is loaded) (Kövesdi, 2010)*

## 3.5 Resistance to transverse force according to (EN_1993-1-5, 2019), new draft

There is no formula in the current Eurocode that covers the patch loading resistance of girders with corrugated web. The latest draft of (EN_1993-1-5, 2019), however, provides a formula for the problem. The design model proposed in this draft is based on the model developed by Kövesdi without considering the contribution from the flange in patch loading resistance. The model can be summarized as following:

The design resistance for corrugated web girders under patch loading can be calculated as follows:

$$F_R = \frac{\chi \cdot k_\alpha \cdot s_s \cdot t_w \cdot f_{yw}}{1.20 \cdot \gamma_{M1}}$$

Factor $k_\alpha$ that consider the effect of corrugation angle is defined as follows:

$$k_\alpha = \frac{a_1 + a_2}{a_1 + a_4}$$

The reduction factor due to local buckling is determined as:

$$\chi = \begin{cases} 1.0, & \bar{\lambda}_p \leq 1.27 \\ \dfrac{1.9}{\bar{\lambda}_p} - \dfrac{0.8}{\bar{\lambda}_p^2}, & \bar{\lambda}_p > 1.27 \end{cases}$$

The relative slenderness is defined as:

$$\bar{\lambda}_p = \sqrt{\frac{f_{yw}}{\sigma_{cr}}}$$

The critical elastic buckling stress can then be calculated from:

$$\sigma_{cr} = \frac{k_\sigma \cdot \pi^2}{12 \cdot (1 - v^2)} \cdot E \cdot \left(\frac{t_w}{a_i}\right)^2$$

This design formula, however, is applicable only in case of a fold length fulfills the following condition:

$$a_i \geq \left(\frac{h_w}{t_w} + 260\right) \cdot \frac{t_w}{11,5}$$

where $a_i$ is the loaded fold length. If more folds are loaded, the maximum fold length ($a_1$ or $a_2$) should be taken.

$k_\sigma$ is a constant set to ($k_\sigma = 1.11$)

It can be observed that the model disregards the contribution from the flange as it is in the case of flat web girders.

## 3.6 Resistance to transverse force according to (Inaam & Upadhyay, 2020)

All the prior studies have been focusing on simply supported girders. The simply supported girder, on the other hand, acts as a cantilever at the support points and that becomes most critical when there is no stiffener over the support section. Inaam and Upadhay (Inaam & Upadhyay, 2020) have investigated the sensitivity of the patch loading capacity to the girder's static system in a recent study published in 2020. The considered parameters and the drown conclusions are summarized as follows:

- Patch load eccentricity: in the case of eccentric patch loading, the smaller outstand of the parallel fold is more significant and has the greatest loss in patch load capacity when compared to the inclined fold. Due to the three-sided support given by the web profile, maximum capacities are obtained for greater outstands of parallel folds at eccentricities of $\frac{e}{b_f} = 0.15\ to\ 0.25$ from the web fold line. See Figure 3.7 and Figure 3.8.
- Loading length: the load carrying capacity of a load increases linearly as the loading length ($s_s$) increases, but the curves plateau at greater loading lengths, with no further increase. Small loading lengths ($s_s$) have a typical patch failure that is local in character, whereas greater loading lengths have a typical shear failure that occurs in the high shear zones towards the supports.
- Longitudinal to inclined folds ratio: single folds with unequal widths $a_1 \neq a_2$ have better load bearing capacities per unit length of corrugation because smaller fold widths with lower w/t ratio offer rotational restriction to broader fold widths. Other limitations, apart from patch load capacity, may influence the final optimal selection of relative fold widths.
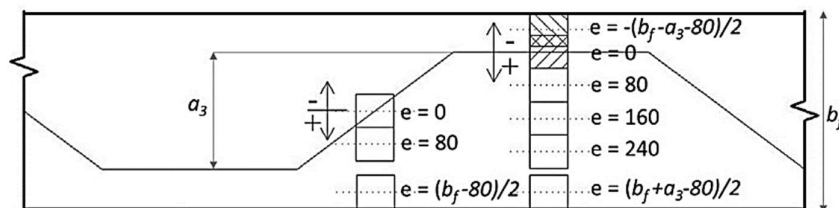


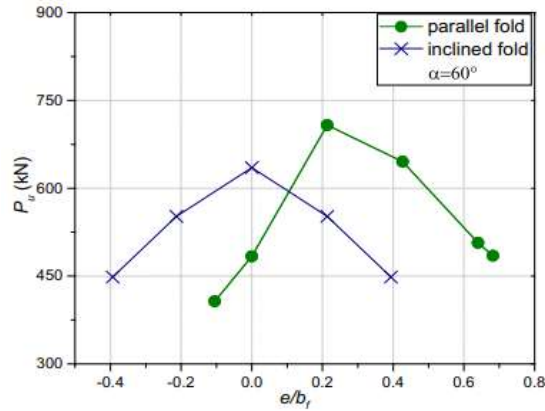*Figure 3.7 Eccentricity from parallel fold (Inaam & Upadhyay, 2020)*

*Figure 3.8 Patch load resistance variation with eccentricity (Inaam & Upadhyay, 2020)*

The design model for patch loading suggested by Inaam & Upadhyay for cantilever system is summarized as the following:

Patch loading resistance can be determined as follows:

$$F_R = \chi_M \cdot t_w \cdot s_s \cdot f_{yw}$$

The reduction factor due to buckling is defined as follows:

$$\chi_M = 0.4718 \cdot \left[\frac{s_s}{2 \cdot (a_1 + a_4)}\right]^{-0.786}$$

Where:

$s_s$ is the loading length

This research reveals that changing the static system from simply supported to cantilever reduces patch loading resistance by up to 22% in the domain of the current study.

## 3.7 Comparison and recommendations

This section compares four design models for patch loading resistance of corrugated web girders. The patch loading resistance of several previous performed tests were compared between the Lou& Edlund, EN-draft2019, Elgaaly and Kövesdi models. Figure 3.9 and Table 3.2 summarize the tests that have been studied. The Kövesdi model, as can be seen, provides the closest data to the test results. Edlund, Elgaaly, and EN1993-1-5(2019) give conservative results. The loading length differs between the tests, and this parameter is not taken into account in the Elgaaly model, resulting in nearly identical capacities for all of the studied tests. The web and the flange are considered to withstand the patch load in Edlund, Elgaaly, and Kövesdi model. The proposed model in Eurocode draft (EN1993-1-5(2019)), on the other hand, ignores the flange contribution, which results in highly conservative results. It can be observed from Table 3.2 that the contribution of the flange can be much larger than the contribution from the web like the Specimen 12 tested by Kövesdi.

*Table 3.2 Previous tests capacities according to Lou& Edlund, EN2019, Elgaaly and Kövesdi models and test results*

| Specimen | Ss [mm] | L [mm] | No. [-] | $F_{exp}$ [kN] | Kövesdi [kN] | Edlund [kN] | EN1993-1-5,2019 [kN] | Elgaaly [kN] |
|----------|---------|--------|---------|----------------|--------------|-------------|----------------------|--------------|

| | | | | | | | | |
|---|---|---|---|---|---|---|---|---|
| Kövesdi specimen 1, inclined | 90 | 1500 | 1 | 754.2 | 710.370 | 650.36 | 170.50 | 684.45 |
| Kövesdi specimen 2, inclined | 200 | 1500 | 2 | 956.48 | 960.43 | 867.15 | 378.88 | 684.45 |
| Kövesdi specimen 3, longitudinal | 90 | 1875 | 3 | 764.75 | 738.14 | 650.36 | 180.93 | 694.62 |
| Kövesdi specimen 4, longitudinal | 200 | 1875 | 4 | 949.02 | 1003.50 | 867.15 | 402.07 | 694.62 |
| Kövesdi specimen 12, corner area | 90 | 1500 | 5 | 772.39 | 710.370 | 650.36 | 170.5 | 684.45 |

*Table 3.3 Dimensions of the studied girders*

| | Specimen 1, Kövesdi | Specimen 2, Kövesdi | Specimen 3, Kövesdi | Specimen 4, Kövesdi | Specimen 12, Kövesdi |
|---|---|---|---|---|---|
| | inclined | inclined | longitudinal | longitudinal | corner |
| L [mm] | 1500 | 1500 | 1875 | 1875 | 1500 |
| $h_w$ [mm] | 500 | 500 | 500 | 500 | 500 |
| $b_f$ [mm] | 225 | 225 | 225 | 225 | 225 |
| Ss [mm] | 90 | 200 | 90 | 200 | 90 |
| $a_1$ [mm] | 210 | 210 | 210 | 210 | 210 |
| $a_3$ [mm] | 145 | 145 | 145 | 145 | 145 |
| $a_2$ [mm] | 230.4 | 230.4 | 230.4 | 230.4 | 230.4 |
| $a_4$ [mm] | 165 | 165 | 165 | 165 | 165 |
| α [Deg] | 39 | 39 | 39 | 39 | 39 |
| $t_f$ [mm] | 20 | 20 | 20 | 20 | 20 |
| $t_w$ [mm] | 6 | 6 | 6 | 6 | 6 |
| $f_{yw}$ [MPa] | 379 | 379 | 379 | 379 | 379 |
| E [GPa] | 200 | 200 | 200 | 200 | 200 |
| υ [-] | 0.3 | 0.3 | 0.3 | 0.3 | 0.3 |
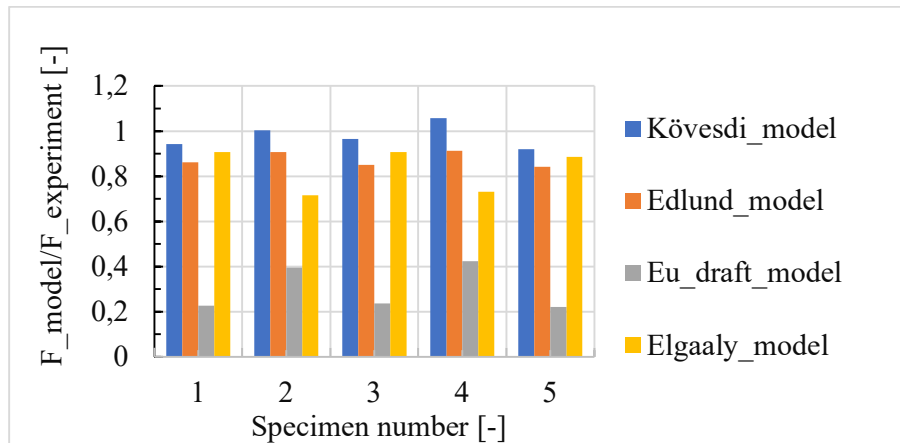
*Figure 3.9 Previous tests capacities according to Lou& Edlund, EN2019, Elgaaly and Kövesdi models and test results*
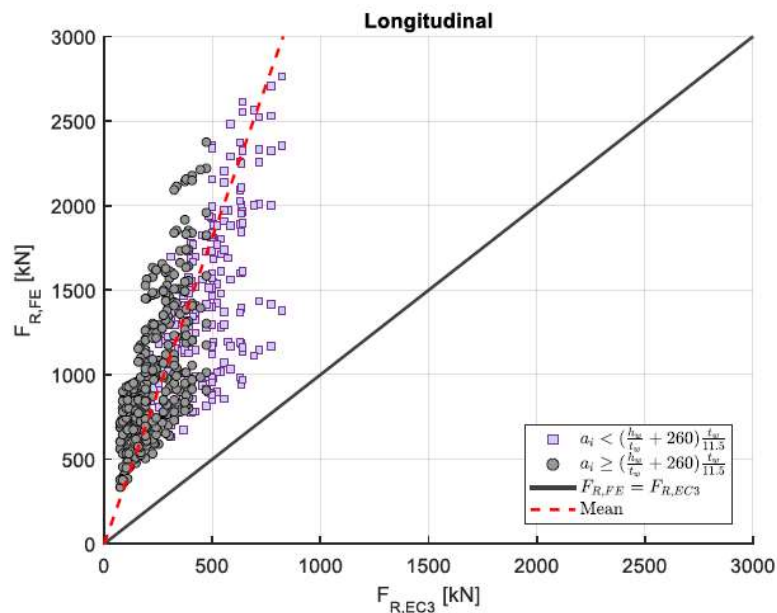


*Figure 3.10 Patch loading resistance from FE-analysis compared to draft of EN1993-1-5, 2019 (SÆMUNDSSON, 2021)*

The conclusions and recommendations that can be drawn from this study are:

- Abundant research has been done on patch loading, and it has been confirmed that the flange contributes to the resistance capacity, however the contribution from the flange is ignored in the Eurocode draft (EN_1993-1-5, 2019). This needs to be reconsidered.
- All studies were done on short loading lengths. Nevertheless, the resistance to patch loading has not been studied for cases where the loading length spans over many waves (such as the case during launching). The shorter loading length might be more essential; nonetheless, the design must be optimized to avoid being too conservative.
- Recently, a master's thesis work was performed at Chalmers university of technology to study the patch loading resistance of corrugated web girders (SÆMUNDSSON, 2021). See Figure 3.10. It was demonstrated that the same conclusion regarding the

flange contribution to the path loading capacity applies for stainless steel. The (EN_1993-1-5, 2019) model yields in so conservative results due to disregarding the flange contribution to patch loading resistance. However, none of the preceding models provides a reliable estimation for the patch loading resistance of corrugated web girders (SÆMUNDSSON, 2021). As a result, the present model in (EN_1993-1-5, 2019) is recommended to be used until a more feasible model is developed.

# 4 Bibliography

Abbas, H. H., Sause, R., & Driver, R. G. (2007). Simplified analysis of flange transverse bending of corrugated web I-girders under in-plane moment and shear. *Engineering Structures*, *29*(11), 2816-2824. https://doi.org/10.1016/j.engstruct.2007.01.006

Al-Emrani, M. (2020). <Book - Steel Structures 2020_V3.pdf>.

Amedment, E.-.-. (2015). Amendment to Stainless steel design rules in Eurocode SS-EN 1993-1-4. In.

Amedment, E.-.-. (2021). Amendment to Stainless steel design rules in Eurocode SS-EN 1993-1-4. In.

B. Johansson, R. M., G. Sedlacek, C. Müller, D. Beg. (2007). <Commentary and worked examples to EN1993-1-5.pdf>.

Baláž, I., & Koleková, Y. (2012). Influence of Transverse Bending Moment in the Flange of Corrugated I-Girders. *Procedia Engineering*, *40*, 26-31. https://doi.org/10.1016/j.proeng.2012.07.050

Basinski, W. (2019). Analysis of the Shear Angle in Corrugated Web Girders. *IOP Conference Series: Materials Science and Engineering*, *471*, 052005. https://doi.org/10.1088/1757-899X/471/5/052005

Denan, F., Osman, M., Saad, S., & others. (2010). The study of lateral torsional buckling behaviour of beam with trapezoid web steel section by experimental and finite element analysis. *International Journal of Research and Reviews in Applied Sciences (IJRRAS)*, *2*(3), 233–240.

Deng, H., Shao, Y.-B., & Hassanein, M. F. (2022). Experimental shear testing of small-scale corrugated web girders used in conventional buildings. *Journal of Constructional Steel Research*, *189*. https://doi.org/10.1016/j.jcsr.2021.107086

Driver, R. G., Abbas, H. H., & Sause, R. (2006). Shear behavior of corrugated web bridge girders. *Journal of structural engineering*, *132*(2), 195–203.

EDVARDSSON, G. E., LUNDQUIST, BENGT. (2014). Influence of Purlins on Lateral-Torsional Buckling of Steel Girders with Corrugated W. In.

Elamary, A. S., Saddek, A. B., & Alwetaishi, M. (2017). Effect of corrugated web on flexural capacity of steel beams. *12*(4), 12.

Elgaaly, M. (1997). Beams with corrugated webs under paartial compression. *Journal of structural engineering*.

EN_1993-1-1. (2005). EN 1993-1-1 General rules and rules for buildings.pdf.

EN_1993-1-1. (2019). EN_1993-1-1_of_SC3_N3022_2019-12-.pdf.

EN_1993-1-4. (2006). EN_1993-1-4_stainless steel.PDF.

EN_1993-1-4. (2020). <CEN-TC250-SC3_N3120_Second_Draft_of_EN_1993-1-4.PDF>

EN_1993-1-5. (2006). EN_1993-1-5 Thin-walled members.pdf.

EN_1993-1-5. (2019). Final draft of EN_1993-1-5  (2019-11-12). In.

et.al., Y. (2008). <2008-CW- Interactive shear buckling- FEM-parametric study.pdf>.

Hassanein, M. F., Elkawas, A. A., El Hadidy, A. M., & Elchalakani, M. (2017). Shear analysis and design of high-strength steel corrugated web girders for bridge design. *Engineering Structures*, *146*, 18-33. https://doi.org/10.1016/j.engstruct.2017.05.035

Hassanein, M. F., & Kharoob, O. F. (2013). Behavior of bridge girders with corrugated webs: (I) Real boundary condition at the juncture of the web and flanges. *Engineering Structures*, *57*, 554-564. https://doi.org/10.1016/j.engstruct.2013.03.004

Hlal, F., Mohra, Naheel. (2021). Stainless Steel Bridge Girders with Corrugated Webs - A parametric study to investigate the sensitivity of Stainless steel girder's shear behaviour to intial imperfection. In.

Inaam, Q., & Upadhyay, A. (2020). Behavior of corrugated steel I-girder webs subjected to patch loading: Parametric study. *Journal of Constructional Steel Research*, *165*, 105896. https://doi.org/10.1016/j.jcsr.2019.105896

Inaam, Q., & Upadhyay, A. (2022). Accordion effect in bridge girders with corrugated webs. *Journal of Constructional Steel Research*, *188*. https://doi.org/10.1016/j.jcsr.2021.107040

Jáger, B., Dunai, L., & Kövesdi, B. (2017a). Flange buckling behavior of girders with corrugated web Part I: Experimental study. *Thin-Walled Structures*, *118*, 181-195. https://doi.org/10.1016/j.tws.2017.05.021

Jáger, B., Dunai, L., & Kövesdi, B. (2017b). Flange buckling behavior of girders with corrugated web Part II: Numerical study and design method development. *Thin-Walled Structures*, *118*, 238-252. https://doi.org/10.1016/j.tws.2017.05.020

Jian-Guo Nie, L. Z., & Mu-Xuan Tao, L. T. (2013). Shear strength of trapezoidal corrugated steel webs. *Journal of Constructional Steel Research*, *85*, 105-115. https://doi.org/http://dx.doi.org/10.1016/j.jcsr.2013.02.012

Jiho Moon, J. Y., & Byung H. Choi, H.-E. L. (2009). Shear strength and design of trapezoidally corrugated steel webs. *Journal of Constructional Steel Research*, *65*, 1198-1205. https://doi.org/doi:10.1016/j.jcsr.2008.07.018

Karlsson, E. (2018). Stainless Steel Bridge Girders with Corrugated Webs. In.

Kollár, D., & Kövesdi, B. (2018). EFFECT OF IMPERFECTIONS AND RESIDUAL STRESSES ON THE SHEAR BUCKLING STRENGTH OF CORRUGATED WEB GIRDERS. 20.

Kollár, D., & Kövesdi, B. (2019). Welding simulation of corrugated web girders - Part 2: Effect of manufacturing on shear buckling resistance. *Thin-Walled Structures*, *141*, 477-488. https://doi.org/10.1016/j.tws.2019.04.035

Kövesdi, B. (2010). <kovesdi_balazs_phd.pdf>

Kövesdi, B., & Dunai, L. (2011). Determination of the patch loading resistance of girders with corrugated webs using nonlinear finite element analysis. *Computers & Structures*, *89*(21-22), 2010-2019. https://doi.org/10.1016/j.compstruc.2011.05.014

Kövesdi, B., Jáger, B., & Dunai, L. (2016). Bending and shear interaction behavior of girders with trapezoidally corrugated webs. *Journal of Constructional Steel Research*, *121*, 383-397. https://doi.org/10.1016/j.jcsr.2016.03.002

LARSSON, M., , , & PERSSON, J. (2013). <Larsson&Persson.pdf>.

Leblouba, M., Barakat, S., & Al-Saadon, Z. (2018). Shear behavior of corrugated web panels and sensitivity analysis. *Journal of Constructional Steel Research*, *151*, 94-107. https://doi.org/10.1016/j.jcsr.2018.09.010

Leblouba, M., Barakat, S., Altoubat, S., Junaid, T. M., & Maalej, M. (2017). Normalized shear strength of trapezoidal corrugated steel webs. *Journal of Constructional Steel Research*, *136*, 75-90. https://doi.org/10.1016/j.jcsr.2017.05.007

Leblouba, M., Barakat, S., Maalej, M., Al-Toubat, S., & Karzad, A. S. (2019). Normalized shear strength of trapezoidal corrugated steel webs: Improved modeling and uncertainty propagation. *Thin-Walled Structures*, *137*, 67-80. https://doi.org/10.1016/j.tws.2018.12.034

Leblouba, M., Junaid, M. T., Barakat, S., Altoubat, S., & Maalej, M. (2017). Shear buckling and stress distribution in trapezoidal web corrugated steel beams. *Thin-Walled Structures*, *113*, 13-26. https://doi.org/10.1016/j.tws.2017.01.002

Luo, R., & Edlund, B. (1996). Ultimate strength of girders with trapezoidally corrugated webs under patch loading. *Thin-Walled Structures*, *24*(2), 135-156. https://doi.org/10.1016/0263-8231(95)00029-1

Moon, J., Yi, J.-W., Choi, B. H., & Lee, H.-E. (2009). Lateral–torsional buckling of I-girder with corrugated webs under uniform bending. *Thin-Walled Structures*, *47*(1), 21-30. https://doi.org/10.1016/j.tws.2008.04.005

Nguyen, N. D., Han, S.-R., Lee, G.-S., & Kang, Y.-J. (2011). Moment modification factor of I-girder with trapezoidal-web-corrugations considering concentrated load height effects. *Journal of Constructional Steel Research*, *67*(11), 1773-1787. https://doi.org/10.1016/j.jcsr.2011.05.002

Richard Sause, & Braxtan, T. N. (2011). Shear strength of trapezoidal corrugated steel webs. *Journal of Constructional Steel Research*, *67*, 223-236. https://doi.org/doi:10.1016/j.jcsr.2010.08.004

SÆMUNDSSON, D., INGÓLFSDÓTTIR, SIGNÝ. (2021). Nonlinear finite element analysis of stainless steel corrugated web girders subjected to patch loading. In.

Sause, R., Abbas, H. H., Wassef, W. G., Driver, R. G., & Elgaaly, M. (2003). Corrugated Web Girder Shape and Strength Criteria. (03), 72.

Transportstyrelsens. (2018). <TSFS 2018_57.pdf>.

Zhang, B., Yu, J., Chen, W., Wang, H., & Xu, J. (2020). Stress states and shear failure mechanisms of girders with corrugated steel webs. *Thin-Walled Structures*, *157*. https://doi.org/10.1016/j.tws.2020.106858

**CHALMERS**